Thesis in requirement for the Doctor of Philosophy (PhD)

Parameter identification for biological models

by

Dirk Fey

Supervisor: Dr. sc. techn. Eric Bullinger

Systems and Modelling Research Unit
Department of Electrical Engineering and Computer Science
Faculty of Applied Sciences
University of Liège, Belgium

Jury members

Prof. Louis Wehenkel, University of Liège (jury president)
Prof. Rodolphe Sepulchre, University of Liège
Dr. Dominique Toye, Assistant Professor, University of Liège
Dr. Damien Ernst, University of Liège
Prof. Dr.-Ing. Rolf Findeisen University Magdeburg, Germany
Seán Commins, PhD, Senior Lecturer, National University of Ireland, Maynooth
Dr. Thierry Bastogne, Maître de Conférences, Université Henri Poincaré, France

Acknowledgements

This thesis would not have been possible without my supervisor Eric Bullinger, whose encouragement and support from the initial to the final level, enabled me to develop an understanding of the subject and develop the here presented methodologies. I could not have wished for a better supervisor providing valuable guidance, while also granting me the freedom to develop my own projects.

I am very grateful to Peter Wellstead, without whom obtaining several scholarships and travel grants would not have been possible. I consider him a valuable mentor.

I would also like to show my gratitude to Seán Comins, who made the second part of my thesis possible. Seán hosted me several times in his lab and taught me much about water maze experiments and behavioural neuroscience.

It is a pleasure to thank Rodolphe Sepulchre, director of Systems and Modelling at the University of Liege, William (Bill) Leithead, director of the Industrial Control Centre at the University of Strathclyde, and Douglas Leith, director of the Hamilton Institute at the National University of Ireland in Maynooth, for having me at their respective institutes.

Further, I am indebted to many of my colleagues and friends, who made working in a research environment stimulating and enjoyable, in particular Diego Oyarzùn, Andrea Weiße, Sung-Ho Hur, Hong Yue, Aristeidis Chatzopoulos, Victoria Neilson and Guillaume Drion and all the others.

Lastly, I offer my regards and blessings to all of those who supported me in any respect during the completion of the project, in particular my wife, my parents and my brother.

Dirk Fey

Contents

Chapter 1

Introduction

From the earliest times on man asked questions about the origin of the world, its meaning and purpose. Science confronts these mysteries with questions, doubts, curiosity and exploratory endeavours, a philosophy that goes back as far as ancient Greece. Pre-Socrates philosophers seeked *natural explanations* in terms of observable forces (such as fire, water, air etc.). Such a explanation is in principle a model of how we think about the world. In modern terms, we can therefore understand science as the identification of models from *observed data* (Ljung, 1999). Ayala (1968) puts it this way

> Science seeks to organise knowledge in a systematic way, endeavouring to discover pattern of relationship among phenomena and processes.

Further, Ayala (1968) gave two more characteristics for science: First, a theory (or hypothesis or model) should be explanatory, i.e. it should explain what we already know, and it should in addition predict something we do not yet know. Second, a theory (or hypothesis or model) should be testable, i.e. it should in principle be possible to invalidate the model by comparing its predictions to new experimental data.

In the public eye, science is often viewed in terms of discoveries. When Alfred Nobel wrote about the conditions of the Nobel price, he was thinking in terms of discoveries, particularly those that are beneficial to humankind. However, viewing science just as the collection of new facts is misleading. Often, scientific progress is more elevated by the introduction of new concepts. In the biological sciences, a new concept was for example introduced by Charles Darwin with the (nowadays seemingly trivial) idea that populations consist of different individuals, which led to the theory of natural selection and evolution. Another example is Erwin Schrödinger with the idea that biological systems follow physical (and chemical) and not metaphysical laws (Schrödinger, 1944), which lay the foundation of modern molecular biology.

Concepts possess more or less abstract representation in form of models. Models are nothing new in biology. An example of a model in the physical sense of the word are laboratory rats. Often, rats in the laboratory act as model organisms used to study diseases that are difficult to study in humans directly. Another, very nice example is provided by James Watson and Francis Crick when discovering the structure of DNA. In their lab, they built a physical,

three dimensional model of the involved chemical elements and their bounds, which they used to guide their intuition into finding the correct configuration (Watson, 1968). Here we also have an example of a mathematical model, in which Crick used the theory of physical chemistry to calculate the stability of the arrangement.

Generally, mathematical models are a vital component of science. Different models or model frameworks often require a different sort of mathematics. I already mentioned the mathematics of physical chemistry, dedicated to the calculation of forces between atoms and molecules. Another example is the application of graph theory to gene regulation and protein interaction networks, where nodes represent genes and proteins and vertices their interactions. Rather recently, another branch of mathematics, namely systems theory spread into biology. In contrast to classical, reductionist biological thinking in which the focus is on studying individual parts, systems theory offers a wholistic approach, in which the focus is on the behaviour emerging from the interaction patterns of the different constituents.

Systems theory was pioneered with the works of Norbert Wiener (1948) and Ludwig von Bertalanffy (1968). Interestingly, Norbert Wiener was inspired by biology. When working on the design of fire control devices during World War II, Wiener observed that anti-aircraft guns exhibit erratic behaviour very similar to tremors in humans. Consulting with Arturo Rosenblueth, a colleague in the neurosciences, he came to the conviction that the behaviour of servomechanisms, of computing machines and of the nervous system, could all be regarded from a unified overall viewpoint. Despite that biological inspiration, systems theory had little impact on biology and most of its success in was engineering. In contrast to engineered systems, facts are often unknown or uncertain in biology. In molecular biology for instance, it is often not known which genes interact with each other, or which proteins are involved in a certain process. This lack of knowledge explains at least partly the long absence and slow progress of systems theory in biology. Further, biology was (and still is) very busy identifying and characterising the components that make up the system, whereas systems theory was busy solving engineering and automatic control problems. Now, in the post genomic era, biology begins to experience a shift in thinking toward a systems perspective; partly driven by the limitations of the reductionist approach, partly driven by a control theoretical community in search of new application areas (Ljung, 2010; Wellstead et al., 2008).

Systems theory is based on dynamic models, and therewith implicitly demands the collection of dynamic data in the form of time series measurements. Recent and ongoing advances in measurement techniques (de Graauw (2009); Szallasi (2006), see also Section 2.2) enable experimental biologists to collect time series data in ever increasing dimension, putting the successful application of systems theory to biology into reachable scope and bringing us back to the beginning of this chapter and the question of how to build these models. Following Ayala's demands on science mentioned earlier, we can lay down some ground rules. To make valuable predictions, we should use experimentally collected data to built a model. Hereby, the complexity of model depends on the amount and quality of data available. In that spirit, my thesis addresses two important questions. First, can we use existing system-theoretical tools to identify biological models? Second, can we develop novel systems theoretical identification methods that are particularly tailored to biology?

About this thesis

This thesis is structured into two parts. Both concern building dynamic models from observed data, but are quite different in perspective, rationale and mathematics.

The first part considers the development of novel identification techniques that are particularly tailored to (molecular) biology and considers two approaches. The first approach reformulates the parameter estimation problem as a feasibility problem. This reformulation allows the invalidation of models by analysing entire parameter regions. The second approach utilises nonlinear observers and a transformation of the model equations into parameter free coordinates. The parameter free coordinates allow the design of a globally convergent observer, which in turn estimates the parameter values, and further, allows to identify modelling errors or unknown inputs/influences. Both approaches are bottom up approaches that require a mechanistic understanding of the underlying processes (in terms of a biochemical reaction network) leading to complex nonlinear models.

The second part is an example of what can be done with classical, well developed tools from systems identification when applied to hitherto unattended problems. In particular, part two of my thesis develops a modelling framework for rat movements in an experimental setup that it widely used to study learning and memory. The approach is a top down approach that is data driven resulting in simple linear models.

Applying systems theoretical tools to biology is often not straightforward, and requires consideration of multiple different aspects. As a consequence, this thesis takes a problem oriented approach that asks at any particular point what is required to solve the problem? Therefore, there is no exhaustive background chapter at the beginning. Rather, the preliminary knowledge for the problems at hand are introduced directly where necessary. I feel this approach fosters the readability of the document.

Part I: Develop theory tailored to biochemical reaction systems

Biochemical reaction systems are a means of understanding biology on a molecular level using dynamic models of intra- and extracellular processes. The question arise of how we can construct these models based on observations in experiments. The systems and control community has developed several methodologies to build dynamic models from experimental data. The theory around these methodologies is commonly referred to as systems identification and enables the user to asses the reliability, quality and predictive power of the identified models. Most, if not all, of systems identification has been developed for technical system and is not applicable to biology. The idea of this thesis is to see the peculiarities of biological systems not as obstacle, but as stepping stone. More concretely, the nonlinearity of biological systems has a certain form, which this thesis exploits to develop novel identification methodologies. As a result these methodologies are particularly tailed to biochemical reaction systems.

Aim:

Develop reliable identification methods that guarantee accuracy by mathematical proof.

Strategy:

Exploit peculiarities of biological systems, in particular the special form of nonlinearity.

Techniques:

The techniques used to achieve the goal are mostly borrowed from systems theory and adjacent fields:

- Sum of squares representation of polynomials
- Linear matrix inequalities and semidefinite programming
- State space transformations
- Observability and nonlinear observers
- Differential geometry and Lie algebraic computations
- Lyapunov and dissipativity theory

Contributions:

The main contributions of Part I can be summarised as follows

- Model invalidation (using sum of squares and semidefinite programming)
  - Extension of a steady state approach in the literature to transients (Fey and Bullinger, 2010)
  - Establishing connections between model/parameter invalidation and observability
- Parameter estimation (using model extensions and nonlinear observers)
  - Extension of a transformation for mass action systems into parameter free coordinates to rational kinetics (Fey et al., 2008)
  - Possibility to estimate time varying parameters and unknown inputs
  - Circumventing observability issues by incorporating known parameters
- Identification of modelling errors
  - Detecting and tracing modelling errors and unknown inputs
- Nonlinear observer design
  - Design of a globally convergent observer using Lie algebra (Fey et al., 2009)

  - Design of a globally convergent observer using dissipativity theory (Fey and Bullinger, 2009)

- Data preprocessing/curve fitting
  - Assessment of the influence of noise and data preprocessing

Part II: Develop modelling framework for the Morris water maze

The Morris water maze is an experimental setup to study spatial learning and memory. Rats are entrained to fulfil a certain navigational task, whereby the path of movement can be recorded easily using a video camera. However, the literature does not use the recorded paths in the analysis of the experiment. Part two of this thesis closes this gap by developing a conceptual and mathematical framework for the analysis of the recorded paths. Thereby a data driven approach is taken in which simple dynamic models of the rat behaviour are constructed and identified. The methodology is generally applicable to other experimental setups where animal movements are tracked.

Aims:

- Develop a framework for analysing recoded movement paths in the Morris water maze.
- Model, identify, analyse and compare two different experiments.

Strategy:

Take a data driven approach using simple discrete time models that can be readily identified using well developed system identification methodologies.

Techniques:

The techniques used to achieve the goal are mostly borrowed from systems identification and adjacent fields:

- Auto- and crosscorrelation analysis
- Random walk, autoregressive and stochastic modelling
- Statistics and identification of distributions
- Model identification (Yule Walker etc.)
- Standard feedback control (PID) and filtering

Contributions:

The main contributions of Part II can be summarised as follows

- Development of a framework that uses recordings of entire swimming paths
- Development of several dynamic models of rat swimming behaviour in the Morris water maze

- Identification of these models in two different experiments, revealing that the feedback strategy and strength depends on the training regime (here, the availability of navigational cues)
  - Three cues: use of immediate information and strong feedback
  - One cue: additional use of past information and weaker feedback
- Analysis and predictions of the identified models
  - In an egocentric, cue based strategy (i.e. self centred, no map) weak feedback resulting in loose or sluggish control is beneficial in cases where the environment provides insufficient information (one cue case)
  - Allocentric strategy (i.e. some sort of mental map or positional information) required to explain observed escape latencies in advanced training stages (i.e. 4 or 5 days of training), but the positional information may be very uncertain/fuzzy.
- Providing a hypothesis of how the model parameters relate to different brain regions and activation of neuronal pathways

Publications

Bullinger, E., Fey, D., Farina, M., and Findeisen, R. (2008). Identifikation biochemischer Reaktionsnetzwerke: Ein beobachterbasierter Ansatz. *AT-Automatisierungstechnik*, 56(5):269–279.

Conzelmann, H., Fey, D., and Gilles, E. D. (2008). Exact model reduction of combinatorial reaction networks. *BMC Systems Biology*, 2:78.

Fey, D. and Bullinger, E. (2009). A dissipative approach to the identification of biochemical reaction networks. In *15th IFAC Symposium on System Identification, Saint Malo, France*, pages 1259–1264.

Fey, D. and Bullinger, E. (2010). Limiting the parameter search space for dynamic models with rational kinetics using semi-definite programming. In *11th Symposium on Computer Applications in Biotechnology, Leuven, Belgium*, pages 150–155.

Fey, D. and Bullinger, E. (2011). Identification of kinetic parameters and modelling errors for biomolecular reaction systems using dissipative observers. *(submitted)*.

Fey, D., Commins, S., and Bullinger, E. (2010). Feedback control strategies for spatial navigation revealed by dynamic modelling of learning in the Morris water maze. *J Comput Neurosci*, (in print).

Fey, D., Findeisen, R., and Bullinger, E. (2008). Parameter estimation in kinetic reaction models using nonlinear observers is facilitated by model extensions. In *17th IFAC World Congress, Seoul, Korea*, pages 313–318.

Fey, D., Findeisen, R., and Bullinger, E. (2009). Identification of biochemical reaction networks using a parameter-free coordinate system. In *Control Theory and Systems Biology* by P. Iglesias and B. Ingalls: 297–316. MIT press.

Part I

Identification of biochemical reaction networks

Chapter 2

Background

2.1 Molecular biology and systems theory

Modelling biological systems on the intracellular level has been a research topic for over half a century. All started in 1943, when Erwin Schrödinger gave three talks in Dublin entitled *What is Life* (Schrödinger, 1943, 1944). One of his central, at that time a revolutionary idea, was that biological systems follow physical laws. In other words, biological systems can be described by mathematical models. For the membrane potential, this was achieved in 1952 by Hodgkin and Huxley, who explained and underlined their experimental data with a mathematical model, a key step in understanding how neurons function (Hodgkin and Huxley, 1952). A few years later, Denis Noble expanded this model to obtain the first mathematical model of the heart (Noble, 1960). Nowadays, Hodkin Huxley models and variants thereof are a vital part of computational neuroscience and widely used in research groups around the world. Part of Hodgkin and Huxley's success relies on the fact that they were able to estimate the model parameters from experimental data. In other areas of molecular biology, such as cell signalling and gene regulation, the identification of mathematical models has proven to be much more challenging.

The advances in biological experimental techniques of the last decades has led to a rapidly growing number of models (Li et al., 2010; Le Novère et al., 2006). In signal transduction, the mitogen activated protein kinase (MAPK) and the epidermal growth factor (EGF) were amongst the first systems to be modelled (Huang and Ferrell, 1996; Kholodenko et al., 1999). From a modelling perspective, cell signalling system are often composed of a number of similar modules or motifs, such as dimerisation processes or phosphorylation cycles. Biologically these modules are diversely implemented, i.e. composed of different molecular species. As a consequence, although having the same interaction pattern, one particular module can exhibit very different behaviours. For example, the MAPK kinase consists of phosphorylation dephosphorylation cycles layered in three stages (Kholodenko et al., 2010). This scheme is implemented by nature in several variations involving different proteins such as ERK1, ERK2 or JNK. A model of the MAPK system can exhibit totally different behaviours such as homeostasis, near perfect adaptation and damped or sustained oscillations, depending on the values of the kinetic parameters (Kholodenko, 2006). This ex-

ample illustrates the importance of choosing the correct parameters, especially if the model is to be used for predictions.

The main bottleneck in obtaining dynamical models of biological systems is the estimation of biological parameters, while structural information like stoichiometry are often known. Unknown parameters can be estimated from time-series data as is common practice in technical applications. Several peculiarities of biological systems hinder a straightforward application of most existing identification methodologies as typically used for technical systems. Biological systems usually have a large number of parameters, though often only a reduced set of experiments are possible, consisting of a few experimental steps and scarce time points. Furthermore, the noise level is usually significant.

Recent years have shown that the control and system theoretical viewpoint and approaches are valuable tools for gaining a deeper understanding of biological systems (Wellstead et al., 2008; Gilles, 2002a). As outlined however, biological systems have particular properties, such as positivity and monotonicity, not often found in technical applications (Sontag, 2005; Sontag et al., 2004). This requires the design of novel methodologies particularly suited for biological systems. Concerning metabolic pathways, a prominent example is metabolic control analysis for sensitivity analysis developed in the 70ies (Heinrich and Schuster, 1996; Fell, 1997). Metabolic control theory exploits the fact that metabolic systems spent most of their time resting in steady state, an assumption not sensible for signalling networks. Concerning signalling networks, such unified theoretical treatments have not yet been established. This is partly due to the fact that signalling systems naturally deal with the temporal integration of ever changing extracellular conditions with the intracellular machinery. As a consequence, the behaviour is often dominated by transient and nonlinear effects. In fact, the nonlinearity of signalling systems often generate the phenomena constituting particular biological functions. Examples are stable limit cycle oscillations in the case of circadian rhythms and cell cycles, or bistable switches in the case of cell fate decisions such as differentiation and apoptosis (Leloup and Goldbeter, 2008; Eissing et al., 2007). From a theoretical perspective, the nonlinearity and behavioural complexity impedes the development of a (unifying) biological theory. As a consequence, the field is diversified with numerous theoretical works treating numerous specialised cases. Recently an entire book *Systems Theory and Systems Biology* edited by Iglesias and Ingalls (2009) was published on the subject. Next year, the *International Journal of Robust and Nonlinear Control* and *Automatica*, both dedicate a special issue to systems biology. In that spirit, my research focuses on the development of identification methodologies that are particularly tailored to biological systems from a systems theoretical perspective.

Before discussing particular aspects and problems of of model identification in biology (including a very limited review of the state of the art) the next two sections introduce to quantitative experimentation and a dynamic modelling of molecular biological systems.

2.2 Quantitative data

Most quantitative measuring methods depend on a combination of size separation and the application of a specific high affinity receptor system. Size

separation is achieved by driving macromolecules of various sizes through a molecular sieve by an electrostatic potential in a process called gel or capillary electrophoresis. The size-resolution of gel electrophoresis is rather limited, which is why subsequent reporter systems are used in order to achieve the desired specificity. The reporter is labelled by incorporating radioactive or fluorescent molecules, which in turn produce readily measurable signals. The quantification of these signals usually exhibits errors of around 10 – 20% or less (Szallasi, 2006).

For nucleic acids, highly specific reporters can be produced with relative ease based on the Watson-Crick pairing. The high specificity of these probes allowed for the elimination of the size-separation step (called Southern blot for DNA, Northern blot for RNA) and led to the automatisation of the process by immobilising either the probe or the sample mixture. These microarray/chip technologies are capable of high throughput, i.e. probing hundreds and thousands of genes simultaneously, however with limited, uncertain accuracy (Draghici et al., 2006).

Proteins are analysed in Western blots. The reporters are called antibodies. Their production still depends on processes that can not easily be controlled, resulting in limited availability and labour intensive production. Despite these difficulties, today's antibodies provide remarkable specificity, not only for individual proteins, but also for diverse posttranslational modifications, such as specific phosphorylation states.

In principle the above described technique can be applied to single cell measurements. However, the isolation of material for Western blots requires extensive and meticulous bench work. An rather convenient alternative is attaching a fluorescent protein to the molecule in question and measuring the fluorescent intensity directly without destroying the cell. The number of different fluorescent proteins that can be fused to other proteins of interest limits the number of measurable proteins. A drawback that can be overcome partially by combining fluorescent labelling with multi parameter flow cytometry (Irish et al., 2006).

The above outlined methodologies are only a partial snapshot of current techniques, however spotlighting those that can provide the quality of data that is necessary for the identification of dynamic models. For a more comprehensive treatment of the subject, I refer to de Graauw (2009) for phospho-proteomics and Gstaiger and Aebersold (2009) for mass spectrometry. The next section introduces to dynamic modelling of biochemical reaction networks in systems biology.

2.3 Dynamic modelling

A common framework for the modelling of biochemical reaction networks are sets of reactions of the following form

$$\alpha_1 \mathrm{S}_1 + \ldots + \alpha_{n_s} \mathrm{S}_{n_s} \rightarrow \beta_1 \mathrm{P}_1 + \ldots + \beta_{n_p} \mathrm{P}_{n_p}, \tag{2.1}$$

where S_i are substrates that are transformed into the products P_i. The factors α_i and β_i are the stoichiometric coefficients of the reactants.

Neglecting spatial and stochastic effects, these reactions are often modelled

with systems of ordinary differential equations:

$$\dot{c} = Nv(c, p), \tag{2.2}$$

where $c \in \mathbb{R}^n_{\geq 0}$ is the vector of concentrations, $p \in \mathbb{R}^{n_p}_{>0}$ the parameter vector and $v \in \mathbb{R}^n_{\geq 0} \times \mathbb{R}^{n_p}_{>0} \mapsto \mathbb{R}^m_{\geq 0}$ the vector of the flows. The stoichiometric matrix $N \in \mathbb{R}^{n \times m}$ depends on the coefficients α_i, β_i and, possibly on factors compensating different units or volumina. For a more detailed introduction, see for example (Klipp et al., 2005; Keener and Sneyd, 2001).

There is a large variety of possible reaction models (Cornish-Bowden, 2004). Here, we restrict the reaction models to the most common ones in signalling networks:

- **mass action**: The flow is proportional to each substrate: $v = k \prod_{i \in I} c_i$ where I is a subset of $1, \ldots, n$ with possibly repeated entries;
- **power law** (S-Systems, generalised mass action) The flow is polynomial in the substrates: $v = k \prod_{i \in [1,n]} c_i^{\alpha_i}$
- **Michaelis-Menten** or **Monod**: for low substrates the flow v depends linearly on the substrate s and saturates for large substrate concentrations at $V_{\max}$: $v = V_{\max} \frac{s}{K_M + s}$. At a substrate concentration of K_M, the flow is half the maximum rate.
- **Hill**: The flow is sublinear for low substrate and saturates for large substrate concentrations at $V_{\max}$: $v = V_{\max} \frac{s^h}{K_M^h + s^h}$. The exponent h is larger than one and at a substrate concentration of K_M, the flow is half the maximum rate.

In biochemical reaction modelling, the stoichiometry is usually known, as is the type of reaction kinetics, in contrary to the often quite uncertain parameters. Thus, the problem can be formulated as follows:

Given: The stoichiometric matrix N and the form of the function $v(c, p)$ describing the reaction rates

Unknown: The kinetic parameters p

The next section introduces to the task of estimating the unknown parameters.

2.4 Classical identification methods and drawbacks

Constructing mathematical models from experimental data is a fundamental element of science (Ljung, 1999). Multiple communities approach the problem differently from different perspectives such as time series analysis, machine learning or manifold learning, with statistics at the core (Ljung, 2010). From a control or systems theoretical perspective, building dynamic models from data is summarised under the term system identification. Taking a systems theoretical perspective, the following sections discuss some aspects of system identification that are relevant in the context of systems biology and this thesis.

Structure vs. parameter identification

Classical control theory reduces the problem of systems identification to parameter estimation. This means we first have parameterise the problem by choosing a model class or model structure, and then estimate the model parameters. Often the term model identification is used when little is know about the structure of the system, i.e. the chosen model class is fairly general, whereas the term parameter estimation is used when a parametrisation is (naturally) given. For example, identifying a finite impulse response system

$$y[n] = b_0 u[n] + b_1 u[n-1] + \dots$$

means estimating the coefficients b_i, i.e. parameter estimation. It is however usually referred to as system identification because no prior assumptions on the structure, i.e. the number coefficients b_i, are made. Finite impulse response systems are a prime example in that respect, because the coefficients are directly given by the impulse response and we can directly see the structure of the system, i.e. all nonzero coefficients. Thus, in this example, the distinction between structural identification and parameter estimation thus degenerates.

Generally however, it makes sense to distinguish structure from parameter identification. In molecular biology, determining which components interact is a form of structure identification and subject of intensive research in the field of bioinformatics (Lee and Tzou, 2009; Li et al., 2008; Csete and Doyle, 2002). We can approach the problem from a systems theoretical point of view by means of a very simple idea (Kholodenko et al., 2002). The interaction pattern of a dynamic system $\dot{c} = f(c)$ is given by its Jacobian $\frac{\partial f}{\partial c}$, in which non zero elements describe which species interact. Kholodenko et al. (2002) derived a methodology of how to estimate a normalised version of the Jacobian based on disturbing each species and measuring the effect on the steady state, which has successfully been used in praxis (Santos et al., 2007). Sontag et al. (2004) relaxed the requirement of having to disturb each species by extending the method to transient, non-steady state conditions using the concept of observability. A drawback is that second and higher order derivatives of the measured variables have to be accurately calculated. This might be unrealistic in a biological setting where data is associated with a high level of noise or uncertainty (Personal correspondence with Prof. B. Kholodenko). In that scenario, taking a probabilistic view might be preferable (Needham et al., 2007; Dojer et al., 2006). In Bayesian learning for example, probabilities are used to represent uncertainties about the interactions to be identified. Before looking at any data, our prior opinions about what the interaction pattern might be can be expressed in a probability distribution over the Jacobian or interaction graph. By looking at the data, Bayesian algorithms revise our opinions and capture these revision in posterior distribution. The posterior distribution then tells us which interactions are most likely.

Structure identification is a huge and quickly moving field; the above examples present only a tiny portion. For a more comprehensive treatment see for example the book *Computational Systems Biology* (Ireton et al., 2009). Further, there are entire databases dedicated to the mapping of molecular biological interactions (STKE, 2010; KEGG, 2010; EcoCyc, 2010). As detailed in the previous section, this thesis assumes that the systems structure is already known. If the structure is known incorrectly, the methodology developed in Chapter 3 can be used to invalidate the model and the methodology developed in Chapters 4

to 6 can be used to identify the error.

Discrete vs. continuous

Discrete-time models are common in engineering. Their estimation is often achieved by minimisation of quadratic functionals (Gadkar et al., 2005; Ljung, 1999). Even in nonlinear cases, discrete identification problems can often be reduced to linear algebra and solved efficiently. In systems biology however, the models are usually time-continuous as described in Section 9. In principle, discretisation makes the machinery of classical, well developed systems theoretical tools available (Rumschinski et al., 2010; Garnier and Wang, 2008). However, these models are the result of first principle modelling and, for example, retain the linearity in the parameters for mass action kinetics. Additionally, time continuous models are less sensitive to noisy measurements common in biology (Garnier et al., 2003). For these reasons, time continuous models are preferable in systems biology, even though there are only few suitable continuous identification algorithms.

Global vs. local

Global, optimisation based parameter estimation algorithms are common in systems biology (Moles et al., 2003; Feng and Rabitz, 2004; Singer et al., 2006). Examples are Monte Carlo based approaches such as simulated annealing and evolutionary strategies (Beyer and Schwefel, 2002), multiple shooting (Peifer and Timmer, 2007) and branch and bound algorithms (Polisetty et al., 2006). These methods formulate the parameter estimation as the minimisation of the error between simulated and measured outputs, subject to the model dynamics as constraints. The resulting optimisation problem is usually non-convex, i.e. difficult to analyse theoretically and the computational complexity for solving it grows significantly with the size of the parameter space (Polisetty et al., 2006). Alternatives are local search strategies such as gradient based methods (Boyd and Vandenberghe, 2004; Zak et al., 2003). The problem with local search strategies is that they can get trapped in local minima. Therewith, their main disadvantage is the need for a good initial guess.

Monte Carlo based, as well as local strategies suffer from the fact that no guarantee of global convergence or optimality can be provided.

Specialised approaches for biological systems

The previous section underpins the necessity for developing novel parameter estimation algorithms that are particularly suited for systems biology (Ljung, 2003). Algebraic approaches that take the model structure explicitly into account (Audoly et al., 2001; Ljung and Glad, 1994; Xia and Moog, 2003), but are only applicable to small systems. Other approaches that are for example based on interval analysis and constraint propagation (Tucker et al., 2007) or a quadratic system description (Karnaukhov and Karnaukhova, 2003) are only applicable in particular cases. Thus, there is still a need for numerical solutions that exploit the structural information.

Chapter 3

Parameter invalidation using semidefinite programming

3.1 Introduction and related work

In principle, the continuous parameter estimation problem can be solved by integrating (2.2). The difficulty with the integration based approach is twofold. On the one hand, an analytic solution of the integral $\int Nv(c,p)dt$ can only be computed in rare special cases, which are generally not relevant in biology. On the other hand, numerical integration requires to specify the unknown parameters p (and initial conditions $c(t=0)$) beforehand. Most parameter estimation methods deal with the dilemma of specifying the unknown parameters by choosing parameter values a priori, numerically integrating the differential equations and then comparing the result with the data a posteriori (Kuepfer et al., 2007). Advanced methods run a loop in which the parameters are updated after each integration step, for example using an evolutionary strategy or a gradient based approach (Peifer and Timmer, 2007; Moles et al., 2003). But even iterative methods do not resolve the fact that only a single parameter set can be considered at a time. Consequently it is impossible to conclude that the best parameter values were found, or that no good solution exists, i.e. that the considered model is inconsistent with the collected experimental data. In fact, the procedure might simply fail to obtain a good parameter estimate.

The above mentioned drawbacks arise from a point-wise checking of the parameter space, which is highly inefficient for a large number of parameters. Here we circumvent this problem by presenting a methodology that is capable of checking entire parameter regions. Instead of providing a parameter estimate, the proposed methodology provides certificates for different parameter regions by proving their inconsistency with experimental data, thus reducing the entire search space to a comparable small fraction containing good solutions (and the true parameters).

The method is based on a polynomial representation of the system dynamics in terms of sum of squares (Parillo, 2003). Such polynomial representation is not

restricted to polynomial kinetics, but also possible for general rational kinetics as they for instance appear in metabolic pathway modelling, as will be shown in Section 3.4. Based on the sum of squares representation, a relaxed semidefinite program is formulated (Boyd and Vandenberghe, 2004). As a consequence of the relaxation it can not be proven that a parameter is consistent with the data, because a solution of the relaxed problem is not necessarily a solution of the original problem. We can however prove inconsistency of entire parameter regions: If the semidefinite program is *infeasible* for a certain parameter region, then this region does *not* contain parameter values consistent with the data. Checking feasibility of the semidefinite program can be done efficiently using high quality software such as SeDuMi and YALMIP, which also provide a high level programming language for implementing the problem (Sturm, 1999; Löfberg, 2004).

First, I review the state of the art, by restricting Section 3.2 to systems with polynomial kinetics in steady state. This facilitates the communication of the main ideas. Afterwards, Sections 3.3 to 3.4 present extensions developed in the course of my PhD studies, with the main contribution being the relaxation of the steady state assumption.

3.2 Review: Steady state analysis for systems with polynomial kinetics

This chapter is based on Kuepfer et al. (2007) and addresses the problem of whether a certain parameter region is consistent with measurements of the species concentrations in steady state.

The problem can be formulated as follows

$$\begin{aligned} \textbf{P1}: \quad & \text{find} && c, p \\ & \text{s.t.} && Nv(c,p) = 0 \\ & && \bar{c}_i - \epsilon_i \leq c_i \leq \bar{c}_i + \epsilon_i && i = 1, \ldots, n \\ & && p_{j,\min} \leq p_j \leq p_{j,\max} && j = 1, \ldots, m \end{aligned}$$

where $\bar{c}_i$ is the measured concentration of species i, ϵ_i the corresponding measurement uncertainty and $p_{j,\min}$, $p_{j,\max}$ lower and upper bounds on the parameter defining the parameter region to analyse.

Expressing the righthand-side of the ordinary differential equations as sum of squares

Often, the reaction rates are linear (affine) in the parameters and polynomial of degree d in the concentrations. i.e. $v(c,p) \in \mathbb{R}[c,p]^{d,1}$. Let

$$\xi^T = \begin{bmatrix} 1 & p_1 & \ldots & c_1 & \ldots & c_1 c_2 & \ldots c_n^d \end{bmatrix} \tag{3.1}$$

be a vector of monomials constituting a basis for $\mathbb{R}[c,p]^{d,1}$, then the reaction rate can be written as a sum of squares (SOS)

$$v_j(c,p) = \xi V_j \xi^T, \qquad j = 1, \ldots, m,$$

where V_j is a symmetric matrix. Therewith a SOS-representation for the righthand-side of the ordinary differential equations (2.2) is given by

$$\sum_j^m N_{i,j} v_j(c,p) = \xi R_i \xi^T, \qquad i = 1,\dots,n,$$

where the symmetric matrices R_i are given by

$$R_i = \sum_j N_{ij} V_j, \qquad i = 1,\dots,n. \tag{3.2}$$

Thus the inequality constraint in Problem $P1$ can be expressed in terms of the monomial basis vector ξ as follows:

$$\xi^T R_i \xi = 0 \qquad i = 1,\dots,n, \tag{3.3}$$

where the symmetric matrices R_i are constructed according to (3.2) and ξ is a monomial basis vector as defined in (3.1).

Dependencies within polynomial basis vector

The monomial basis vector consists of linearly independent functions. Nevertheless, nonlinear couplings have to be respected. For example, let $\xi_{10} = c_1$, $\xi_{11} = c_2$ and $\xi_{15} = c_1 c_2$, then it must hold that $\xi_{10}\xi_{11} = \xi_{15}$. In analogy to the previous section, these dependencies can be expressed as SOS

$$\xi^T D_i \xi = 0, \qquad i = 1,\dots,n_d$$

where D_i is a symmetric matrix and n_d the number of nonlinear dependencies in the polynomial basis vector.

Measurements and parameter regions as constraints

Let $\mu(p,c)$ be the mapping of the parameters p and states c to basic vector of monomials, i.e.

$$\xi = \begin{bmatrix} 1 \\ \mu(p,c) \end{bmatrix}.$$

By construction, the elements of μ are monotone and therefore assume their minima and maxima for $(p_{\min}, c_{\min})$ and $(p_{\max}, c_{\max})$ respectively. The inequalities $c_{i,\min} \le c_i \le c_{i,\max}$ and $p_{j,\min} \le p_j \le p_{j,\max}$ are thus covered by

$$B\xi \ge 0, \qquad \text{with } B = \begin{bmatrix} \vdots & \vdots \\ -\mu_j(p_{\min}, c_{\min}) & e_j^T \\ \mu_j(p_{\max}, c_{\max}) & -e_j^T \\ \vdots & \vdots \end{bmatrix},$$

where e_j is the is the j-th Euclidean unit vector, i.e.

$$e_{j,i} = \begin{cases} 1 & \text{if } i = j \\ 0 & \text{otherwise.} \end{cases}$$

Relaxation to a semidefinite program

A relaxation of the original problem is now found by defining $X = \xi\xi^T$ (Parillo, 2003). The resulting non-convex constraint $\text{rank}(X) = 1$ is dropped in the semidefinite program. Several other convex constraints arising from the definition of X such as $X_{11} = 1$ and $X \succeq 0$ are still used.

$$\begin{aligned}
\textbf{RP1} \quad \text{find} \quad & X \in \mathbb{S} & \\
\text{s.t.} \quad & \text{tr}(R_i X) = 0 & i = 1, \ldots, n \\
& \text{tr}(D_i X) = 0 & i = 1, \ldots, n_d \\
& e_1^T X e_1 = 1 & \\
& BXe_1 \geq 0 & \\
& BXB^T \geq 0 & \\
& BXe_1 \succeq 0, &
\end{aligned}$$

where $e_1 = [1,\ 0,\ \ldots]^T$, n is the number of species and and n_p the number of nonlinear dependencies in the polynomial basis vector ξ.

3.3 Extension to transients

The previous section considered steady state analysis, i.e. $\dot{c} = 0$. This section extends the methodology to include dynamics, i.e. $\dot{c} \neq 0$. The approach requires the knowledge of the time derivative of the states $\dot{c}$. In principle this can be achieved by measuring $c(t)$ at at least two proximate time points and calculating $\dot{c} = \frac{c(t_2) - c(t_2)}{t_2 - t_1}$. In practice, curve-fitting techniques in which basic functions $\psi_i(t)$ with well known derivatives $\dot{\psi}_i(t)$ are fitted to the measurements, are preferable because of better accuracy and measurement noise reduction.

The problem can be formulated as follows

$$\begin{aligned}
\textbf{P2}: \quad \text{find} \quad & c, \dot{c}, p & \\
\text{s.t.} \quad & Nv(c,p) - \dot{c} = 0 & \\
& c_{i,\min} \leq c_i \leq c_{i,\max} & i = 1, \ldots, n \\
& p_{j,\min} \leq p_j \leq p_{j,\max} & j = 1, \ldots, n_p \\
& \dot{c}_{i,\min} \leq c_i \leq \dot{c}_{i,\max} & i = 1, \ldots, n
\end{aligned}$$

where $c_{i,\min}$, $c_{i,\max}$, $\dot{c}_{i,\min}$, $\dot{c}_{i,\max}$ are lower and upper bounds on the measurements of the species concentrations and their derivatives respectively, and $p_{j,\min}$, $p_{j,\max}$ are lower and upper bounds defining the parameter region which is to analyse. Similarly to Section 3.2 this section finds a relaxation of the problem to a semidefinite program using sum of squares.

Representing the ordinary differential equations as sum of squares

Recall that Section 3.2 established a sum of squares representation for the righthand-side of the differential equations

$$\dot{c}_i = \xi^T R_i \xi. \tag{3.4}$$

Using the extended version of the basis vector of monomials

$$\zeta^T = \begin{bmatrix} \xi^T & \dot{c} \end{bmatrix},$$

The equality (3.4) is equivalent to

$$\zeta^T Q_i \zeta = 0 \qquad \text{with } Q_i = \begin{bmatrix} R_i & S_i \\ S_i^T & 0 \end{bmatrix}, \qquad i = 1, \ldots, n, \tag{3.5}$$

and with the matrix R_i as in (3.2) and with the matrix S_i of dimension $\dim \xi \times n$ defined elementwise, i.e. the element k, l of S_i is

$$S_{i_{k,l}} = \begin{cases} -1/2 & \text{if } k = 1, l = i \\ 0 & \text{otherwise} \end{cases}.$$

Therewith the equality in Problem $P2$ is expressed by

$$\zeta^T Q_i \zeta = 0, \qquad i = 1, \ldots, n. \tag{3.6}$$

Measurements and parameter regions as constraints

Setting up the constraints is virtually the same as in Section 3.2. The only difference is that the mapping μ has to be extended to include $\dot{c}$, i.e.

$$(p, c, \dot{c}) \mapsto \zeta : \qquad \zeta = \begin{bmatrix} 1 \\ \mu(p, c) \\ \dot{c} \end{bmatrix}.$$

The inequalities are set up with the extended mapping

$$\nu(p, c, \dot{c}) = \begin{bmatrix} \mu(p, c) \\ \dot{c} \end{bmatrix}.$$

leading to the matrix B

$$B = \begin{bmatrix} \vdots & \vdots \\ -\nu_j(p_{\min}, c_{\min}, \dot{c}_{\min}) & e_j^T \\ \nu_j(p_{\max}, c_{\max}, \dot{c}_{\max}) & -e_j^T \\ \vdots & \vdots \end{bmatrix}, \tag{3.7}$$

covering with $B\zeta \geq 0$ the inequality constraints in Problem $P2$.

Relaxation to a semidefinite program

Based on (3.6) and (3.7), the relaxed problem in the transient case is the following semidefinite program

$$\begin{array}{lll} \textbf{RP2} \quad \text{find} & Z \in \mathbb{S} & \\ \quad \text{s.t.} & \operatorname{tr}(Q_i Z) = 0 & i = 1, \ldots, n \\ & \operatorname{tr}(D_i Z) = 0 & i = 1, \ldots, n_d \\ & e_1^T Z e_1 = 1 & \\ & BZe_1 \geq 0 & \\ & BZB^T \geq 0 & \\ & BZe_1 \succeq 0, & \end{array}$$

where the Q_i are defined in (3.5), B is defined in (3.7) and $Z \in \mathbb{S}$ is the relaxed version of $\zeta\zeta^T$ corresponding to X in Section 3.2.

Example: Simple toy model

This Section illustrates the proposed methodology using a simple toy model that has an analytical solution. This allows to validate the proposed approaches.

Consider the following system of reactions

$$S + E \rightharpoonup C + E, \qquad\qquad C \rightharpoonup S.$$

Using the law of mass action the concentrations are described by the following system of ordinary differential equations

$$\frac{d}{dt}\begin{bmatrix} c \\ e \\ s \end{bmatrix} = \begin{bmatrix} 1 & -1 \\ 0 & 0 \\ -1 & 1 \end{bmatrix} \mathbf{v}(\mathbf{c}, p), \qquad\qquad \mathbf{v}(\mathbf{c}, p) = \begin{bmatrix} \tilde{k}_1 s\, e \\ p_2 c \end{bmatrix},$$

where c, e, s are the concentrations of C, E, S respectively and k_1 and p_2 are the kinetic parameters. Using that e is constant ($\dot{e} = 0$) we can set $p_1 = k_1 e$ as a constant parameter. Further using the conservation law $s(t) + c(t) = S_0$, the system is described by a single ordinary differential equation for the concentration of C

$$\dot{c} = \begin{bmatrix} 1 & -1 \end{bmatrix} \mathbf{v}(c, p), \qquad\qquad \mathbf{v}(c, p) = \begin{bmatrix} p_1 S_0 - p_1 c \\ p_2 c \end{bmatrix}.$$

A monomial basis vector for this system is

$$\zeta = \begin{bmatrix} 1 & p_1 & p_2 & S_0 & c & \dot{c} \end{bmatrix},$$

which allows the application of the method as described in Section 3.3. However, due to the simplicity of the system we can also analyse the problem analytically as follows. By setting $\dot{c} = 0$ we can see that in steady state the parameter p_1 depends linearly on the parameter p_2 with $p_1 = \frac{\bar{c}}{S_0 - \bar{c}} p_2$, where $\bar{c}$ denotes the steady state concentration of C (see Figure 3.1). In the case of perfect measurements, this dependency is a one dimensional line in the parameter space. In the case of uncertain measurements (i.eupper and lower bounds on the measured concentration), this dependency results in a two dimensional cone in the parameter space (see Figure 3.1 for an example with 10% measurement accuracy). In the dynamic case, the concentration changes over time depending on the initial condition $c(t = 0) \neq \bar{c}$. When $\dot{c}$ is measured or estimated from measurement of c at several time points t_i, the cone of admissible parameter regions changes over time. Figure 3.1 illustrates this time dependency for $t = 0$ and $t = 1$. Since the parameters have to be consistent at all time points, only the intersection contains admissible parameter values, and in fact also the true parameter values.

Example: Lotka-Volterra model

The famous LotkaVolterra equations describe the population dynamics of two interacting species, with one being the prey, the other being a predator:

$$\begin{aligned} \dot{c}_1 &= c_1(p_1 - c_2), \\ \dot{c}_2 &= c_2(-p_2 + c_1), \end{aligned}$$

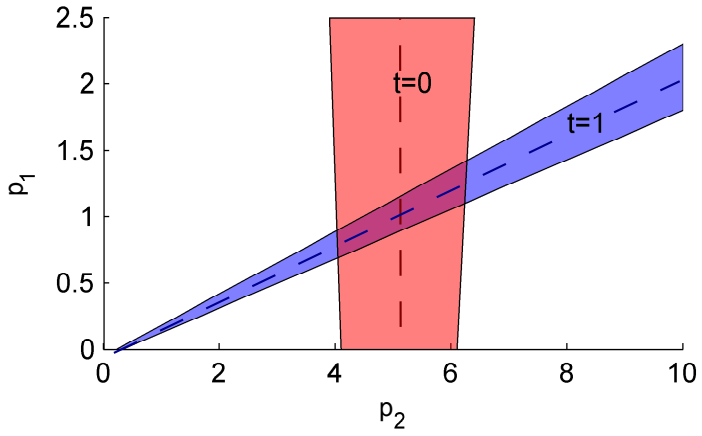

Figure 3.1: Consistent parameter regions for measurements at two different points in time. Red: for the transient at $t = 0$. Blue: in steady state ($t = 1$). The dashed lines indicate the parameter dependencies for perfect measurements. The true parameter value that generated the data is the intersection of both dashed lines. The cones represent the admissible parameter values for 10% measurement uncertainty. Only the intersection is consistent with both measurements.

where c_1 and c_2 are the concentration (e.g. number of animals per habitat) of prey and predator respectively, and p_1 and p_2 are parameters describing the birth rate of the prey and the mortality rate of the predator (Murray, 2007).

The model is used to illustrate that the proposed methodology is applicable to systems with periodic (non-steady-state) trajectories. The model was chosen because it is well studied and results obtained by the proposed methodology can thus be verified easily. The semidefinite program was constructed according to Section 3.3 with the monomial basis vector

$$\zeta = \begin{bmatrix} 1 & p_1 & p_2 & S_0 & c_1 & c_2 & \dot{c}_1 & \dot{c}_2 \end{bmatrix}.$$

Feasibility checking on a grid of parameter regions resulted in small oval-shaped parameter regions. For measurements at different time points, these regions were slightly different, such that the admissible parameter region could be reduced slightly by taking the intersection.

The two examples nicely illustrate that the methodology is applicable to measurements of transients, and that combining measurements at two or more time points significantly reduces the region of admissible parameters.

3.4 Extension to rational kinetics

The presented methodology is easily extended to systems with rational kinetics. All that is required for the relaxation to a semidefinite program as presented in the previous sections is a sum of squares representation of the system of ordinary

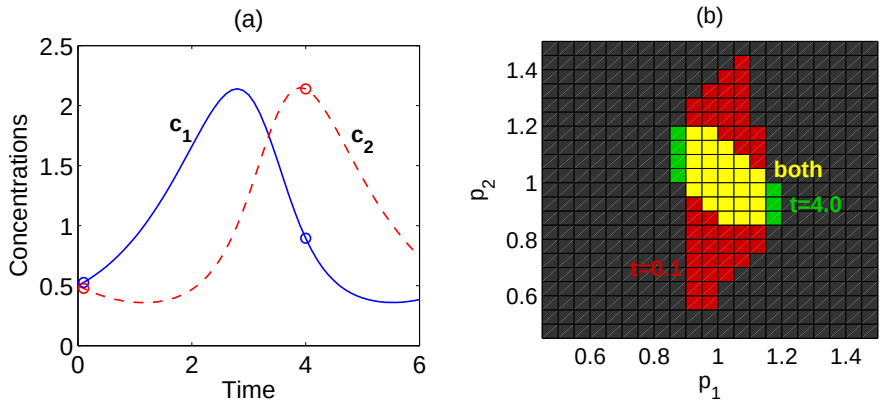

Figure 3.2: Simulation results of the Lotka-Volterra example. **(a)** Trajectories that generated the in-silico data. Circles indicate the time points where the feasibility problem was checked. **(b)** Consistent parameter regions for two different points in time. Only the intersection is consistent with both measurements. Results were obtained with 10% measurement uncertainty.

differential equations

$$\dot{c} = Nv(c,p), \qquad \text{with } v_j(c,p) = \frac{r(c,p)}{q(c,p)}, \tag{3.8}$$

where $r, q \in \mathbb{R}[c,p]$ are polynomial functions.

A polynomial representation of system (3.8) is easily obtained by multiplying left- and righthand-side of each equation with all denominators of $v(c,p)$, yielding

$$\sum_j N_{i,j} p_j(c(t_l),p) = \prod_{k\neq j} q_k(c(t_l),p) - \dot{c}_i(t_l) \prod_k q_k(c(t_l),p),$$

which can be expressed as

$$0 = f_i(z), \qquad i = 1,\ldots,n$$

where $z^T = \begin{bmatrix} p^T & c^T & \dot{c}^T \end{bmatrix}$ and $f \in \mathbb{R}[z]^{2d}$ is a multivariate polynomial. Let the degree of this polynomial be $2d < \infty$ and let ζ be a basis of $\mathbb{R}[z]^d$ consisting of monomials, then there exists a symmetric matrix $Q \in \mathbb{S}^{d\times d}$ such that

$$f_i(z) = \zeta^T Q_i \zeta, \qquad i = 1,\ldots,n.$$

In practice, the polynomial representations is often sparse, i.e. the matrices Q_i have common zero-rows and -columns. Then these zero-rows and -columns in Q_i as well as the corresponding monomials in the basis ζ should be removed (Waldherr et al., 2008). Let $\tilde{Q}_i$ be these reduced matrices and let $\tilde{\zeta}$ be the corresponding reduced basis, then Q_i is to be used in the semidefinite programm $RP2$, and the matrices B have to be constructed according to the monotone mapping $(c,p,\dot{c}) \mapsto \tilde{\zeta}$ as described in Section 3.3.

Example using rational kinetics: Double phosphorylation cycle with Michaelis-Menten kinetics

Consider the following reaction scheme of a double phosphorylation cycle

$$K_1 \underset{v_2(P)}{\overset{v_1(R)}{\rightleftharpoons}} K_2 \underset{v_4(P)}{\overset{v_3(R)}{\rightleftharpoons}} K_3,$$

where the reaction rates follow Michaelis Menten kinetics

$$v_1 = p_1 \frac{RK_1}{P_1 + K_1}, \qquad v_3 = p_3 \frac{RK_2}{P_3 + K_2},$$
$$v_2 = p_2 \frac{PK_2}{P_2 + K_2}, \qquad v_4 = p_4 \frac{PK_3}{P_4 + K_3}.$$

Here, R and P act as enzymes for the phosphorylation and dephosphorylation process respectively. We can consider the concentration of R as an input, allowing us to stimulate the system, whereas we assume for simplicity that P is constant with $P = 1$. Using the conserved moiety $K_1 + K_2 + K_3 = K_0 = 1$ the resulting system of ordinary differential equations is

$$\dot{K}_1 = -p_1 \frac{RK_1}{P_1 + K_1} + p_2 \frac{R(1 - K_1 - K_3)}{P_2 + (1 - K_1 - K_3)}, \tag{3.9a}$$
$$\dot{K}_3 = p_3 \frac{(1 - K_1 - K_3)}{P_3 + (1 - K_1 - K_3)} - p_4 \frac{K_3}{P_4 + K_3}. \tag{3.9b}$$

If both states are measured, i.e. $y = \begin{bmatrix} K_1 & K_2 \end{bmatrix}^T$, the estimation of the parameters in v_1 and v_3 is decoupled from the estimation of the parameters in v_2 and v_4. In the following we focus on estimation of the parameters in v_1 and v_2. We bring (3.9a) into polynomial form and substitute $K_1 = y_1, \dot{K}_1 = \dot{y}_1, K_3 = y_3$:

$$\begin{aligned} P_2 y_1 \dot{y}_1 + P_2 y_1 R + P_2 \dot{y}_1 P_1 - y_1^2 \dot{y}_1 - y_1^2 R - y_1 \dot{y}_1 y_2 - y_1 \dot{y}_1 P_1 - y_1 y_2 R - \dots \\ \dot{y}_1 y_2 P_1 + y_1^2 + y_1 \dot{y}_1 + y_1 y_2 + y_1 P_1 + y_1 R + \dot{y}_1 P_1 + y_2 P_1 - y_1 - P_1 = 0. \end{aligned} \tag{3.10}$$

Figure 3.3 shows a simulated time course of the system in response to a step input ($R = 1$) and the corresponding parameter dependencies in (3.10). Although generally nonlinear, the parameter dependencies are linear in steady state (because (3.10) is affine in the parameters for $\dot{y}_1 = 0$).

3.5 Extension to partial state / output measurements

One of the drawbacks of the sdp approaches described so far is that all states have to be measured. Such a scenario is rather unrealistic for real biological problems. In general, only some of the states, or even a function of the states, can be measured. Mathematically, we can take this fact into account by introducing an output function describing the relation of states and measurement. To that purpose, this section considers systems of the form

$$\dot{c} = f(c, p), \qquad y = h(c, p),$$

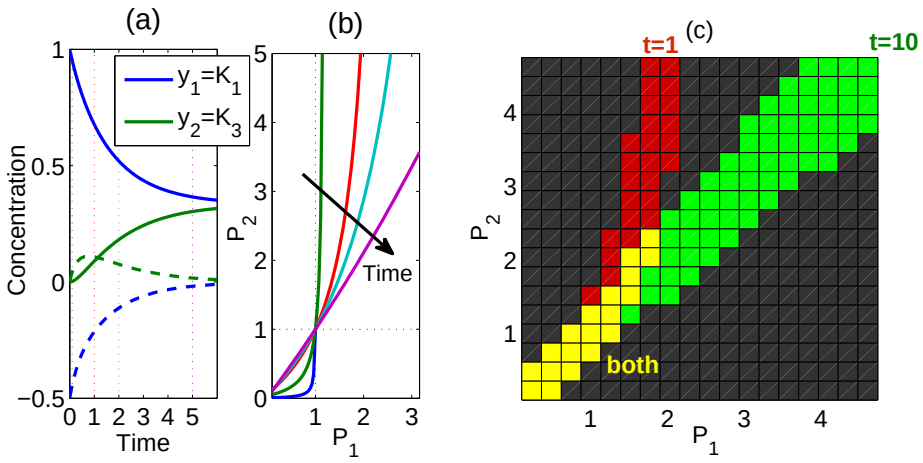

Figure 3.3: Rational kinetics: Double phosphorylation cycle with Michaelis-Menten kinetics. **(a)** System response to a step input. Solid lines show concentrations of unphosphorylated kinase K_1 and double phosphorylated kinase K_3, dashed lines their respective time derivatives. Dotted lines indicate the time-points where the parameter dependencies (3.10) where evaluated. **(b)** Parameter-dependencies between the two Michaelis Menten constants P_1 and P_2 as given by (3.10) for different time-points. Dotted lines indicate the true parameter values. The dependencies are linear in steady state. **(c)** Consistent/inconsistent parameter regions obtained via semidefinite programming with a relative uncertainty of $\pm 10\%$.

where $f = Nv(c,p)$ contains the reaction kinetics and stoichiometry and $h(c,p)$ is the output function describing the measurement.

What we need to do in order to set up a sdp as described in the previous sections is to reconstruct the states c from the measurements y and their derivatives:.

$$\begin{aligned} y &= h(c,p), \\ \dot{y} &= \frac{\partial h}{\partial c} f(c,p), \\ &\vdots \end{aligned}$$

3.5.1 Simple extension using only the differential equations

In the simplest case, we can reconstruct the unmeasured states only using the differential equations themselves, i.e. only using the first output derivative $\dot{y}$. A necessary condition for this to work is that at least half the states are measured. Consider the following system

$$\begin{bmatrix} \dot{c}_1 \\ \dot{c}_2 \end{bmatrix} = \begin{bmatrix} f_1(c_1, c_2, p) \\ f_2(c_1, c_2, p) \end{bmatrix} \qquad y = \begin{bmatrix} I & 0 \end{bmatrix} \begin{bmatrix} c_1 \\ c_2 \end{bmatrix},$$

where, without loss of generality, c_1 denotes the measured and c_2 the unmeasured states. Therewith the output derivative is simply $L_f h = f_1$. If the mapping $f_1 : c_2 \mapsto y$ is injective, there exists a dissection with

$$\begin{bmatrix}\dot{y}_1\\ \dot{y}_2\end{bmatrix} = \begin{bmatrix}f_{11}(c_1, c_2, p)\\ f_{12}(c_1, c_2, p)\end{bmatrix} \qquad \text{where } \begin{bmatrix}y_1\\ y_2\end{bmatrix} = y,\ \begin{bmatrix}f_{11}\\ f_{12}\end{bmatrix} = f_1,$$

such that $f_{11} : c_2 \mapsto \dot{y}_1$ is invertible. Substituting the partial state estimate $c_1 = y$ into this invertible part and solving for the unmeasured states gives

$$\begin{aligned} c_1 &= y \\ c_2 &= f_{11}^{-1}(y, \dot{y}_1, p). \end{aligned}$$

Finally, substituting the above solution into the second part of the dissection f_{12} gives the parameter conditions

$$\dot{y}_2 \overset{!}{=} f_{12}(y, f_{11}^{-1}(y, \dot{y}_1, p), p). \tag{3.11}$$

If (3.11) is at least rational, it can be brought into polynomial form by multiplying through with the denominator. Let $\pi_{\text{num},i}$ and $\pi_{\text{den},i}$ be the numerator and denominator of the components of $f_{12}(y, f_{11}^{-1}(y, \dot{y}_1, p), p)$ respectively, then (3.11) is with $z^T = \left[y^T, \dot{y}^T, p^T\right]$ for nonvanishing denominators equivalent to

$$\pi_{\text{den},i} - \dot{y}_{2,i}\pi_{\text{num},i} =: \pi_i(z) = 0,$$

where $\pi_i \in \mathcal{R}[z]^{2d}$ is a multivariate polynomial of degree $2d \leq \infty$. Let ζ be a basis of $\mathcal{R}[z]^{2d}$ consisting of monomials, then there exists a symmetric matrix $Q \in \mathcal{S}^{d\times d}$ such that

$$\pi_i(z) = \zeta^T Q_i \zeta = 0,$$

which can be used to set up the sdp as described earlier.

Sufficient conditions for the existence of a sums of squares representation

The question whether the parameter condition (3.11) can be brought into polynomial form depends on f_{11}. Clearly, a sufficient condition is that f_{11}^{-1} is rational. Therewith we can formulate the following theorem.

Lemma 3.1 If f_{11} is affine in the unmeasured states c_2, i.e. it can be written as $f_{11} = A(c_1, p)c_2 + b(c_1, p)$ then the parameter condition (3.11) is rational and can be written as a sum of squares $\zeta^T Q \zeta = 0$. ∎

Proof. Because $v(c, p)$ is rational, $b(c_1, p)$, $A(c_1, p)$ and therewith $A^{-1}(c_1, p)$ are rational. Consequently $c_2 = A^{-1}(c_1, p) \cdot (\dot{c}_1 - b(c_1, p))$ is rational. ∎

The following theorem establishes the connection to the stoichiometry for mass action systems and provides a sufficient condition in terms of the stoichiometry.

Theorem 3.1 Consider mass action systems and assume that at most one unmeasured species occurs in each reaction. Further assume that all reactions orders with respect to the unmeasured states are one, i.e. the corresponding stoichiometric coefficient is one. Then the parameter condition (3.11) is rational and can be written as a sum of squares $\zeta^T Q \zeta = 0$. ■

Proof . The proof follows directly from Lemma 3.1. To see this, note that with the above assumptions the reaction rates are affine in the unmeasured states c_2. ■

Note that the above theorem is also valid for reduced mass action systems. Often, mass action systems are described with a reduced set of differential equations using conserved moieties. Conserved moieties arise from dependencies in the stoichiometric matrix $N_{\text{dep}} = L_0 N_{\text{indep}}$ resulting in the state dependencies

$$c_{\text{dep}}(t) = L_0 c_{\text{indep}}(t) + c_{\text{dep}}(0) - L_0 c_{\text{indep}}(0).$$

Substituting the above state dependencies back into the differential equations gives the reduced system. Because the differential equations are affine in c_2 and the state dependencies are affine, the reduced system is affine in c_2 and we can apply Lemma 3.1.

Remark Because the procedure does not use the differential equations of the unmeasured states f_2, no information can be obtained about parameters only occurring in f_2. ■

Example partial state measurement using only the differential equations: Phosphorylation cycle

Consider the following phosphorylation/dephosphorylation cycle

$$K_1 + R \underset{v_2}{\overset{v_1}{\rightleftharpoons}} K_2 \xrightarrow{v_3} K_3 + R,$$
$$K_3 + P \underset{v_5}{\overset{v_4}{\rightleftharpoons}} K_4 \xrightarrow{v_6} K_1 + P,$$

where the reaction rates follow mass action kinetics

$$v_1 = p_1 R K_1, \qquad v_2 = p_2 K_2, \qquad v_3 = p_3 K_2,$$
$$v_4 = P K_3, \qquad v_5 = p_2 K_4, \qquad v_6 = p_3 K_4.$$

Here, R and P act as enzymes for the phosphorylation and dephosphorylation process respectively. The conserved moieties $K_1 + K_2 + K_3 + K_4 = K_0 = 1$, $P + K_4 = P_0 = 1$ and $R + K_2 = R_0$ allow us eliminate the states K_4, R and P. We can consider the concentration of R_0 as an input, allowing us to stimulate the system, whereas we assume for simplicity that P_0 is constant with $P_0 = 1$. The resulting system of ordinary differential equations is

$$\dot{K}_1 = -p_1(1 - K_2)K_1 + p_2 K_2 + p_3(1 - K_1 - K_2 - K_3), \tag{3.12a}$$
$$\dot{K}_2 = p_1(1 - K_2)K_1 - p_2 K_2 - p_3 K_2, \tag{3.12b}$$
$$\dot{K}_3 = p_3 K_2 - (K_1 + K_2 + K_3)K_3 + p_2(1 - K_1 - K_2 - K_3). \tag{3.12c}$$

Measuring the unphosphorylated and phosphorylated kinase $y_1 = K_1$ and $y_2 = K_3$, allows to solve (3.12a) for the unmeasured state

$$K_2 = \frac{p_1 y_1 + \dot{y}_1 - p_3 + p_3 y_1 + p_3 y_2}{p_2 - p_3 + p_1 y_1}.$$

Substituting the solution into (3.12c) and bringing into polynomial form gives

$$\begin{aligned} &- p_2 p_1 y_2 y_1 - p_2 p_1 y_1^2 - p_1 y_2^2 y_1 - p_1 y_2 y_1^2 - p_2^2 y_2 - p_2^2 y_1 - p_2 y_2^2 - \\ &\quad p_2 y_2 y_1 - p_1 y_2 y_1 - p_1 y_1 \dot{y}_2 + p_1 y_1 p3 + y_2 p_3^2 + y_1 p_3^2 + p_2^2 - p_2 \dot{y}_1 - \\ &\qquad p_2 \dot{y}_2 - y_2 \dot{y}_1 + y_2 p_3 + \dot{y}_1 p_3 + \dot{y}_2 p_3 - p_3^2 = 0, \end{aligned}$$

which can be used to set up the semidefinite programme. Figure 3.4 shows the response of the system to a step input of R, the corresponding parameter dependencies and feasible parameter regions as obtained by sdp. For the purpose of simplicity of presentation, Fig. 3.4 assumed $p_3 = 1$, i.e.

$$\begin{aligned} &- p_2 p_1 y_2 y_1 - p_2 p_1 y_1^2 - p_1 y_2^2 y_1 - p_1 y_2 y_1^2 - p_2^2 y_2 - p_2^2 y_1 - p_2 y_2^2 - p_2 y_2 y_1 - \dots \\ &- p_1 y_2 y_1 - p_1 y_1 \dot{y}_2 + p_2^2 - p_2 \dot{y}_1 - p_2 \dot{y}_2 + p_1 y_1 - y_2 \dot{y}_1 + 2 y_2 + \dot{y}_1 + y_1 + \dot{y}_2 - 1 = 0. \end{aligned} \tag{3.13}$$

Because (3.13) is quadratic, it has two solutions when solved for either parameter in dependence of the other, e.g. $p_2(p_1) = F_1(p_1) \pm F_2(p_1)$. The solutions depend of course on the measured outputs and their derivatives $y_1(t)$, $\dot{y}_1(t)$, $y_2(t)$ and $\dot{y}_2(t)$, which change over time. This time dependence is illustrated in Figure 3.4b, which also shows that both solutions are positive for a wide range of parameters. Further the Figure shows that the time-dependent solutions intersect at the true parameter value.

Building the semidefinite programme with (3.13) and checking its feasibility over a parameter grid gives similar results. Because the sdp analyses the problem on a grid of parameter regions with size of 0.2 in each direction, the true solution is not recovered exactly. Instead we obtain a small parameter region that contains the true solution (see Fig. 3.4c).

3.5.2 General considerations using higher order Lie derivatives

Consider the system

$$\dot{c} = f(c, p) \qquad\qquad y = h(c, p),$$

where the function $h : c \mapsto y$ describes the output measurements. Its observability space is defined as

$$\mathcal{O} = \left\{ h, \quad L_f h, \quad L_f^2 h, \quad \cdots \right\},$$

where the operator L_f is the Lie derivative. If the system is observable, choosing (at least) n linearly independent functions $\Phi^T = \left[\phi_1, \quad \cdots, \quad \phi_n \right] \in \mathcal{O}$ enables us to reconstruct the states from the outputs and their time derivatives. To

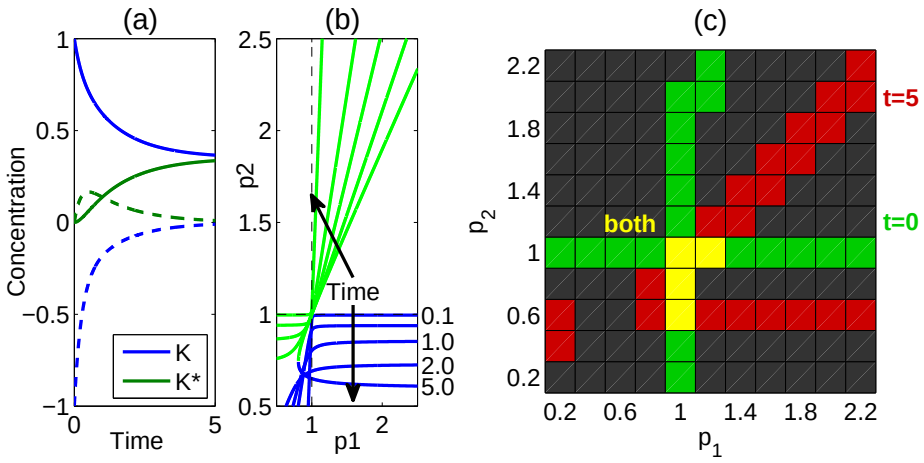

Figure 3.4: Partial state measurement using only the differential equations: Phosphorylation cycle. Unphosphorylated and phosphorylated kinase was measured $y_1 = K_1$, $y_2 = K_3$. but not the complex K_2. **(a)** Systems response to a step input of R. Concentrations of measured quantities: unphosphorylated and phosphorylated kinase (solid), and their respective time derivatives (dashed). **(b)** Parameter dependencies for measurements at different time points as given by (3.13). **(c)** Feasible parameter regions for two time points: $t = 0.1$ and $t = 5$.

that end, let $z \in \{y, \quad \dot{y}, \quad \cdots\}$ the outputs and their derivatives corresponding to the chosen mapping Φ, then inversion of Φ reconstructs the states:

$$z = \Phi(c, p) \qquad \rightarrow \qquad c = \Phi^{-1}(z, p)$$

To get information about the parameters, we derive parameter condition using (at least) one more linearly independent functions in $\mathcal{O}$. Let $\tilde{g}_j := L_f^k h_i$ be those functions, then

$$L_f^k h_i(c, p) = \tilde{g}_j(\Phi^{-1}(z, p), p) =: g_j(z, p) \stackrel{!}{=} y_i^{(k)} \tag{3.14}$$

must hold true. Because z and $y_i^{(k)}$ are known from measuring the outputs, (3.14) provides conditions for feasible parameters.

Uniform observability

Preferably, one would use successive derivatives, i.e.

$$\Phi_i = \begin{bmatrix} L_f^0 \\ \vdots \\ L_f^{k_i - 1} \end{bmatrix} h_i(c, p) \qquad \Phi = \begin{bmatrix} \Phi_1 \\ \vdots \\ \Phi_m \end{bmatrix}$$

where n is the number of states and m the number of measured outputs. If the system is uniformly observable, the observability map $\Phi(c)$ can be inverted and the parameter conditions are

$$y_i^{k_i} = L_f^{k_i} h_i \circ \Phi^{-1}(z, p),$$

where $z = \begin{bmatrix} y_1, & \cdots, & y_1^{(k_1-1)} & \cdots, & y_m^{(k_m-1)} \end{bmatrix}$.

A sufficient condition for the existence of a sums of squares representation

A sufficient condition for the parameter condition (3.14) to be rational is that the differential equations describing the system are rational in the measured and affine in the unmeasured states.

Theorem 3.2 Assume that the system is observable, and further, that it is rational in the measured states and affine in the unmeasured states, i.e. it can be written as

$$\dot{c} = \begin{bmatrix} \dot{c}_1 \\ \dot{c}_2 \end{bmatrix} = A(c_1, p)c_2 + b(c_1, p), \qquad y = c_1,$$

where $A(c_1, p)$ and $b(c_1, p)$ are a matrix and a vector with entries that are rational functions of c_1 and p. Then the parameter condition (3.14) is rational (defining a semi-algebraic variety) and can be represented by a sos $\zeta^T Q \zeta$. ■

Proof. The derivative of the output is an affine function of the unmeasured states c_2

$$\dot{y} = \dot{c}_1 = A_1(c_1, p)c_2 + b_1(c_1, p).$$

We show by induction that all output derivatives of any order are affine functions of c_2. Define

$$z_k = \begin{bmatrix} y & \dot{y} & \cdots & y^{(k)} \end{bmatrix}$$

as the vector containing the output and its derivatives up to order k.
Induction basis:

$$\dot{y} = A_1(z_0, p)c_2 + b_1(z_0, p)$$

is affine in c_2.
Induction step: Assume that the j-th derivative of the output is affine in c_2 and can be written as

$$y^{(j)} = A_{1,j}(z_j, p)c_2 + b_{1,j}(z_j, p).$$

Then

$$y^{(j+1)} = \frac{\partial A_{1,j}(z_j, p)}{\partial z_j}\dot{z}_j c_2 + \frac{\partial b_{1,j}(z_j, p)}{\partial z_j}\dot{z}_j + A_{1,j}(z_j, p)\dot{c}_2.$$

Substituting $\dot{c}_2 = A_1(z_0, p)c_2 + b_1(z_0, c_2)$ yields an affine function in c_2 that can be written as

$$y^{(j+1)} = A_{1,j+1}(z_{j+1}, p)c_2 + b_{1,j+1}(z_{j+1}, p)$$

Because the system is observable, we can pick n linearly independent functions defining an affine system of equations

$$z = \mathcal{A}(z, p)c_2 + \mathcal{B}(z, p),$$

where $z \in \{y, \quad \dot{y}, \quad \cdots\}$. Its inverse is a rational function of z

$$c_2 = \mathcal{A}(z,p)^{-1}\big(z - \mathcal{B}(z,p)\big),$$

wherewith the parameter condition is a rational function and can be brought into polynomial form by multiplying through with the denominators. ■

The above theorem established an important fact, namely that for systems that are affine in the unmeasured states, the inverse of the observability map is rational. Therewith, the parameter condition can be formulated as a sum of squares as described in the previous sections.

Example partial state measurement using higher order derivatives: Double phosphorylation cycle

Consider the following phosphorylation/dephosphorylation cycle

$$K_1 + R \xrightarrow{v_1} K_2 + R \xrightarrow{v_2} K_3 + R,$$
$$K_3 + P \xrightarrow{v_3} K_2 + P \xrightarrow{v_4} K_1 + P,$$

where the reaction rates follow mass action kinetics

$$v_1 = p_1 R K_1, \qquad v_2 = p_2 R K_2,$$
$$v_3 = p_3 P K_3, \qquad v_4 = p_4 P K_2.$$

Here, R and P act as enzymes for the phosphorylation and dephosphorylation process respectively. The conserved moiety $K_1 + K_2 + K_3 = K_0 = 1$, allow us eliminate the state K_2. We can consider the concentration of R as an input, allowing us to stimulate the system, whereas we assume for simplicity that P is constant with $P = 1$. The resulting system of ordinary differential equations is

$$\dot{K}_1 = -p_1 R K_1 + p_3 P(1 - K_1 - K_3), \tag{3.15a}$$
$$\dot{K}_3 = -p_4 P K_3 + p_2 R(1 - K_1 - K_3). \tag{3.15b}$$

Measuring the unphosphorylated and phosphorylated kinase $y_1 = K_3$ gives the observability equations

$$L_f h = -p_4 P K_3 + p_2 R(1 - K_1 - K_3) \tag{3.16a}$$
$$L_f^2 h = -p_2 R(-p_1 R K_1 + p_3 P({}_1 - K_1 - y_1)) \ldots + (-p_2 R - p_4 P)(p_2 R({}_1 - K_1 - y_1) - p_4 P y_1) + p_2({}_1 - K_1 - y_1)\dot{R}. \tag{3.16b}$$

Solving (3.16a) for the unmeasured state K_1 and substituting into (3.16b) yields the parameter dependencies, for which a semidefinite programme can be constructed as described earlier.

Figure 3.5a shows the response of the system to a step input for R. For simplicity of presentation, the two phosphorylation and dephosphorylation parameters respectively were assumed to be equal, i.e. $p_1 = p_3$ and $p_2 = p_4$. The parameter dependencies change for measurements at different time points, intersecting at the true value (Fig. 3.5b). By evaluating the sdp at different time points, we can invalidate most of the parameter space, revealing that only a small region can contain feasible parameters (Fig. 3.5c).

3.6 Critical assessment of own work

Practical applicability is an important aspect of systems identification. This section discusses some practical aspects with respect to the proposed methodology.

3.6.1 Identifiability

Identifiability asks the question whether it is in principle (theoretically) possible to estimate all unknown parameters from (noise free) experimental data. Generally, this is not an easy question to answer, and multiple approaches exist in the literature (Audoly et al., 2001; Ljung and Glad, 1994). Following the considerations of the previous sections, we can state the following theorem concerning (practical) identifiability.

Theorem 3.3 If the manifolds defined by the parameter condition (3.14) intersect in a single point only, then the system is identifiable. Further, the sole intersection point is the unique solution of the parameter estimation problem.■

Therewith, identifiability is not a necessary precondition for the presented approach. Rather, we could argue that the system is identifiable if the sdp returns only a tiny, connected parameter region. However, this is not necessarily the case: The sdp solution might be an artifact of the relaxation and the original problem might not have a solution at all.

3.6.2 Effects of noise, sampling and curve fitting

In practise, derivatives can not be measured directly. Rather they have to be estimated from measuring time courses over a certain interval. Direct calculation of derivatives using finite differences is very noise sensitive, it is therefore beneficial to employ some sort of smoothing or filtering on the raw data. Throughout this section I fitted simple exponential functions to artificially generated, noisy data using the Matlab curve fitting toolbox. I found that fitting exponential functions gives better results compared to standard regressors such as polynomials or splines. This is not surprising, considering that linear differential equations possess solutions of exponential form, but might partly be due to the fact that the here considered examples were in essence homeostasis systems in which the trajectories are relaxations from an initial condition to a steady state, or from an old steady state to a new one in response to a constant stimulus. In contrast to the exponential functions used here, splines and polynomials tend to oscillate and might therefore be better suited for fitting limit cycles or other systems with oscillatory responses.

Example: Phosphorylation cycle and curve fitting

Consider the example from Section 3.5.1. Figure 3.6 shows the time course of (3.12) to the initial condition $K_1 = 0$, $K_3 = 0$, which resemble simple first and second order exponential responses of the form

$$A(1 - \exp(-t/T_1)) + B(1 - \exp(-t/T_2)).$$

These exponential functions were fitted to artificially generated data. We generated the artificial data by drawing measurement noise from a normal distribution $y_i(t_j) = (1 + N(0, 0.1))c_i(t_j)$ at 12 logarithmically spaced sample intervals. Logarithmic spaced sampling is beneficial to uniformly spaced sampling intervals (for systems relaxing to (a new) steady state). Figure 3.6 shows the true trajectories, measurements and fitted trajectories. Because fitting noisy data does not recover the true trajectory perfectly, the parameter dependencies do not all intersect in one point (the true parameter value). For any two given time points, the p-dependencies might intersect at a different value, or even not intersect despite coming close. From a theoretical point of view, it is therefore of important to assign sufficiently large measurement uncertainty ϵ in the sdp:

$$y^{(j)}_{i,\min} = (1 - \epsilon) \cdot y^{(j)}_{i,\text{fitted}}, \tag{3.17}$$

$$y^{(j)}_{i,\max} = (1 + \epsilon) \cdot y^{(j)}_{i,\text{fitted}}, \tag{3.18}$$

From a practical point of view, the sdp is likely to be feasible even if the parameter dependencies do not intersect, depending on how much *slag* the parameter region provides. Depending on how trustworthy the measurements and the fitted trajectories are, one can solve the semidefinite programme with tighter or looser upper and lower bounds. Figure 3.6 shows that choosing looser bounds increases the feasible parameter region, but that the problem still has a solution for neglectable small uncertainty $\epsilon = 0.0001$.

3.6.3 Modularisation

Depending on what states are measured, not all parameters are correlated. We have seen in the example in Section 3.4 that the parameters p_1 and p_2 are decoupled from the parameters p_3 and p_4 (see (3.9)). In the example, the decoupling arose from the fact that all states were measured, and the differential equations of K_1 and K_2 only depends on k_1, k_2 and k_3, k_4 respectively. In general, large systems that can be decomposed into subsystems are decoupled by measuring the states linking the subsystems.

Example of modularisation: MAPK

Consider the Mitogen-activated protein kinases (MAPK) as example. As already mentioned in the introduction (Section 2.1), MAPK systems consist of phosphorylation dephosphorylation cycles layered in three stages (Fig. 6.2). MAPK systems are implemented by nature in several variations involving not only different molecules such as ERK1 (also known as MAPK3), ERK2 (also known as MAPK1), Jun N-terminal kinase (JNK) and p38 MAPK but also different feedback patterns such as inhibition of Raf phosphorylation by ERK (Kholodenko et al., 2010). Therewith MAPK system form universal modules of cell signalling networks regulating various cellular activities, such as gene expression, mitosis, differentiation, proliferation and cell survival/apoptosis (Kholodenko, 2006).

As can be seen from the graph in Fig. 6.2, Raf, MEK and ERK form three modules only coupled through their respective phosphorylated or doublephosphorylated forms. By measuring these forms, the parameters in each module can be analysed independently.

The above fact hold true independently of the reaction kinetics used. For simplicity of illustration, we restrict ourselves to mass action kinetics in the following. Then the MAPK system in Fig. 6.2 can be modelled with the following rate equations

$$v_1 = p_1 u \mathrm{K}_1 \qquad v_2 = p_2 \mathrm{K}_2, \tag{3.19a}$$
$$v_3 = p_3 \mathrm{K}_2 \mathrm{KK}_1 \qquad v_4 = p_4 \mathrm{K}_2 \mathrm{KK}_2, \tag{3.19b}$$
$$v_5 = p_5 \mathrm{KK}_3 \qquad v_6 = p_6 \mathrm{KK}_2, \tag{3.19c}$$
$$v_7 = p_7 \mathrm{KK}_3 \mathrm{KKK}_1 \qquad v_8 = p_8 \mathrm{KK}_3 \mathrm{KKK}_2, \tag{3.19d}$$
$$v_9 = p_9 \mathrm{KKK}_3 \qquad v_{10} = p_{10} \mathrm{KKK}_2. \tag{3.19e}$$

Reactions 3 to 6 and 7 to 10 are two double phosphorylation cycles as treated earlier in Section 3.5.2. Thus, by measuring $y_1 = [\mathrm{Raf_p}] = K_2$, $y_2 = [\mathrm{MEK_{pp}}] = KK_2$ and $y_3 = [\mathrm{ERK_{pp}}] = KKK_2$, we can use (3.16) to analyse the parameter identification problem.

Figure 3.8 illustrates the modularised approach. Here, the double phosphorylation model was used to identify tier two and three of the described MAPK system, with the true parameters $p_i = 1$ for phosphorylation, $p_i = 0.2$ for dephosphorylation. The identification assumed equal phosphorylation and dephosphorylation rates in each tier $p_3 = p_4$, $p_5 = p_6$, $p_7 = p_8$ and $p_9 = p_{10}$.

3.7 Perspective

This chapter presented a methodology for checking consistency of entire parameter regions with experimental data. The sum of squares decomposition enabled us to formulate the problem as a semidefinite programme that can be solved efficiently. The methodology is an extension of the steady state approach using full state measurements presented in Kuepfer et al. (2007) to transients using partial state measurements. Using transient data significantly reduces the space of feasible parameters, as biochemical systems are usually not identifiable in steady state. A particular advantage is that measuring all states is generally not required. If the system is observable, it suffices to measure only a subset of the states. In fact, observability analysis can be used to identify a set of suitable measurements.

3.7.1 Relation to barrier certificates

Similar approaches to the here presented one in the literature use the so called barrier certificates to certify parameter regions inconsistent with data and model (Anderson and Papachristodoulou, 2009). Similar to a Lyapunov function, a barrier certificate $B(x, p, t)$ is a function depending on the states, parameters and time. Given two measurements x_1, x_2 at different time points, the idea is to find a real-valued function that for some parameter region $P \ni p$ has a higher value at the second time point compared to the first time point $B(x_2, p, t_2) - B(x_1, p, t_1) > 0$ but at the same time is nonincreasing along the trajectory $\frac{\partial B}{\partial x} f + \frac{\partial B}{\partial t} \leq 0$. Such construction obviously creates a contradiction and it can be concluded that the parameter region P is inconsistent with the measurement.

The advantage of a barrier certificate is that it incorporates the righthandside of the differential equations between the measurement points. Generally this

may allow to find tighter bounds on the feasible parameter regions compared to the simple method proposed here (Sections 3.2 to 3.4) that only uses the differential equations at the measured time points.

The drawback of a barrier certificate is that it requires the construction of a polynomial function, which is computationally demanding for complicated systems. The number of decision variables required for this construction increases polynomially with the number of states. In contrast, the here presented method (Sections 3.2 to 3.4) does not require the construction of a certificate function and the number of decision variables increases only linearly with the states.

3.7.2 Relation to other approaches

Compared to other approaches in the literature the main advantages of the presented approach are

- Checking of entire parameter regions (as opposed to single, sampled points in the parameter space as in heuristic approaches)
- Generally applicable to all biochemical reaction networks (as opposed to small systems with particular, often biologically irrelevant kinetics)
- Solving or simulating the system of ordinary differential equations is not required
- Computational inexpensive (when compared to barrier certificates or heuristic sampling methods)

From an theoretical perspective the approach connects aspects of differential algebra (Lie derivatives) to semi-algebraic varieties (polynomial parameter conditions define a subdimensional manifold in the parameter space). In fact, the approach is closely related to the Ritt's algorithm, which states that every globally identifiable model structure can be rearranged to a linear regression (Ljung, 2010). The advantage of formulating the problems as semidefinite programme (as opposed to linear regression) is that identifiability in no longer required. Rather, unidentifiability is a result of the analysis, as unidentifiable parameters depend on each other.

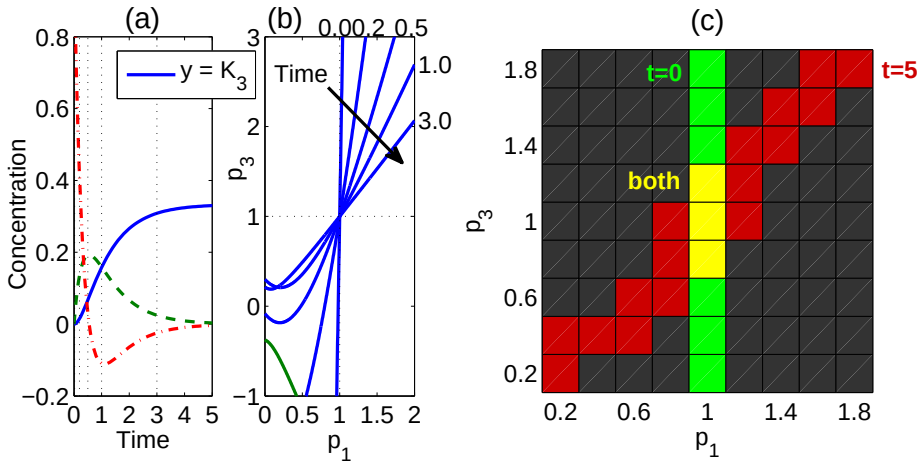

Figure 3.5: Partial state measurement using higher order Lie derivatives: Double phosphorylation cycle. Only the double phosphorylated kinase $y = K_3$ was measured. **(a)** Systems response to a step input of R. Concentrations of double phosphorylated kinase (solid), and its first (dashed) and second (dash-dotted) time derivative. **(b)** Parameter dependencies for measurements at different time points. **(c)** Feasible parameter regions for two time points: $t = 0$ and $t = 5$.

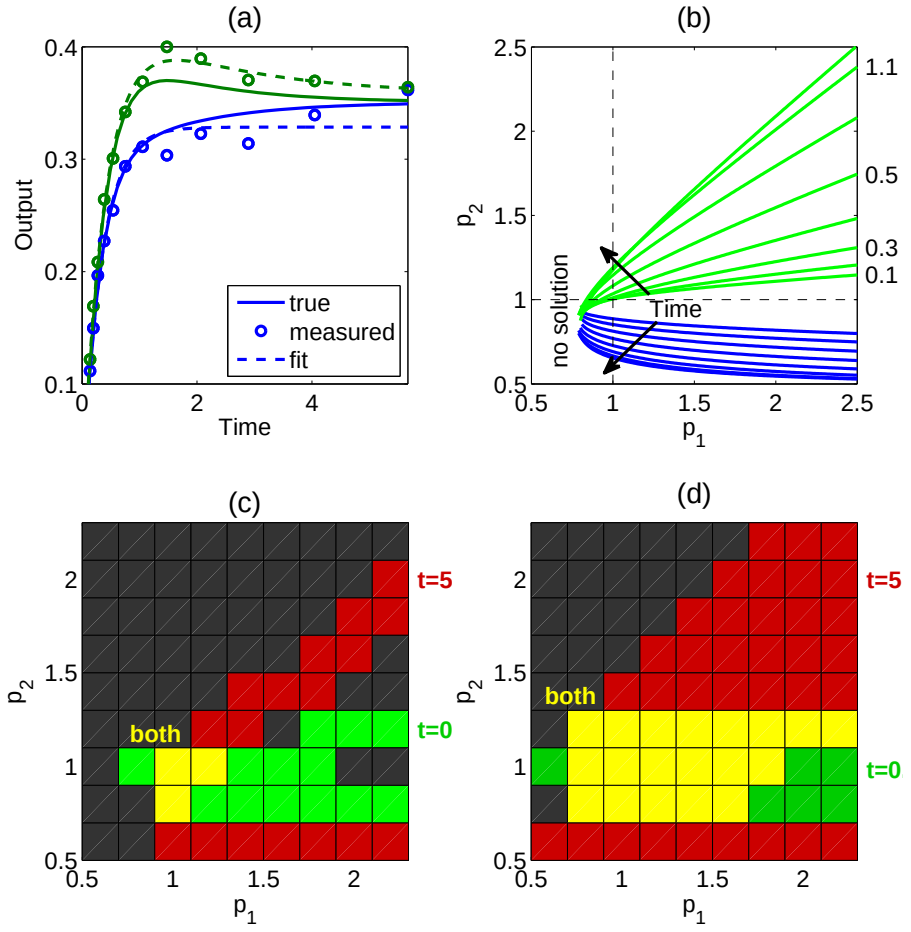

Figure 3.6: Effect of curve fitting: Phosphorylation cycle (with partial state measurement, i.e. complexes not measured) **(a)** Time course of the measured states K_1 (blue) and K_3 (green) to the initial condition $K_1 = 0$, $K_3 = 0$. Solid: True time course (simulated); Circles: Time discrete measurements corrupted with 10% Gaussian noise; Dashed: Fitted timecourse. **(b)** Parameter dependencies using the fitted timecourse. **(c)** Results sdp with 0.02% uncertainty, i.e. $\epsilon = 0.01/100$; **(d)** Results sdp with 10% uncertainty, i.e. $\epsilon = 5/100$.

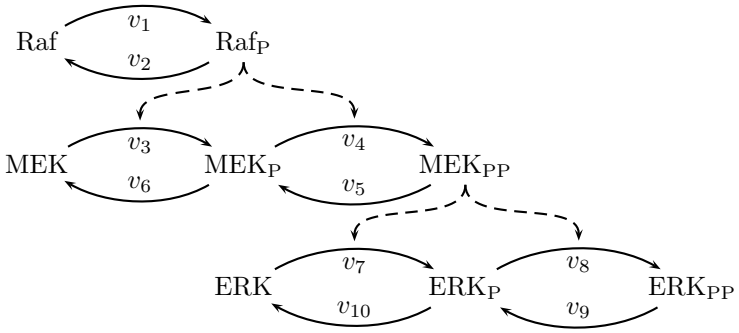

Figure 3.7: Basic structure of MAPK systems at the example of Raf-MEK-ERK.

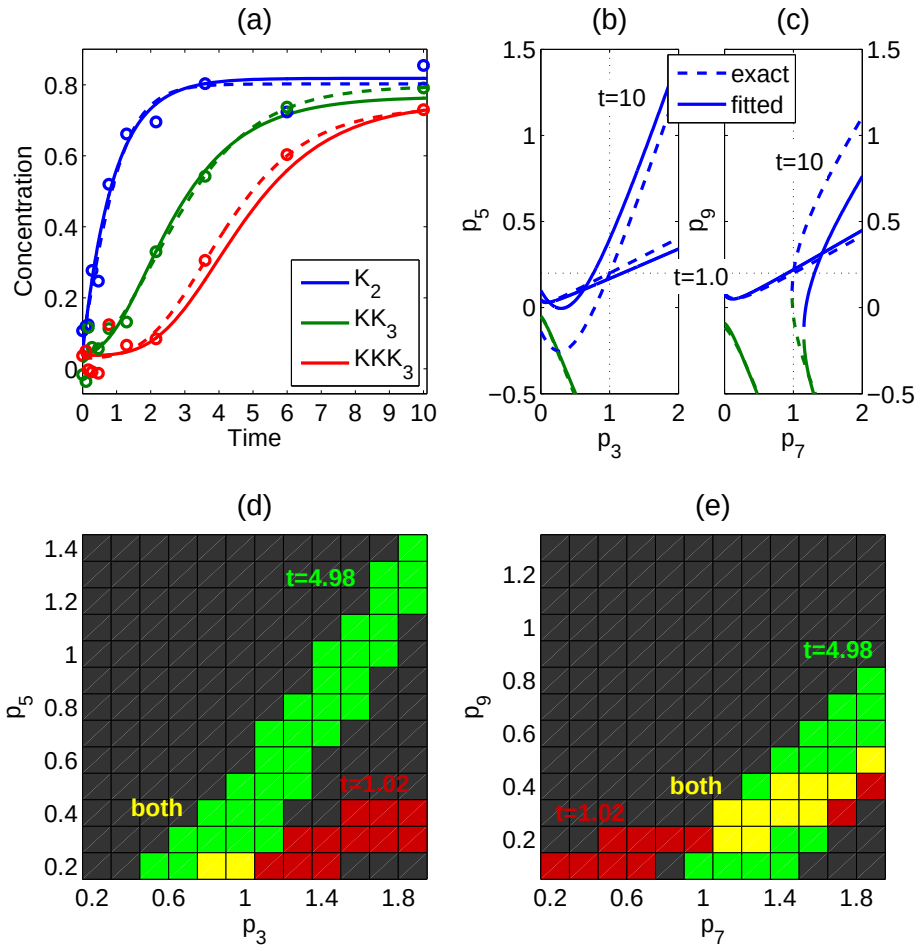

Figure 3.8: Modularisation: MAPK with mass action kinetics. **(a)** Time course of the measured states with K_2 (blue) beeing phosphorylated Raf, KK_3 (green) double phosphorylated MEK and KKK_3 (red) double phosphorylated ERK. Solid: True time course (simulated); Circles: Time discrete measurements corrupted with 10% Gaussian noise; Dashed: Fitted timecourse. **(b)** Analytical solution of the parameter dependencies for different time-points using the fitted timecourse. The identification assumed $p_3 = p_4$ and $p_5 = p_6$, $p_7 = p_8$ and $p_9 = p_{10}$. **(c)** Results of sdp for tier two, i.e. p_3 and p_5. **(d)** Results of sdp for tier two, i.e. p_7 and p_9.

Chapter 4

Parameter estimation using state space extensions and observers

4.1 Introduction and Related work

The parameter estimation problem is closely related to the state estimation problem as both consider the estimation of unknown quantities. In loose terms, an observer is a mathematical system that estimates internal, non-measured states. Observer based approaches to parameter estimation require a certain system extension. Assuming that the parameters are constant, we can formally extend the state space with the parameters, i.e.

$$\begin{bmatrix} \dot{c} \\ \dot{p} \end{bmatrix} = \begin{bmatrix} f(c,p) \\ 0 \end{bmatrix}. \tag{4.1}$$

Given the above system, an observer can achieve a combined state and parameter estimation. However, designing observers for system (4.1) carries two difficulties: parameter dependency and nonlinearity (see also Chapter 5.2). The parameter dependency triggers observability issues; for example, linearisations of (4.1) are generally not observable in steady state (Farina et al., 2006). The nonlinearity of the problem means that the observer depends on the unknown states as in contrast to linear systems there is no separation principle (Xia and Zeitz, 1997). As a consequence, global convergence for all $p \in \mathcal{R}$ can generally not be achieved (Farina et al., 2007; Dochain, 2003).

This chapter proposes an alternative to the state space extension with $\dot{p} = 0$. We can transform the system into parameter free coordinates by exploiting properties particular to biochemical reaction systems, thus facilitating the observer design. The methodology is based on Farina et al. (2006), who proposed a parameter independent system description for mass action systems. However, many biological models employ more complicated kinetics, such as Michaelis Menten and Hill kinetics (see also Section 9). This chapter generalises the transformation into parameter free coordinates to kinetics with rational terms.

4.2 Parameter-free coordinates for autonomous (closed) systems

This section proposes an state space extension that transforms the system into parameter free coordinates. The transformation takes the systems structure explicitly into account. The approach is first illustrated for a system with a single reaction, before the general extension scheme is presented.

Example Let us consider the following system with $k > 0$, $K > 0$

$$\dot{c} = -v(c), \tag{4.2a}$$

$$v(c) = k\frac{c^2}{c+K}. \tag{4.2b}$$

Assuming that c and therefore v are positive, it is possible to derive the differential equation for the relative rate of change of the reaction rate, in essence taking the logarithm and time derivative of (4.2b). Before doing that, we introduce the new state

$$M = c + K$$

with the derivative

$$\dot{M} = \dot{c}.$$

Now, taking the logarithm and time derivative of (4.2b) gives

$$\begin{aligned}\frac{\dot{v}}{v} &= \frac{d}{dt}\log v = \frac{d}{dt}\left(\log k + 2\log c - \log M\right)\\ &= 2\frac{\dot{c}}{c} - \frac{\dot{M}}{M}.\end{aligned}$$

Substituting $\dot{c} = -v$ yields an extended system

$$\begin{aligned}\dot{c} &= -v\\ \dot{M} &= -v\\ \dot{v} &= v\left(-2\frac{v}{c} + \frac{v}{M}\right)\end{aligned}$$

in which the right-hand-side is parameter free. ■

As the example illustrates, the states of the parameter free extended system consists of the concentrations c, the denominators of the reaction rates M and the reaction rates v.

In general, the approach considers reaction kinetic systems

$$\dot{c} = N(v, p)$$

allowing for fluxes of the form:

$$v_i = k_i \prod_{j=1}^{n} \frac{c_j^{\nu_{ij}}}{K_{ij}^{\eta_{ij}} + c_j^{\eta_{ij}}}, \tag{4.3}$$

where $K_{ij} > 0$, $\nu_{ij} \geq 0$ and $\eta_{ij} \geq 0$. If $\eta_{ij} = 0$, then the arbitrary parameter K_{ij} shall be equal to 1. The general formulation of (4.3) contains mass action kinetics, generalised mass action kinetics, Michaelis-Menten- and Hill-kinetics as well as their products. For example, setting $\eta_{ij} = 0$ leads to a mass action model.

For $0 < \nu_{ij} < 1$, the flux v_i is not Lipschitz in $c_j = 0$. To ensure the existence and uniqueness of solutions, we assume that all concentrations are strictly positive.

Assumption 4.1 The parameters p and the concentrations c are strictly positive along trajectories of (4.1) and bounded, i.e. $0 < \underline{\delta} \leq c_i(t, c_0) \leq \overline{\delta} < \infty$ holds for all species i and all initial conditions c_0 for some positive constants $\underline{\delta} < \overline{\delta}$.■

This condition is satisfied in many biological application, in particular for models of metabolic pathways.

To simplify the presentation, define the following matrix-valued function $M : \mathbb{R}^n_{\geq 0} \to \mathbb{R}^{m \times n}$

$$M_{ij} = K_{ij}^{\eta_{ij}} + c_j^{\eta_{ij}}. \tag{4.4}$$

As the example illustrates, the mapping

$$\Theta : \quad \begin{bmatrix} c \\ p \end{bmatrix} \mapsto \begin{bmatrix} c \\ M(c,p) \\ v(c,p) \end{bmatrix} \tag{4.5}$$

is diffeomorph if Assumption 4.1 holds, defining an smooth and bijective state-space transformation of the original system (4.1) into an equivalent extended system that is parameter free. This means, considering M_{ij} and v_i as additional states, complementing the natural states c_j, results in ordinary differential equations that do not depend on the parameters. We can state the following theorem.

Theorem 4.1 Let the concentrations be strictly positive, the flows of the form of (4.3), with known exponents ν_{ij} and η_{ij}. Then, the following two systems are equivalent:

$$\dot{c} = Nv(c,p) \tag{4.6a}$$
$$\dot{p} = 0 \tag{4.6b}$$

with

$$p = \begin{bmatrix} k_1 & \dots & k_m & K_{11} & \dots & K_{mn} \end{bmatrix}^T, \tag{4.6c}$$

and

$$\dot{c} = Nv \tag{4.7a}$$
$$\dot{M}_{ij} = \eta_{ij} c_j^{\eta_{ij}-1} e_j^T N v \tag{4.7b}$$
$$\dot{v} = \operatorname{diag}(v)\Big(\nu\big(\operatorname{diag}(c)\big)^{-1} N v - \tilde{m}\Big), \tag{4.7c}$$

where

$$\tilde{m}_i = \sum_j \frac{\eta_{ij} c_j^{\eta_{ij}-1} e_j^T N v}{M_{ij}}.$$ ■

Proof.

a) Equation (4.7a) follows directly from (4.6a).

b) The dynamic description of M is obtained by differentiation along the trajectory of (4.6) and using (4.7a)

$$\frac{d}{dt} M_{i,j} = \eta_{i,j} c_j^{\eta_{i,j}-1} \dot{c}_j = \eta_{i,j} c_j^{\eta_{i,j}-1} \sum_{k=1}^{n_r} N_{i,k} v_k.$$

c) We multiply both sides of (4.3) with the denominator and take the logarithm

$$\sum\nolimits_{j=1}^{n_c} \log\left(K_{i,j}^{\eta_{i,j}} + c_j^{\eta_{i,j}}\right) + \log\left(r_i\right) \;=\; \log\left(\hat{r}_i\right) + \sum\nolimits_{j=1}^{n_c} \nu_{i,j} \log\left(c_j\right).$$

Again taking the time derivative and using (4.4) yields

$$\sum_{j=1}^{n_c} \frac{\dot{M}_{i,j}}{M_{i,j}} + \frac{\dot{r}_i}{r_i} = \sum_{j=1}^{n_c} \nu_{i,j} \frac{\dot{c}_j}{c_j}.$$

Rearranging gives

$$\dot{r}_i = r_i \left(\sum_{j=1}^{n_c} \nu_{i,j} \frac{\dot{c}_j}{c_j} - \sum_{j=1}^{n_c} \frac{\dot{M}_{i,j}}{M_{i,j}} \right).$$

Finally, Substituting $\dot{c}_j$ and $\dot{M}_{i,j}$ using (4.7a) and (4.7b) respectively yields the differential equations for the reaction rates (4.7c). ■

If some parameters values are already known, the proposed methodology can be adjusted in a straightforward way to not estimate them again. There are basically two cases. First, the parameter is a Hill or Michaelis-Menten constant K_{ij}. Then, there exists a state M_{ij}, which depends on K_{ij} and on some concentrations. This state can therefore be expressed as an algebraic equation of other states and does not require a differential equation. In the second case, the parameter is proportional to a flow, i.e. k_i in a flow v_j. This flow then also contains no unknown, only other states and thus its differential equation can be replaced by an algebraic equation. The reduced extended system is a differential algebraic system of index one. The algebraic equations can easily be eliminated, thus reducing the state space dimension by the number of known parameters.

Summarising, any biochemical reaction model consisting of flows modelled as in (4.3) can be transformed into a system that is free of parameters. This

system has an extended state vector and depends only on structural properties of the original system.

The extended state is denoted by $x \in \mathbb{R}^{n_x}_{>0}$

$$x = \begin{bmatrix} c \\ m \\ v \end{bmatrix}, \tag{4.8}$$

where m is the vector of all non-zero entries of

$$\operatorname{vect} M = \begin{bmatrix} M_{11} & \cdots & M_{m1} & M_{12} & \cdots & M_{mn} \end{bmatrix}^T,$$

and the extended system by

$$\dot{x} = f(x) \tag{4.9a}$$
$$y = h(x). \tag{4.9b}$$

To simplify the observer design, we introduce the assumption that the output is a subset of the concentrations and flows. This is the case in many biological applications.

Assumption 4.2 The output $y(t) \in \mathbb{R}^{n_y}$ is a subset of the concentrations c and the flows v, i.e.

$$y = h\left(\begin{bmatrix} c \\ m \\ v \end{bmatrix}\right) = \begin{bmatrix} H_c & 0 & 0 \\ 0 & 0 & H_v \end{bmatrix} \begin{bmatrix} c \\ m \\ v \end{bmatrix}, \tag{4.10}$$

where the columns of H_c and of H_v are a subset of the columns of the corresponding identity matrices. ■

4.2.1 Parameter independent form with inputs

The scheme can easily extended to include inputs. Then, the original system writes as

$$\dot{c} = Nv(c, p, u_c) + N_u u_v,$$

with the reaction kinetics

$$v_i = k_i \prod_j \frac{c_j^{\nu_{ij}} u_c^{\nu_{u,ij}}}{M_{ij}} \qquad \text{where} \qquad M_{ij} = c_j^{\eta_{ij}} + M_{ij},$$

and where u_c and u_v are inputs representing concentrations and fluxes respectively. Although the mapping (4.5) is now input dependent, it still transforms the system into extended coordinates (parameter free coordinates) in exactly the same manner. The corresponding extended system is

$$\dot{c} = Nv + N_u u_v, \tag{4.11a}$$
$$\dot{M}_{ij} = \eta_{ij} c_j^{\eta_{ij}-1} e_j^T (Nv + N_u u_v), \tag{4.11b}$$
$$\dot{v} = \operatorname{diag}(v)\left(\nu\big(\operatorname{diag}(c)\big)^{-1}(Nv + N_u u_v) + \nu_u\big(\operatorname{diag}(u_c)\big)^{-1}\dot{u}_c - \tilde{m}\right), \tag{4.11c}$$

where

$$\tilde{m}_i = \sum_j \frac{\eta_{ij} c_j^{\eta_{ij}-1} e_j^T (Nv + N_u u_v)}{M_{ij}}.$$

Assuming that the possibly time dependent inputs $u_c = u_c(t)$ are differentiable, the dependence of the extended system on time derivatives of u_c does not pose a problem. We can define $u^T = \begin{bmatrix} u_v^T & u_c^T & \dot{u}_c^T \end{bmatrix}$ and write the system compactly as

$$\dot{x} = f(x, u) \tag{4.12a}$$
$$y = h(x). \tag{4.12b}$$

Remark Step and pulse inputs can be handled either using a differentiable approximation in the form of steep sigmoidal functions e.g. $u_c = A_0(1+\tanh(t-T_0))$ or by changing the initial condition accordingly and setting $\dot{u}_c = 0$. ■

4.3 Proposed parameter estimation scheme

Based on the parameter free systems description we can propose the following parameter estimation scheme

1. Transformation of the system of ordinary differential equations into a parameter independent form;
2. Estimation of all states in the parameter free coordinates using an observer;
3. Back transformation to obtain the paraments.

Step one is an alternative to the classical extention by $\dot{p} = 0$ and transforms the parameter estimation problem into a state estimation problem. The extended states can be estimated using a suitable observer (step two). Step three is the back transformation into original coordinates, which gives the actual parameter estimate. Inversion of (4.5) yields an explicit expression. In particular, using (4.4), the parameters $K_{ij}(t)$ can be estimated via

$$\hat{K}_{ij}(t) = \begin{cases} \left(\hat{M}_{ij}(t) - \hat{c}_j(t)\right)^{1/\eta_{ij}} & \text{for } \eta_{ij} > 0, \\ 1 & \text{for } \eta_{ij} = 0. \end{cases} \tag{4.13a}$$

Finally, the estimation of the parameters $k_i(t)$ is possible using (4.3)

$$\hat{k}_i(t) = \hat{v}_i(t) \prod_j^{n_c} \frac{\hat{M}_{ij}(t)}{\hat{c}_j(t)^{\nu_{ij}}} \tag{4.13b}$$

in the input free case, and

$$\hat{k}_i(t) = \hat{v}_i(t) \prod_j^{n_c} \frac{\hat{M}_{ij}(t)}{\hat{c}_j(t)^{\nu_{ij}} u_c(t)^{\nu_{u,ij}}} \tag{4.13c}$$

in the input case.

Because the observer has to be initialised with an unknown initial condition, the parameter estimate is time dependent. It converges to the true, constant values if and only if the observer converges.

4.4 Perspective

This chapter presented the transformation in step one as an alternative to the classical state space extension $\dot{p} = 0$. The transformation explicitly takes into account the particular nonlinearities of biological systems. The main advantage of the transformation is that the right hand sides of the resulting ordinary differential equations (4.7) and (4.11) do not depend on the parameters, but only on the stoichiometry and the states. The parameters are hidden in the initial conditions as $x_0 = \Phi(c_0, p)$. A further advantage of the transformed system is that the measurements are often a subset of the coordinates c and v as fluxes can for example be measured using ${}_{13}$C labelling (Costenoble et al., 2007). This simple output function also helps in the observer design, which is discussed in the following two chapters.

Chapter 5

Design of a normal form observer

5.1 Introduction

The parameter-free system (4.7) simplifies the design of an observer as the system does not contain any unknown parameters in the right-hand side. The estimation of the parameters of the original system requires the estimation of the extended state vector of the transformed system. Systems theory uses so called observers, which are mathematical systems often consisting of an (approximated) copy of the true system and and feedback injection of the predicted output error. Concretely, let

$$\dot{x} = f(x), \qquad y = h(x)$$

be the extended system as described in Section 4.2 with unknown states x and measured output y. Then the system

$$\dot{z} = f(z) + L(z)(y - h(z)),$$

is an observer if the (possibly state dependent gain) L is chosen such that the estimate converges toward the true state, i.e $z(t) \to x(t)$ for $t \to \infty$.

In the linear case, observer design is rather easy, because of the separation principle. Consider the following linear time invariant system

$$\dot{x} = Ax, \qquad y = Cx$$

and the observer

$$\dot{z} = Az + L(y - Cz),$$

then the observer error $e = x - z$ is given by

$$\begin{aligned} \dot{e} &= Ax - Az + L(Cx - Cz) \\ &= Ae - LCe = (A - LC)e. \end{aligned}$$

A main result of linear observer theory is that if the so called observability matrix

$$\begin{bmatrix} C \\ CA \\ \vdots \\ CA^{-1} \end{bmatrix}$$

has full rank, the system is called observable and we can choose L such that $A - LC$ is Hurwitz and the observer converges $z(t) \to x(t)$. This result is independent of the particular trajectory to be observed because the error dynamics do not depend on the (unknown) states of the system. This is called the separation principle.

Unfortunately, there is no separation principle in the nonlinear case. The complexity of the problem requires more advanced mathematics, in which the observer design depends on many aspects of the system to be observed. Observability and convergence can often only be proven locally or in particular cases.

5.2 Classical nonlinear observer design

The classical theory of nonlinear observers uses a nonlinear analogue to the observability matrix for linear systems, the observability map

$$\Phi(x) = \begin{bmatrix} \Phi_1(x) \\ \Phi_2(x) \\ \vdots \\ \Phi_p(x) \end{bmatrix}, \qquad \Phi_i(x) = \begin{bmatrix} \mathrm{L}_f^0 h_i(x) \\ \mathrm{L}_f^1 h_i(x) \\ \vdots \\ \mathrm{L}_f^{n_i-1} h_i(x) \end{bmatrix}, \qquad \sum_{i=1}^{p} n_i = n. \tag{5.1}$$

If the observability map is locally invertible, i.e. if

$$Q := \frac{\partial \Phi}{\partial x}$$

is nonsingular, then the system is called locally observable. We can view Q as the nonlinear analogue to the observability matrix in the linear case. If the observability map has a continous inverse, then $z = \Phi(x)$ transform the system with

$$\dot{z} = \frac{\partial \Phi}{\partial x} f \circ \Phi^{-1}(z).$$

into observability canonical coordinates. The corresponding state-space description is:

$$\begin{aligned} \dot{\xi} &= J\xi + B\phi(\xi) \\ y &= C\xi, \end{aligned} \tag{5.2}$$

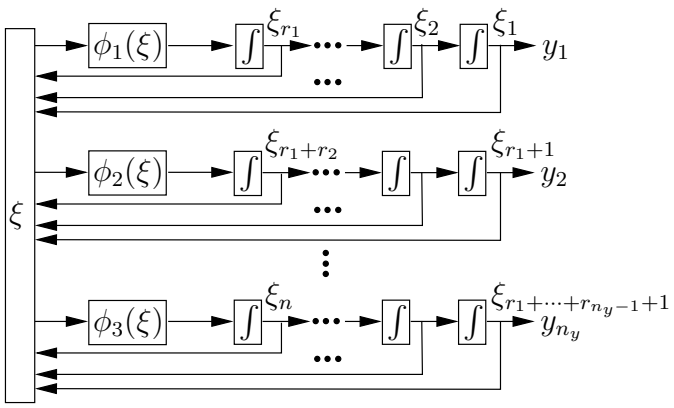

Figure 5.1: Sketch of the observer canonical form.

where

$$J = \begin{bmatrix} J_1 & & \\ & \ddots & \\ & & J_{n_y} \end{bmatrix}, \qquad J_i = \begin{bmatrix} 0 & 1 & & 0 \\ & & \ddots & \\ & & & 1 \\ 0 & \dots & \dots & 0 \end{bmatrix} \in \mathbb{R}^{r_i \times r_i},$$

$$B = \begin{bmatrix} B_1 & & \\ & \ddots & \\ & & B_{n_y} \end{bmatrix}, \qquad B_i = \begin{bmatrix} 0 & \dots & 0 & 1 \end{bmatrix}^T \in \mathbb{R}^{r_i \times 1},$$

$$C = \begin{bmatrix} C_1 & & \\ & \ddots & \\ & & C_{n_y} \end{bmatrix}, \qquad C_i = \begin{bmatrix} 1 & 0 & \dots & 0 \end{bmatrix} \in \mathbb{R}^{1 \times r_i}.$$

In observability coordinates, the states correspond to the output y and its derivatives $\dot{y}$ to $y^{(r_i)}$, and the nonlinearities are concentrated in the function $\phi(\xi)$, see Fig. 5.1. Clearly, the transformation into the observability canonical form (5.2) is only possible if $\Phi(\cdot)$ is invertible, which requires a suitable choice of outputs and the number of their derivatives. For a detailed discussion see for example Xia and Zeitz (1997) or Schaffner and Zeitz (1999).

Several methods exists to design observers for systems in observability cannonical form. Usually, they employ a simulation term $A\tilde{z} + B\phi(\tilde{z})$ (a copy of the system) and a correction term that feeds back the error of measured y and estimated output $\tilde{y} = C\tilde{z}$, and can therewith be written in the form

$$\frac{d}{dt}\tilde{z} = A\tilde{z} + B\phi(\tilde{z}) + L \cdot [y - C\tilde{z}], \tag{5.3}$$

whereby the design of the gain matrix $L \in \mathbb{R}^{n \times p}$ differs, for example using Lyapunov functions, pole placement, or high gain (Schaffner and Zeitz, 1999; Xia and Zeitz, 1997; Gauthier et al., 1992). In any case, some additional calculations are necessary to obtain the observer in original coordinates x. Differentiating

$\tilde{x} = \Phi^{-1}(\tilde{z})$ gives

$$\frac{d}{dt}\tilde{x} = \frac{\partial \Phi^{-1}}{\partial \tilde{z}} \frac{d\tilde{z}}{dt} = Q^{-1}[A\tilde{z} + B\phi(\tilde{z})] + Q^{-1}L[y - \tilde{y}]$$

Substituting $z = \Phi(x)$ gives the observer in original coordinates

$$\frac{d}{dt}\tilde{x} = f(x) + Q^{-1}(x) \cdot L(\theta) \cdot [y - h(x)]. \tag{5.4}$$

Here we used the fact that $f = Q^{-1}\bar{f} \circ \Phi$ where $\bar{f}(\tilde{z}) = A\tilde{z} + B\phi(\tilde{z})$.

From the above considerations, it is clear that the observer only exists if Q^{-1} exists, i.e. if the system is locally observable. If some points on the trajectory are not locally observable, the observers fails. Vargas et al. (2003) proposed a modification to resolve this issue, in terms of an event based observer. An event is a connected set of time points along a trajectory where the inversion of Q is numerically ill conditioned:

$$T_{\text{Event}} = \{t \in \mathbb{R} : \quad \left|\frac{\lambda_{\min}}{\lambda_{\max}}\right| < \delta\}$$

where $\lambda_{\min}$ and $\lambda_{\max}$ are the absolute smallest and largest eigenvalue of $Q(x(t, x_0))$ respectively, and $\delta > 0$ is some predefined value. During such an event, Q is close to singular, the inversion of Q is numerically infeasible and the correction term in (5.4) gets very large. A solution that enables to simulate (5.4) despite the ill-conditioned Q is to switch the correction term $Q^{-1}(x)L(\theta)$ in (5.4) to zero for the time of the event T_{event}. Therewith, the event based observer is given by

$$\frac{d}{dt}\tilde{z} = A\tilde{z} + B\phi(\tilde{z}) + Q^{inv}(\tilde{z}) \cdot L(\theta) \cdot [y - h(\tilde{z})],$$

whereby

$$Q^{inv} = \begin{cases} Q^{-1} & \text{if } \left|\frac{\lambda_{\min}}{\lambda_{\max}}\right| \geq \delta, \\ 0 & \text{if } \left|\frac{\lambda_{\min}}{\lambda_{\max}}\right| < \delta. \end{cases} \tag{5.5}$$

Unfortunately, global observability can not be guaranteed for the event based observer, i.e. there are initial conditions for which the observer fails to give an accurate estimate (see Fig. 5.3). Here, the system is not locally observable in steady state and the correction term is set to zero according to (5.5), thus trapping the observer in the steady state.

Farina et al. (2006) demonstrated that the parameters of biochemical reaction systems are usually not locally observable in steady state (unless reaction rates are measured). Together with the above results, this renders classical and event based observers unsuitable for parameter estimation.

5.3 Design of an approximative observer

Approximative observer design is an approach to estimate the states of a system in cases where local observability can not be guaranteed (Vargas and Moreno,

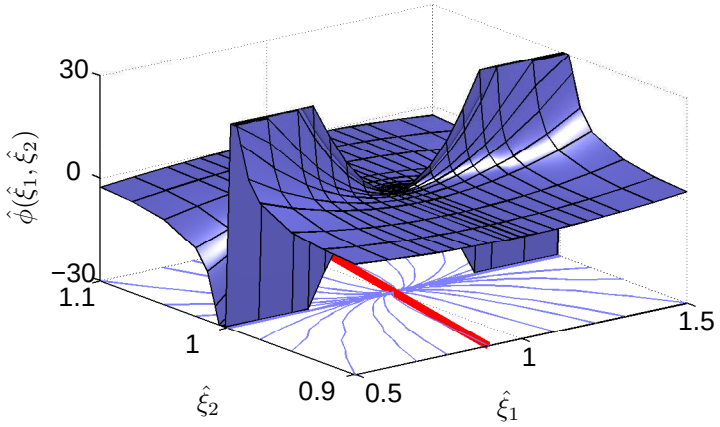

Figure 5.2: Illustration of an approximation $\hat{\phi}(\cdot)$ of the discontinuous function $\phi(\hat{\xi}_1, \hat{\xi}_2) = -\frac{(\hat{\xi}_1-1)^2}{\hat{\xi}_2-1}$. The approximation $\hat{\phi}(\cdot)$ is equal to $\phi(\cdot)$ on $\hat{\xi}_1 = \hat{\xi}_2$ (the thick red line in the contour plot) and globally bounded (with magnitude 30).

2005). As discussed in the previous section, local observability is a prerequisite for classical observer design that is often violated for biochemical reaction systems. When the systems is not locally observable everywhere, Q^{-1} is singular for some time point(s) causing singularities in the observer (see Section 5.2). The problem can be avoided by observing in observability coordinates directly. Then the observer consists of a dynamic part in observability coordinates and an algebraic part

$$\begin{aligned} \frac{d}{dt}\tilde{z} &= A\tilde{z} + B\phi(\tilde{z}) + L(\theta)\cdot[y - C\tilde{z}], \\ \tilde{x} &= \Phi^{-1}(\tilde{z}). \end{aligned} \tag{5.6}$$

Clearly, such an observer only exists if $\Phi(\cdot)$ is invertible. Further, because $\frac{\partial \Phi}{\partial x}$ is not invertible everywhere, $\phi(\cdot)$ might not Lipschitz and the system in observability coordinates might have several solutions. Then the observer requires continous extensions of the characteristic nonlinearity $\phi(\cdot)$ (Vargas and Moreno, 2005).

In the context of the biochemical reaction systems considered here, we can resolve this problem by bounding the nonlinearity of the observer such that no error on the true trajectory is introduced. This is illustrated in Fig. 5.2 where the true trajectory corresponds to $\hat{\xi}_1 = \hat{\xi}_2$.

The next theorem discusses the properties of an observer based on the one proposed by Vargas and Moreno (2005). This is a high-gain observer whose states converge with arbitrary precision to the states of the system in observability canonical form.

Theorem 5.1 Choose coefficients $l_j^{(i)}$ in such a way that $s^{r_i} + \sum l_j^{(i)} s^j$ is a Hurwitz polynomial, or equivalently, that $J - LC$ with $L_i = \begin{bmatrix} l_{r_i-1}^{(i)} & \dots & l_0^{(i)} \end{bmatrix}$ is a Hurwitz matrix and a bounded approximation $\hat{\phi}(\cdot)$ such that $\hat{\phi}(\xi) = \phi(\xi)$

on the true trajectory $\xi(t, \xi_0)$. Then, for any $\epsilon > 0$ there exists a $\theta > 0$ such that the observer

$$\begin{aligned}
\dot{\hat{\xi}} &= J\hat{\xi} + B\hat{\phi}(\hat{\xi}) + \Theta L(y - C\hat{\xi}) \\
\hat{x} &= \Phi^{-1}(\hat{\xi}) \\
\Theta &= \begin{bmatrix} \Theta_1 & & \\ & \ddots & \\ & & \Theta_{n_y} \end{bmatrix}, \qquad L = \begin{bmatrix} L_1 & & \\ & \ddots & \\ & & L_{n_y} \end{bmatrix}, \\
\Theta_i &= \operatorname{diag}\begin{bmatrix} \theta & \dots & \theta^{r_i} \end{bmatrix},
\end{aligned}$$

estimates the state ξ with ϵ precision in finite time. In other words, there exists a $T \geq 0$ such that

$$\|\hat{\xi}(t) - \xi(t)\| \leq \epsilon \qquad \text{for all } t \geq T. \qquad \blacksquare$$

Proof . Following Vargas and Moreno (2005), we have to show that $\hat{\phi}$ is a continuous extension of ϕ. Considering the rational form of the reaction kinetics and the extended system, it is clear that all Lie derivatives $L_f^i h(x)$ are rational functions. Further, using Assumption 4.1 we see that the denominators do not vanish and that $L_f^i h(x)$ are continuous and bounded. In particular the characteristic nonlinearities $\phi_i = L_f^{r_i} h_i$ is continuous and bounded on the true trajectory, i.e. there are constants Ω_i such that $-\Omega_i \leq \phi_i(x(t)) \leq \Omega_i$ and we can define $\hat{\phi}_i(x) = \operatorname{sign}(\phi_i(x)) \max(\phi_i(x), \Omega_i)$.

$$\hat{\phi}_i(x) = \begin{cases} \Omega_i \operatorname{sign}(\phi_i(x)) & \text{if } |\phi_i(x)| > \Omega_i \\ \phi_i(x) & \text{else} \end{cases}. \qquad \blacksquare$$

The high gain parameter θ can be used to tune the speed of convergence. However, θ also amplifies the noise in the data and should thus not be chosen too high.

The observer coordinates can be transformed back into the coordinates of the original system with the help of the inverse of the observability map Φ^{-1}.

$$\hat{x} = \Phi^{-1}(\hat{\xi}) \tag{5.8a}$$

For each time point t, $\hat{x}(t)$ can be calculated, directly leading to estimates of the concentrations $\hat{c}$. Using (4.4), the parameters $K_{ij}(t)$ can be estimated via

$$\hat{K}_{ij}(t) = \begin{cases} \left(\hat{M}_{ij}(t) - \hat{c}_j(t)\right)^{1/\eta_{ij}} & \text{for } \eta_{ij} > 0, \\ 1 & \text{for } \eta_{ij} = 0. \end{cases} \tag{5.8b}$$

Finally, the estimation of the parameters $k_i(t)$ is possible using (4.3)

$$\hat{k}_i(t) = \hat{v}_i(t) \prod_j^{n_c} \frac{\hat{M}_{ij}(t)}{\hat{c}_j(t)^{\nu_{ij}}}. \tag{5.8c}$$

Clearly the parameter estimate is time dependent. It converges to the true, constant values if and only if the observer converges. One of the main disadvantages of the proposed methodology is the necessity of transforming the extended system into observability canonical form. Another constraint is the sensitivity to noise, inherent to high-gain observers.

5.3.1 Example circadian rhythm

In order to provide a proof of concept the presented approach is tested on a simple gene regulation model of the circadian rhythm in neurospora. The model describes day-night oscillations of the frequency protein (FRQ) by a nonlinear feedback loop within its gene expression (Leloup et al., 1999)

$$\dot{M} = r_3 - r_5 \qquad r_1 = k_s M \qquad r_3 = v_s \frac{K_1^4}{K_1^4 + F_n^4}$$

$$\dot{F}_c = r_1 - r_4 - r_2 + r_{2'} \qquad r_2 = k_1 F_c \qquad r_4 = v_d \frac{F_c}{K_d + F_c}$$

$$\dot{F}_n = r_2 - r_{2'} \qquad r_{2'} = k_2 F_n \qquad r_5 = v_m \frac{M}{K_M + M}.$$

Here M denotes the concentration of FRQ mRNA, F_c and F_n the concentration of FRQ protein in the cytosol and nucleus respectively, r_1 denotes the rate of translation, r_2 and $r_{2'}$ of transport in and out the nucleus, r_3 of transcription, r_4 and r_5 of degradation. By using the above reaction rates and defining the Hill variables

$$m_1 = K_1^4 + F_n^4, \qquad m_2 = K_d + F_c, \qquad m_3 = K_M + M,$$

the model is extended as described in the previous section.

Table 5.1 explores different designs of $\Phi(\cdot)$, i.e. different combinations of outputs and their derivatives, to analyse observability. Thereby it is advisable to limit the order of the derivatives for two reasons. First, to keep the observer design simple, and second to minimise numerical errors. If for a particular choice of $\Phi(\cdot)$ the corresponding observability matrix $Q = \frac{\partial \Phi}{\partial x}$ has full rank $n = 12$, the extended neurospora model is observable and thus identifiable.

Outputs & their degree n_i									
M	F_c	F_n	r_1	r_2	$r_{2'}$	r_3	r_4	r_5	rank(Q)
3	2	3	-	-	-	-	2	2	12
-	2	3	-	-	-	3	2	2	11
1	2	3	-	-	-	2	2	2	12
5	3	4	-	-	-	-	-	-	11
5	4	3	-	-	-	-	-	-	12
-	2	3	3	-	-	-	2	2	11
3	2	-	-	-	3	-	2	2	12
-	2	-	2	1	3	-	2	2	10

Table 5.1: Selection of the observability analysis of the neurospora model, each row corresponds to one particular design of Φ with the entries being the degree n_i as in (5.1). Observability and thus identifiability is achieved for full rank of $Q = \frac{\partial \Phi}{\partial x}$, i.e. rank($Q$) $= n = 12$.

A biologically feasible output, which also enables a simple observer design, is for example measuring the species concentrations (Leloup et al., 1999) and degradation rates (Shu and Hong-Hui, 2004):

$$y = \begin{bmatrix} M & F_c & F_n & r_4 & r_5 \end{bmatrix}^T.$$

A suitable choice of Φ for this output with invertible $Q = \frac{\partial \Phi}{\partial x}$ is for instance given by (see Table 5.1 row 1)

$$\Phi = \begin{bmatrix} M & \dot{M} & \ddot{M} & F_c & \dot{F}_c & F_n & \dot{F}_n & \ddot{F}_n & \dot{r}_4 & r_5 & \dot{r}_5 \end{bmatrix}^T.$$

Remark Note that the system is also observable if only the concentrations are measured $y = [M\ F_c\ F_n]$ (see Table 5.1 row 5). ■

The observer design has to be performed carefully, because calculating the determinant of Q identifies a loss of local observability if one of the following conditions holds:

$$r_2 = r_{2'},\ r_3 = r_5,\ r_1 + r_{2'} = r_2 + r_4, \qquad F_c(r_2 - r_{2'}) = F_n(r_1 + r_{2'} - r_2 - r_4).$$

Despite the fact that at these points Φ^{-1} is non-Lipschitz, Φ^{-1} is still continuous under the image of Φ since $\Phi \circ \Phi^{-1} = id$, thus permitting the observer design.

Both observer structures, (5.4) and (5.3), were implemented, whereby for (5.4) the modified version of Q^{-1} as in (5.5) was used. A trial and error procedure revealed best results for a condition number in (5.5) of $\delta = 10^{-4}$.

In a simulation study with the originally published parameters, artificial data was generated in order to test the method. The observers are initialized with 100% deviation from the true initial condition $\tilde{x}_i(0) = 2 \cdot x_i(0)$ for the non-measured variables $i = 4, \cdots, 9$. For this initial condition, the event based observer (5.4) fails (Figure 5.3a), whereas the ϵ-approximative observer (5.3) converges (Figure 5.3b). There are periods where observer error increases due to the reduced observability properties of the system (Figure 5.3 Row 3).

Applying (5.8) on the state estimate for each time point gives the parameter estimate. As Figure 5.4 shows, this parameter estimate is time dependent, converging nicely towards the true values. Spikes occurs where local observability and thus local identifiability is lost. Consequently a readout of the parameter values that spares these spiky regions is preferable to e.g. least squares fitting (Table 5.2).

5.3.2 Example MAPK and discussion

The proposed methodology is illustrated using the Mitogen-activated protein kinases (MAPK) introduced earlier in Section 3.6.3. In contrast to Section 3.6.3, the here presented model employs Michaelis Menten kinetics (Kholodenko, 2000). Further, the model contains a negative feedback loop from ERK to Raf, leading to an oscillatory behaviour. The model contains eight states and ten reactions with a total of 21 parameters. Figure 5.5 shows the overall network structure. The substrate concentrations are

$$c = \begin{bmatrix} \text{Raf-1} & \text{Raf-1}_\text{p} & \text{MEK} & \text{MEK}_\text{p} & \text{MEK}_\text{pp} & \text{ERK} & \text{ERK}_\text{p} & \text{ERK}_\text{pp} \end{bmatrix}^T,$$

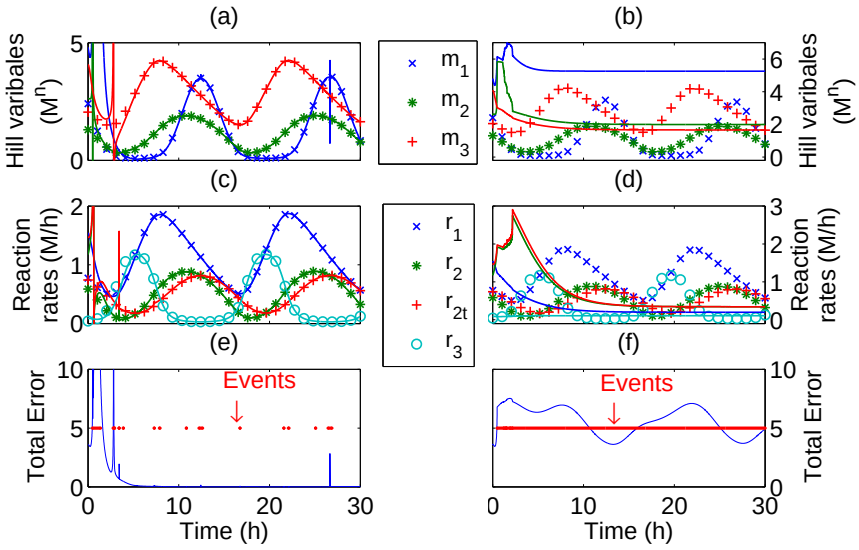

Figure 5.3: Comparison of event based and approximative observer at the example of the circadian rhythm. **(a-d)** The real (markers) and estimated (solid) trajectories of the non measured states for both observer structures with gain parameter $\theta = 1.5$. **(e-f)** The Euclidean error of the estimated states $\sqrt{\sum_j^n (x_{j,\text{est}} - x_{j,\text{real}})^2}$. The red markings indicate where events occur on the observed trajectory and the error can increase. **(a,c,e)** Approximative observer. **(b,d,f)** Event based observer.

	k_s	k_1	k_2	v_s	v_d	v_m	K_1	K_d	K_m
True	0.5	0.5	0.6	1.6	1.4	0.505	0.5	0.13	0.5
15h	0.50	0.50	0.60	1.63	1.39	0.505	0.55	0.13	0.50
25h	0.50	0.50	0.60	1.62	1.40	0.504	0.53	0.13	0.50

Table 5.2: True parameters that generated the simulated data for testing the parameter estimation method using the approximative observer, and readout of the estimated parameters at 15h and 25h. Units: k_i (h^{-1}), v_i (nMh^{-1}), K_i (nM).

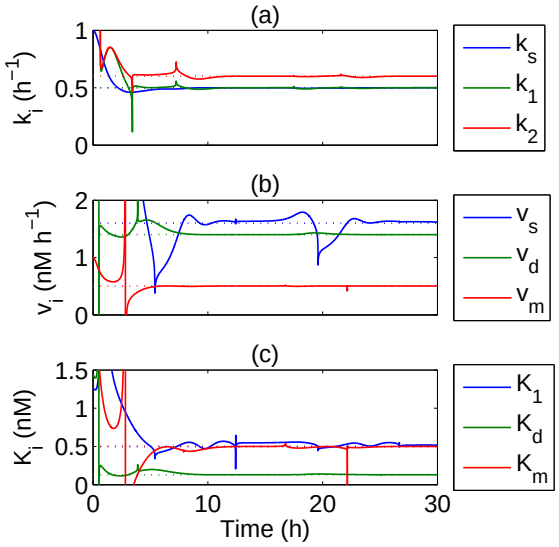

Figure 5.4: Parameter estimates of the circadian rhythm. As the observer converges, the parameter estimates of the ϵ-approximative observer (5.3) converge to the true values (dotted, constant). **(a)** Parameters of the mass action reactions. **(c)** Maximal flux parameters of Hill and Michaelis Menten reactions. **(c)** Half activation parameters of Hill and Michaelis Menten reactions.

and the system dynamics can be described by

$$\dot{c} = Nv,$$

$$N = \begin{bmatrix} -1 & 1 & & & & & & & & \\ 1 & -1 & & & & & & & & \\ & & -1 & & & 1 & & & & \\ & & 1 & -1 & 1 & -1 & & & & \\ & & & 1 & -1 & & & & & \\ & & & & & & -1 & & & 1 \\ & & & & & & 1 & -1 & 1 & -1 \\ & & & & & & & 1 & -1 & \end{bmatrix},$$

where the reaction kinetics are of the following form:

$$v_1 = \frac{k_1 K_I^{\nu_I}}{K_I^{\nu_I} + \mathrm{ERK_{pp}}^{\nu_I}} \frac{\text{Raf-1}}{K_1 + \text{Raf-1}}, \qquad v_6 = k_6 \frac{\mathrm{MEK_p}}{K_6 + \mathrm{MEK_p}},$$

$$v_2 = k_2 \frac{\text{Raf-1}_\mathrm{p}}{K_2 + \text{Raf-1}_\mathrm{p}}, \qquad v_7 = k_7 \mathrm{MEK_{pp}} \frac{\mathrm{ERK}}{K_7 + \mathrm{ERK}},$$

$$v_3 = k_3 \text{Raf-1}_\mathrm{p} \frac{\mathrm{MEK}}{K_3 + \mathrm{MEK}}, \qquad v_8 = k_8 \mathrm{MEK_{pp}} \frac{\mathrm{ERK_p}}{K_8 + \mathrm{ERK_p}},$$

$$v_4 = k_4 \text{Raf-1}_\mathrm{p} \frac{\mathrm{MEK_p}}{K_4 + \mathrm{MEK_p}}, \qquad v_9 = k_9 \frac{\mathrm{ERK_{pp}}}{K_9 + \mathrm{ERK_{pp}}},$$

$$v_5 = k_5 \frac{\mathrm{MEK_{pp}}}{K_5 + \mathrm{MEK_{pp}}}, \qquad v_{10} = k_{10} \frac{\mathrm{ERK_p}}{K_{10} + \mathrm{ERK_p}}.$$

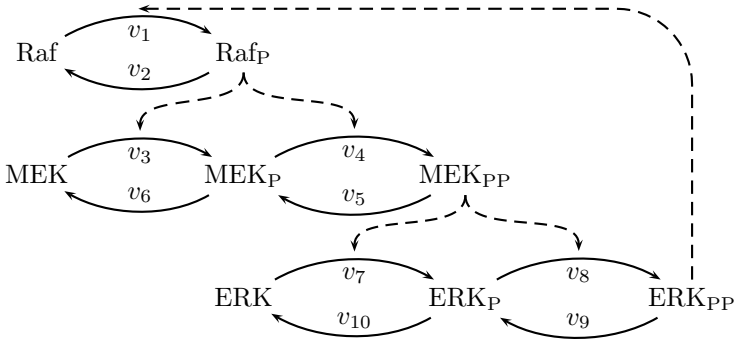

Figure 5.5: Reaction scheme of the mitogen-activated protein kinase cascades.

Parameter	**Value**	**Parameter**	**Value**
ν_I	2.0	K_I	18
k_1	2.5	K_1	50
k_2	0.25	K_2	40
k_3	0.025	K_3	100
k_4	0.025	K_4	100
k_5	0.75	K_5	100
k_6	0.75	K_6	100
k_7	0.025	K_7	100
k_8	0.025	K_8	100
k_9	1.25	K_9	100
k_{10}	1.25	K_{10}	100

Table 5.3: Parameters of the MAP kinase model (Kholodenko, 2000).

The extended state vector consists of the concentrations c, the flows v and the denominators or the flows $m = \begin{bmatrix} m_{11} & m_{12} & m_2 & m_3 & \dots & m_{10} \end{bmatrix}^T$

$$
\begin{aligned}
m_{11} &= K_I^{\nu_I} + \mathrm{ERK}_{\mathrm{pp}}^{\nu_I}, & m_6 &= K_6 + \mathrm{MEK}_{\mathrm{p}},\\
m_{12} &= K_1 + \text{Raf-1}, & m_7 &= K_7 + \mathrm{ERK},\\
m_2 &= K_2 + \text{Raf-1}_{\mathrm{p}}, & m_8 &= K_8 + \mathrm{ERK}_{\mathrm{p}},\\
m_3 &= K_3 + \mathrm{MEK}, & m_9 &= K_9 + \mathrm{ERK}_{\mathrm{pp}},\\
m_4 &= K_4 + \mathrm{MEK}_{\mathrm{p}}, & m_{10} &= K_{10} + \mathrm{ERK}_{\mathrm{p}}.\\
m_5 &= K_5 + \mathrm{MEK}_{\mathrm{pp}},
\end{aligned}
$$

The parameters values are the same as in Kholodenko (2000) and listed in Table 5.3. The parameters can be grouped into two vectors k and K:

$$
k = \begin{bmatrix} k_1 K_I^{\nu_I} \\ k_2 \\ \vdots \\ k_{10} \end{bmatrix}, \qquad K = \begin{bmatrix} K_I \\ K_1 \\ \vdots \\ K_{10} \end{bmatrix}.
$$

The term $k_1 K_I^{\nu_I}$ is identified as a single parameter. As $K_I^{\nu_I}$ is estimated separately, k_1 can also be obtained. The exponent ν_I is assumed to be known.

It is obvious that the time derivatives of c and m do not depend on the

parameters K and k. Simple calculations show that this also holds for the time derivatives of v. For example,

$$\begin{aligned}\dot{v}_1 &= -\frac{k_1 K_I^{\nu_I}}{K_I^{\nu_I} + \mathrm{ERK}_{\mathrm{pp}}^{\nu_I}} \nu_I \mathrm{ERK}_{\mathrm{pp}}^{\nu_I - 1} \dot{\mathrm{ERK}}_{\mathrm{pp}} \frac{\text{Raf-1}}{K_1 + \text{Raf-1}} \\ &\quad + \frac{k_1 K_I^{\nu_I}}{K_I^{\nu_I} + \mathrm{ERK}_{\mathrm{pp}}^{\nu_I}} \frac{\dot{\text{Raf-1}}(K_1 + \text{Raf-1}) - \text{Raf-1}\dot{\text{Raf-1}}}{\left(K_1 + \text{Raf-1}\right)^2} \\ &= -v_1 \frac{\nu_I c_8^{\nu_I - 1} \dot{c}_8}{m_{11}} + v_1 \frac{\dot{c}_1 (m_{12} - c_1)}{m_{12} c_1} \\ &= -v_1 \frac{\nu_I c_8^{\nu_I - 1} e_8^T N v}{m_{11}} + v_1 \frac{e_1^T N v (m_{12} - c_1)}{m_{12} c_1}.\end{aligned}$$

The extended state space is given by

$$x = \begin{bmatrix} c \\ m \\ v \end{bmatrix}. \tag{5.9}$$

Using all concentrations c and flows v as outputs, a possible choice for the observability map is

$$\Phi(x) = \begin{bmatrix} c \\ \dot{c} \\ v \\ \dot{v} \\ \ddot{v}_1 \end{bmatrix}. \tag{5.10}$$

This mapping is bijective, but not locally invertible. In the neighbourhood of the points where the observability map is not locally invertible, its inverse and $\phi(\cdot)$ are ill-conditioned. Therefore, in the observer $\phi(\xi)$ is approximated by

$$\hat{\phi}(\xi) = \begin{cases} -\delta & \text{if } \phi(\xi) \leq -\delta, \\ \phi(\xi) & \text{if } -\delta < \phi(\xi) < \delta, \\ \delta & \text{if } \phi(\xi) \geq \delta, \end{cases}$$

where $\delta = 30$. Similarly to (Vargas et al., 2003), events are defined as the set of time points where the observability map is ill-conditioned:

$$T_{\mathrm{Event}} = \left\{ t : \frac{\sigma_{\min}}{\sigma_{\max}} < 10^{-6} \right\},$$

where $\sigma_{\min}$ and $\sigma_{\max}$ are the smallest and largest singular values of $\partial\Phi/\partial x$. This avoids problems due to the non-existence or ill-conditioning of the inverse.

For illustration purposes, the observer polynomials have zeros at 1 and 1.1 for the second order systems and also at 1.2 for the third order system, while the high-gain parameter is 4.

The parameters estimation is possible at any time point, using (5.8). However, during an event, the estimation might be severely perturbed. Therefore, it is reasonable to estimate the parameter at non-event time points.

A closer analysis of the parameter estimation and in particularly their fluctuations reveals that the parameters of v_1, i.e. k_1, K_1 and K_I are not well

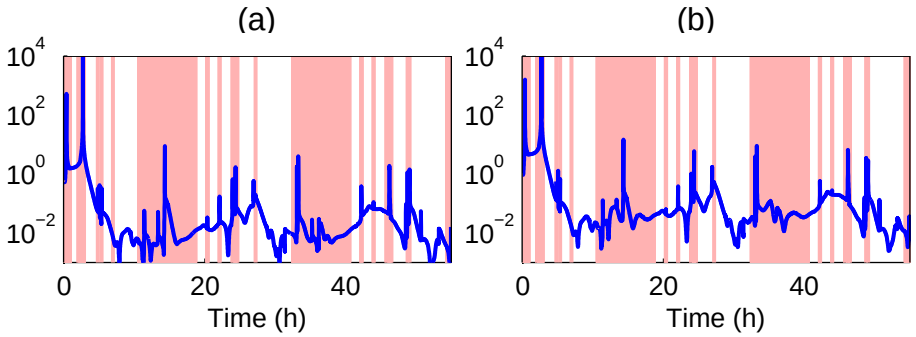

Figure 5.6: Estimation error of the MAPK model. The light-red markings indicate where events occur during which the extended system is not or only poorly identifiable. **(a)** State estimation error in observer coordinates. **(b)** Parameter estimation error.

estimated. This is particularly visible whenever $\mathrm{ERK_{pp}}$ (c_8) is large, see Figure 5.7. The inhibition term of v_1

$$v_I(\mathrm{ERK_{pp}}) = -\frac{k_1 K_I^{\nu_I}}{K_I^{\nu_I} + \mathrm{ERK_{pp}}^{\nu_I}} \tag{5.11}$$

is shown in Figure 5.7. For $\mathrm{ERK_{pp}}$ much larger than K_I, the relative sensitivity

$$S_{v_I}^{K_I}(\mathrm{ERK_{pp}}) = \frac{K_I}{\mathrm{ERK_{pp}}} \frac{\partial v_I(\mathrm{ERK_{pp}}, K_I)}{\partial K_I} \tag{5.12}$$

approaches zero. Whenever $\mathrm{ERK_{pp}}$ is large, the flow v_1 and its sensitivity on K_I is significantly reduced. This means the effect of the parameters K_I is negligible. Thus the parameter can hardly be identified, see Figure 5.7.

To circumvent this identifiability problem, the three parameter of v_1 are estimated when c_8 is low, e.g. at $t = 26.5$ min ($V_1 = 150.01$, $K_1 = 50.01$, $K_I = 17.95$) and the differential equations corresponding to the extended states are defined via algebraic equations as described in Section 4.2Then, the reduced extended state vector (without v_1 as output and without v_1, m_{11} and m_{12} as states) is estimated.

Comparing the two simulations reveals that the identifiability problem not only causes large fluctuations in the estimation, but also reduces the observability (gray marking), see Figure 5.8 compared to Figure 5.6. The reduced estimation slightly degrades the estimation error, see Figure 5.9. This is in particular the case for the parameters in reactions close to v_1, while more downstream reaction parameters are well estimated, see for example the estimation of k_2 and K_7 in Figure 5.9.

The example demonstrates the applicability of the proposed parameter estimation method. The parameters can be estimated with relatively small errors. The example highlights that practical identifiability is often time-dependent. Here, three parameters are identified in a first round, before all other are in a second estimation simulation.

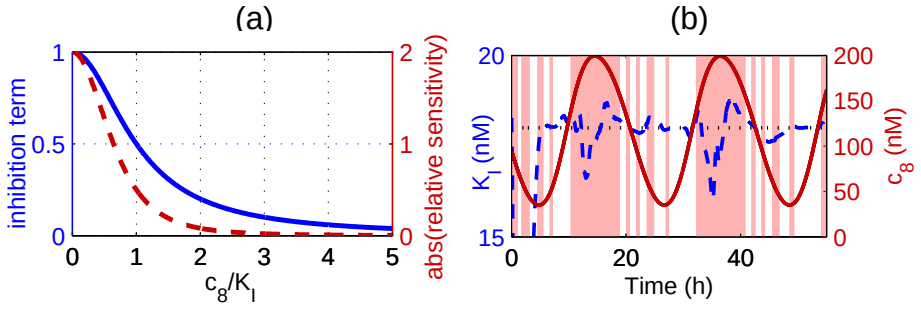

Figure 5.7: Illustration of the poor identifiability of the parameters of v_1 for high concentrations of $\mathrm{ERK_{pp}}$ (c_8). **(a)** Inhibition term (black, solid) and relative sensitivity (gray dashed line) as a function of the inhibitor concentration c_8. **(b)** Time course of $\mathrm{ERK_{pp}}$ (c_8, solid line) and the estimate of K_I (dashed line, with true value dotted). For large values of $\mathrm{ERK_{pp}}$, the estimation deteriorates and the system is poorly observable (gray markings).

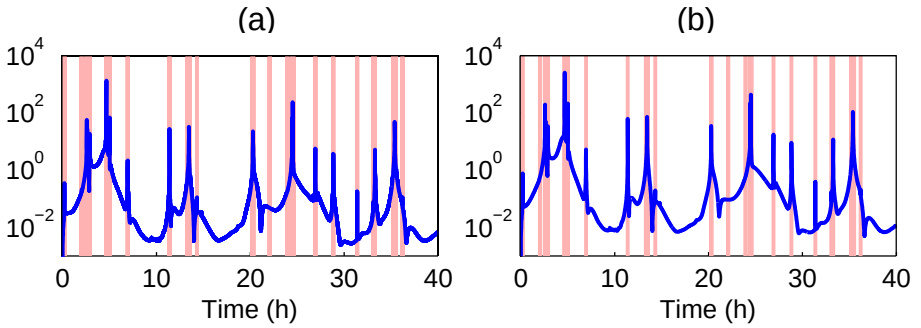

Figure 5.8: Error of the reduced estimation problem. Two step approach: First, model extention with reactions and Hill variables, but only the parameters of v_1, m_{11} and m_{12} where read out. Second, model extension for all reactions and Hill variables except v_1, m_{11} and m_{12} and read out of the remaining parameters. **(a)** State estimation error in observer coordinates. **(b)** Parameter estimation error.

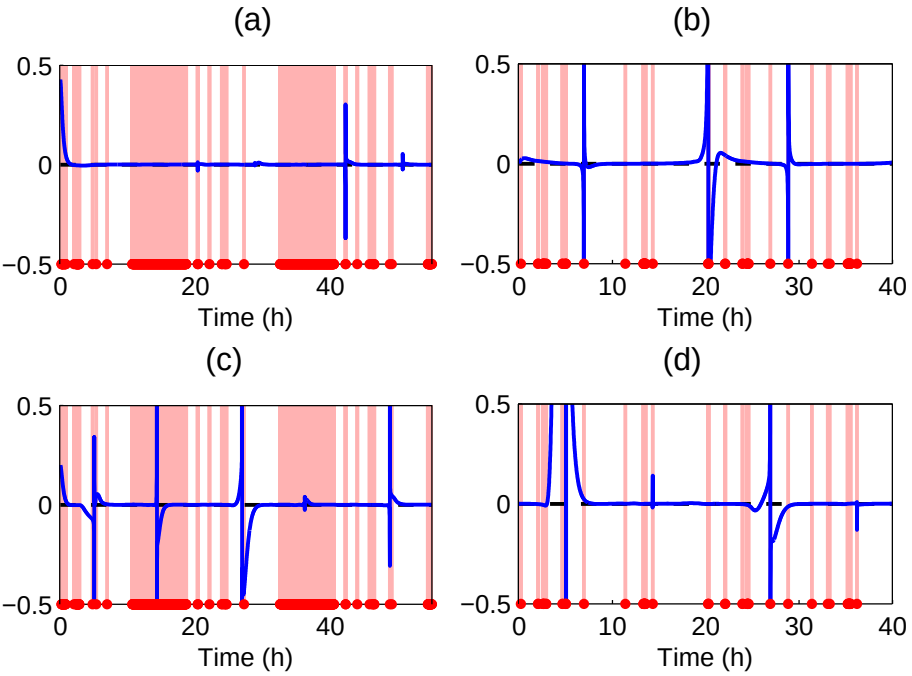

Figure 5.9: Comparision of the full (left column) and reduced (right column) estimation problem for parameters k_2 (top row) and K_7 (bottom row). Gray marking indicate where the trajectory is poorly observable. **(a, b)** Relative estimation error of k_2 **(c, d)** Relative estimation error of K_7 **(a, c)** Estimation uses the full extended state; **(b, d)** Estimation uses the reduced state, i.e. without v_1, m_{11}, m_{12}.

5.4 Summary and conclusions

The proposed parameter estimation methodology consists of three main steps. First, the system is transformed into a parameter-free system as described in Chapter 4. This requires only the knowledge of structural information such as the stoichiometry and the type of reaction kinetics. The second step is the design of an observer for the extended system in observability canonical form as described in this chapter. Obviously, the observer does also not depend on the parameters. The third and final step is the back-transformation of the observer states into the state space of the extended system. The parameters can be recovered in a straight-forward manner.

In the parameter free form, observers (state estimators) can be used to solve the parameter estimation problem. Unfortunately classical observer design for the here considered class of systems suffers from two drawbacks. First, global convergence can not be guaranteed. Second, classical observers can only be used if local observability holds. However, local observability is often violated somewhere on the trajectory (Section 5.2) or in steady state (Farina et al., 2006). Thus, special nonlinear observers are required.

This chapter presented the design of an nonlinear observer in observability cannonical form that is globally convergent and does not require local observability. Its main advantage is that it explicitly takes into account the structural information. In contrary to commonly used heuristic approaches, the proposed method guarantees the uniqueness of the parameter estimate.

Drawbacks of the proposed method are the necessity of transforming the extended system into observability canonical form, the need of time-continuous measurements or approximations thereof and the possibility of noise sensitivity. The latter two points can be dealt with using appropriate measurement filtering. The first point however limits the applicability of the method to systems of not too large dimension, as it requires expensive Lie algebraic computations. The next chapter presents an observer design avoiding this drawback.

Chapter 6

Design of a dissipative observer

As already mentioned, the parameter-free system (4.7) enables us to use observers for parameter estimation. In order to avoid the drawbacks associated with normal form observers, this chapter uses the concept of dissipativity to design an observer.

6.1 Introduction

The concept of dissipativity was proposed by Willems (Willems, 1972a,b) as an extension of Lyapunov theory to open system. Consider the state space system

$$\dot{x} = f(x,u), \qquad\qquad y = h(x,u),$$

a real valued function of the input and output $s(u,y)$ called the supply rate and a state function $V(x)$ called the storage function.

Definition 6.1 The system is called dissipative (with respect to the supply rate s) if

$$V\big(x(t_2)\big) - V\big(x(t_1)\big) \leq \int_{t_1}^{t_2} s\big(u(t),y(t)\big)dt$$

hold for all u, y, x and t_1, t_2 with $t_2 \geq t_1$. ■

The dissipativity condition can be checked without knowing $x(t)$, i.e. without having to solve the differential equations. Assume that $V(\cdot)$ is differentiable, then the above dissipativity condition is equivalent to

$$\frac{\partial V}{\partial x}(x,u) \leq s\big(u,h(x,u)\big)$$

holds for all x and u. To see that dissipativity is an extension of Lyapunov, note that if the input is absent, the dissipativity reduces with $s(u,y) = 0$ to the Lyapunov condition $\frac{\partial V}{\partial x}(x) \leq 0$.

Similarly to Lyapunov, we can understand dissipativity intuitively in terms of (generalised) energy. An open system interacts with its environment through

the inputs and outputs. The supply function $s(u, y)$ describes how a certain quantity (mass flow, power, entropy flow etc.) flows in and out of the system. The function $V(x)$ describes how much of the supply is stored in the system. The difference of what supplied and what is stored is dissipated, i.e. gets lost. The dissipation inequality states the the dissipation is nonnegative.

If we want to show that a system is dissipative, we need to find suitable supply and storage functions. In the linear-quadratic case, the system is assumed to be linear and the supply rate is assumed to be a quadratic form. However, because of $y = h(x, u)$ we can as well assume that the supply is quadratic in u and x, yielding

$$\begin{aligned} \dot{x} &= Ax + Bu, \\ s(u, x) &= u^T Q u + u^T S x + x^T R x, \end{aligned}$$

where Q and R are symmetric matrices. In the linear-quadratic case it suffices to check quadratic storage functions $V(x) = x^T P x$, where P is a symmetric matrix. With

$$\frac{\partial V}{\partial x}(\dot{x}) = x^T (A^T P + PA) x$$

the dissipativity condition becomes

$$x^T (A^T P + PA) x \leq u^T Q u + u^T S x + x^T R x,$$

which is equivalent to the matrix inequality

$$\begin{bmatrix} A^T P + PA - R & PB - S^T \\ B^T P - S & -Q \end{bmatrix} \preccurlyeq 0.$$

The matrix inequality is linear in the unknown matrices parameterising the supply and storage functions and can be solved effetely using computational tools such as YALMIP and SeDuMi (Löfberg, 2004; Sturm, 1999).

Dissipativity is very well suited for analysing interconnected systems. Consider two connected state space systems

$$\begin{aligned} \dot{x} &= f(x, u), & y &= h(x, u) \\ \dot{z} &= \tilde{f}(z, y), & u &= \tilde{h}(z, y), \end{aligned}$$

i.e. the output of the each system is the input of the other, with the supply and storage functions $s(u, y), V(x)$ and $\tilde{s}(y, u), \tilde{V}(z)$. Then a storage function of the closed loop system is the sum of both individual storage function and the dissipativity condition becomes

$$\frac{d}{dt}\big(V(x) + V(z)\big) \leq s(u, y) + \tilde{s}(y, u).$$

By matching the supply rates $\tilde{s}(y, u) = -s(u, y)$, we obtain the Lyapunov inequality $\frac{d}{dt}\big(V(x) + \tilde{V}(z)\big) \leq 0$, where we can define $\hat{V} : \hat{V}(x, z) = V(x) + \tilde{V}(z)$ as a Lyapunov function candidate. Assume $(x, z) = (0, 0)$ is a fix point of the interconnected system and assume further that $\hat{V}$ is positive definite, i.e. $\hat{V}(0, 0) = 0$ and $\hat{V}(x, z) > 0$ holds for all $(x, z) \neq 0$ Then the fix point is stable if the Lyapunov inequality holds with $\leq$ and asymptotically stable if it holds

with $<$. This illustrates how dissipativity can be used to analyse stability of interconnected systems.

The following sections use the here introduced concepts of interconnected systems and dissipativity with quadratic storage and supply functions in order to design an observer. Section 6.2 develops a general design scheme in terms of matrix inequalities. Section 6.4 applies the design to the extended, parameter free system, before its use for parameter estimation is discussed at the example of the MAPK system in Section 6.5

6.2 Dissipative observer

Dissipativity was applied to the observer design by Osario and Moreno (Osorio and Moreno, 2006; Moreno, 2008). The underlying idea is to decompose the nonlinear system into the interconnection of a linear dynamical system (A, G, F),

$$\dot{x} = Ax + Gw, \tag{6.1a}$$

$$\tilde{y} = Fx = \begin{bmatrix} y \\ \sigma \end{bmatrix} = \begin{bmatrix} Cx \\ Hx \end{bmatrix}, \tag{6.1b}$$

where y denotes the measured and σ the unmeasured output, and a static, possibly time-varying nonlinearity

$$w = \Psi(\sigma, u, t). \tag{6.1c}$$

Generally, an observer is a dynamic system that estimates all (unmeasured) states x from the measured output y. Moreno (Moreno, 2008) proposed a Luenberger observer for system (6.1) composed of an copy of the system equations (6.1) and two additional correction terms feeding back the error of predicted $C\xi$ and measured output y

$$\dot{\xi} = A\xi + G\Psi\big(\xi + N \cdot (C\xi - y), u, t\big) + L \cdot (C\xi - y), \tag{6.2}$$

where the matrices L and N are design parameters.

For analysing the convergence of the estimate, i.e. $\xi(t) \to x(t)$ for $t \to \infty$, it is convenient to look at the error of the estimate $e = \xi - x$. Straight forward calculation shows that the dynamics of the error are given by

$$\dot{e} = A_L e + G\upsilon \tag{6.3a}$$

$$z = H_N e \tag{6.3b}$$

$$\upsilon = -\Phi(z, x, u, t), \tag{6.3c}$$

where

$$A_L = A + LC, \tag{6.3d}$$

$$H_N = H + NC \tag{6.3e}$$

$$\Phi(z, x, u, t) = \Psi(x, u, t) - \Psi(x + z, u, t). \tag{6.3f}$$

Remark The nonlinearities $\Psi(\sigma, u, t)$ and $\Phi(z, \sigma, u, t)$ may be time varying and depend on the input, which usually is also a function of the time u=u(t). For readability reasons, the remainder of this document does not denote this functional dependence explicitly, i.e. we write for instance $\Phi(z, \sigma)$ and implicitly assume that the stated conditions hold true for all u, t. ■

To ensure convergence of the estimate, $e = 0$ must be a globally attractive steady state of system (6.3).

System (6.3) is a linear dynamical system (6.3a) with a input dependent, static nonlinear state feedback (6.3c). From (6.3f) it is clear that for vanishing error $e_{\mathrm{ss}} = 0$ the feedback becomes zero $\upsilon = 0$, and that $e_{\mathrm{ss}} = 0$ is indeed a steady state. This steady state condition holds for any input $u(t)$ and any trajectory $x(t, x_0)$.

To achieve that $e_{\mathrm{ss}} = 0$ is a globally stable steady state, we combine a dissipativity condition on the linear part (6.3a) with a matched dissipativity condition on the nonlinear feedback (6.3c).

Definition 6.2 (from Osorio and Moreno, 2006) The nonlinear part of the error dynamics Φ is called (Q, S, R)-dissipative if there exists a non positive semidefinite quadratic form

$$\omega(\Phi, z) = \Phi^T Q \Phi + 2\Phi^T S z + z^T R z \geq 0, \tag{6.4}$$

for all x, u and t. ■

Definition 6.3 (from Osorio and Moreno, 2006) The error dynamics are called ($-R$, S^T, $-Q$)-state strictly dissipative, if there are matrices L and N, a matrix $P = P^T \succcurlyeq 0$[1] and a scalar $\epsilon > 0$ such that

$$\begin{bmatrix} PA_L + A_L^T P + \epsilon P + H_N^T R H_N & PG - H_N^T S^T \\ G^T P - S H_N & Q \end{bmatrix} \preccurlyeq 0. \tag{6.5}$$

■

Osario and Moreno Osorio and Moreno (2006) derived the following theorem, proving exponential convergence of the observer error.

Theorem 6.1 (Dissipative Observer from Osorio and Moreno, 2006) Assume that the nonlinearity Φ is (Q, S, R)-dissipative and the linear part (A_L, H_N) is $(-R, S^T, -Q)$-state strictly dissipative, then the system (6.2) is a globally exponential observer for the closed loop system (6.1), i.e. it holds

$$\|e(t)\|_2 \leq \sqrt{\frac{\lambda_{\max}(P)}{\lambda_{\min}(P)}} \|e(0)\|_2 \exp\left(-\frac{1}{2}\epsilon t\right). \qquad ■$$

The inequalities (6.4) and (6.5) are nonlinear in the unknowns. The next section derives sufficient conditions for solving these inequalities, by transforming them into linear matrix inequalities.

[1] Throughout this manuscript, the curly symbols $\preccurlyeq$ and $\succcurlyeq$ refer to inequalities in terms of semi-definiteness.

6.3 Sufficient conditions for the dissipative observer

To simplify the observer design, the dissipativity conditions are reformulated as linear matrix inequalities (LMIs), which semidefinite programming can solve efficiently.

Nonlinear part

First we consider the dissipativity condition of the nonlinear part, for which we formulate the following theorem.

Theorem 6.2 Assume the nonlinearity Φ satisfies the sector condition $\|\Phi(z,x)\|_2 \leq \delta\|z\|_2$, then the condition

$$\sigma^R_{\min} \geq \sigma^Q_{\max}\delta^2 + 2\delta\|S\|_2, \tag{6.6}$$

where $\sigma^R_{\min}$ and $\sigma^Q_{\max}$ are the smallest and largest singular values of $R \succcurlyeq 0$ and $Q \preccurlyeq 0$ respectively, guarantees that the nonlinear dissipativity condition (6.4) is satisfied for all z. ■

Proof. Consider the dissipativity of the nonlinear part in (6.4). To compensate for negative influences of Q and S, R needs to be sufficiently large. A sufficient condition is $R \succcurlyeq 0$ and $Q \preccurlyeq 0$ together with

$$z^T R z \geq -\Phi^T Q \Phi - 2\Phi^T S z.$$

This condition is satisfied if

$$\sigma^R_{\min}\|z\|_2^2 \geq \sigma^Q_{\max}\|\Phi\|_2^2 + 2\|S\|_2 \cdot \|\Phi\|_2 \cdot \|z\|_2.$$

Using $\|\Phi(z,x)\|_2 \leq \delta\|z\|_2$ we obtain

$$\sigma^R_{\min}\|z\|_2^2 \geq \sigma^Q_{\max} \cdot \delta_2^2 \cdot \|z\|_2^2 + 2 \cdot \|S\|_2 \cdot \delta \cdot \|z\|_2^2,$$

which concludes the proof. ■

The above theorem assumes that R is positive semidefinite. As will become clear in the next section, this assumption makes sense and is motivated by the dissipativity condition of the linear part (see (6.7)).

Linear part

A Schur complement on the upper left element of the matrix inequality (6.5) yields

$$\begin{bmatrix} -R^{-1} & H_N & 0 \\ H_N^T & PA_L + A_L^T P + \epsilon P & PG - H_N^T S^T \\ 0 & G^T P - S H_N & Q \end{bmatrix} \preccurlyeq 0. \tag{6.7}$$

From here we can directly see that $R \succcurlyeq 0$ and $Q \preccurlyeq 0$. Further, (6.7) is a linear matrix inequality in the unknowns R^{-1}, P, Q, L, N and $S^* = SH_N$. Thus, for a given ϵ, (6.7) can be solved efficiently using semidefinite programming. In particular, solving (6.7) gives the observer gain matrices L and N.

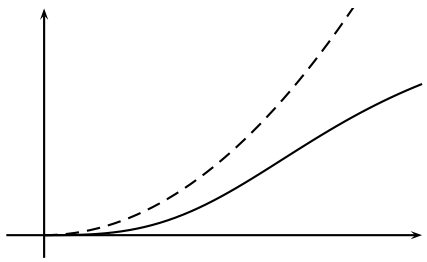

Figure 6.1: Bounding Φ using a quadratic term.

Matrix inequality

Recall however, that $\omega(\Phi, z) > 0$ must also hold. Using Theorem 6.2 we achieve that by posing (6.6) as additional constraint for (6.7). Unfortunately, the two inequalities are coupled in a nonlinear fashion. This is resolved by adding two constraints, first setting $S = 0$ and second defining a lower bound for the singular values of R. Under these conditions, (6.6) is equivalent to the following LMIs in the unknowns Q and R^{-1}

$$R^{-1} \prec \frac{1}{\sigma^R_{\min}}, \tag{6.8}$$

$$\sigma^R_{\min} \geq \|Q\|_2 \, \delta^2. \tag{6.9}$$

To see this, note that $(\sigma^R_{\min})^{-1} = \sigma^{R^{-1}}_{\max}$ and that R is symmetric positive definite, i.e. $\sigma^{R^{-1}}_{\max}$ equals the largest eigenvalue of R^{-1}.

Remark We set $S = 0$ because the nonlinear coupling $S = S^*(H + NC)^{-1}$ prevents us from formulating an LMI representation for the upper bound on $\|S\|_2$ required in (6.6). In the case $\dim(\sigma) = \dim(x) = n_x$ we could alternatively demand $H_N \in \mathbb{R}^{n_x, n_x}$ to be non-singular, and after solving (6.7), calculate S as $S = S^* H_N^{-1} = S^*(H + NC)^{-1}$. ∎

Summarising, the above considerations derived simple, linear conditions guaranteeing that both nonlinear dissipativity conditions (6.2) and (6.2) are satisfied. For convenience these conditions are collected in the following system of linear matrix inequalities:

$$P \succ 0, \tag{6.10a}$$

$$R^{-1} \prec \frac{1}{\sigma^R_{\min}}, \tag{6.10b}$$

$$\sigma^R_{\min} \geq \|Q\|_2 \delta^2, \tag{6.10c}$$

$$\begin{bmatrix} -R^{-1} & H_N & 0 \\ H_N^T & PA_L + A_L^T P + \epsilon P & PG \\ 0 & G^T P & Q \end{bmatrix} \preccurlyeq 0. \tag{6.10d}$$

To solve the system of LMIs, we choose a desired convergence rate ϵ of the observer and a lower bound $\sigma^R_{\min}$ on the singular values of R.

Sufficient condition for the existence of a solution for an arbitrarily large δ

Theorem 6.3 If the pair (A, C) is observable, then the system of LMIs (6.10) is solvable for any given $\delta < \infty$. ∎

Proof. Note that if (A, C) is observable, then there exists an L such that $A_L = A - LC$ is Hurwitz and $PA_L + A_L^T P + \epsilon P$ is negative definite. For sufficiently large P, the LMI (6.7) is diagonal dominant. Thus, the LMI (6.7) is solvable for all $R \succ 0$ and $Q \prec 0$. ∎

6.4 Dissipative observer for the parameter-free system

For the extended system (4.11), a dissipative observer design is very well suited as the system is fully known and can be written as a Lur'e system, i.e. the feedback of a linear dynamical and a static nonlinear part. With

$$H = I, \qquad G = \begin{bmatrix} 0 \\ I \end{bmatrix},$$

the system (4.11) is of the form (6.1), where in the simplest case, the linear part contains just the stoichiometry

$$A = \begin{bmatrix} 0 & 0 & N \\ 0 & 0 & 0 \end{bmatrix} \tag{6.11a}$$

and the nonlinear part contains the functions f_M and f_v

$$\Psi(\sigma, u, t) = \Psi(x, u) = \begin{bmatrix} f_M(x, u) \\ f_v(x, u) \end{bmatrix}. \tag{6.11b}$$

An alternative is to use the Jacobian at some reference point x_{ref} $A_\Psi = (\frac{\partial}{\partial x} f)(x_{\text{ref}})$ wherewith

$$A = \begin{bmatrix} 0 & 0 & N \\ & A_\psi & \end{bmatrix}$$

and

$$\Psi(x, u) = \begin{bmatrix} f_M(x, u) \\ f_v(x, u) \end{bmatrix} - G A_\Psi x. \tag{6.12}$$

Obviously, we would like to apply Theorem 6.2, for which we have to show that Φ satisfies the sector condition. The following lemma provides sufficient conditions.

Lemma 6.1 Assume that the Jacobian of the nonlinearity Ψ is bounded in a surrounding of the trajectory $x(x_0, t)$ of the true system with $\|\frac{\partial}{\partial}\Psi\|_2 \leq \frac{1}{2}\Delta < \infty$. Assume further, that Ψ is globally bounded with $\Psi(x) \leq \frac{1}{2}\Omega < \infty$. Then there exists a constant $\delta > \Delta$ such that $\Phi(z, x)$ satisfies the sector condition $\|\Phi(z, x)\|_2 \leq \delta \|z\|_2$. ∎

Proof. The proof considers two cases. First, for $0 \leq \|z\|_2 \ll 1$, consider the Taylor expansion of Φ w.r.t z around $z = 0$

$$\Phi(z, x) = \Phi(0, x) + \frac{\partial \Phi}{\partial z}(0, x)z + \mathcal{O}^2(z)$$

Considering the definition of Φ, we see that $\Phi(0, x) = \Psi(x) - \Psi(x + 0)$ and $\frac{\partial \Phi}{\partial}(0, x) = -\frac{\partial \Psi}{\partial}(0, x)$, wherewith

$$\Phi(z, x) = 0 - \frac{\partial \Psi}{\partial x}(x)z + \mathcal{O}^2(z)$$

Because $\|z\|_2$ is small, the linear part in the Taylor series dominates the quadratic part, and we can choose a constant $\delta > \Delta \geq \frac{\partial \Psi}{\partial x}$ such that the sector condition is satisfied. Second, for $\|z\|_2 > 0$, consider a proof by contradiction. Assume that there is a z_Ω for which the sector condition is not satisfied. Because of $\|z_\Omega\|_2 > 0$ and $\|\Phi(z_\Omega, x)\|_2 \leq \Omega$, we obtain a contradiction by choosing $\delta \geq \frac{\Omega}{\|z_\Omega\|_2}$. ∎

With Assumption 4.1 follows from the rational form of the reaction kinetics that the norms of $\Psi(x)$ and its Jacobian $\frac{\partial}{\partial x}\Psi(x)$ possess upper bounds for any trajectory $x(t, x_0)$. This is not necessarily true for the observer $\Psi(x + z)$. Therefore we bound $\Psi(x + z)$ artificially with $\hat{\Psi}(x + z)$ such that no error is introduced on the true trajectories, i.e. $\hat{\Psi}(x(t, x_0)) = \Psi(x(t, x_0))$.

A simple construction for the observer nonlinearity is

$$\hat{\Psi}_i(x + z) = \begin{cases} \Psi_{\min} & \text{if } \Psi_i(x + z) > \Psi_{\min} \\ \Psi_i(x + z) & \text{if } \Psi_{\min} \leq \Psi_i(x + z) \leq \Psi_{\max} \\ \Psi_{\max} & \text{if } \Psi_i(x + z) < \Psi_{\max} \end{cases},$$

where $\Psi_{\min}$ and $\Psi_{\max}$ respectively are lower and upper bounds on the elements of Ψ on the true trajectory, i.e. it holds that

$$\Psi_{\min} \leq \Psi x(t, x_0) \leq \Psi_{\max}.$$

Summarising, the above construction guarantees that the assumptions of Lemma 6.1 are satisfied, Theorem 6.2 can be applied and the system of LMIs in (6.10) guarantees global convergence of the observer.

6.5 Example MAPK

The proposed methodology is illustrated using a model of the Mitogen-activated protein kinases (MAPK) as introduced earlier in Section 3.6.3. In order to facilitate the readability of the document, the mathematical descriptions are recapitulated below.

Figure 6.2 shows a sketch of the overall network structure. The systems

Table 6.1: Parameters of the MAPK model that generated the artificial data.

p_1	p_2	p_3	p_4	p_5	p_6	p_7	p_8	p_9	p_{10}
1	0.1	0.8	1.1	0.4	0.2	0.9	1.2	0.5	0.3

reaction scheme is

$$\begin{aligned}
K_1 + u &\xrightarrow{v_1} K_2 + u,\\
K_2 + P_1 &\xrightarrow{v_2} K_2 + P_1,\\
KK_1 + K_2 &\xrightarrow{v_3} KK_2 + K_2 \xrightarrow{v_4} KK_3 + K_2\\
KK_3 + P_2 &\xrightarrow{v_5} KK_2 + P_2 \xrightarrow{v_6} KK_1 + P_2\\
KKK_1 + KK_3 &\xrightarrow{v_7} KKK_2 + KK_3 \xrightarrow{v_8} KKK_3 + K_3\\
KKK_3 + P_3 &\xrightarrow{v_9} KKK_2 + P_3 \xrightarrow{v_{10}} KKK_1 + P_3.
\end{aligned}$$

We obtain a system of ordinary differential equations $\dot{c} = Nv$ using the vector of concentrations

$$c = \begin{bmatrix} K_1 & K_2 & KK_1 & KK_2 & KK_3 & KKK_1 & KKK_2 & KKK_3 \end{bmatrix}^T$$

and the stoichiometric matrix

$$N = \begin{bmatrix}
-1 & 1 & & & & & & & & \\
1 & -1 & & & & & & & & \\
 & & -1 & & & 1 & & & & \\
 & & 1 & -1 & 1 & -1 & & & & \\
 & & & 1 & -1 & & & & & \\
 & & & & & & -1 & & & 1 \\
 & & & & & & 1 & -1 & 1 & -1 \\
 & & & & & & & 1 & -1 &
\end{bmatrix}. \tag{6.13}$$

The reaction rates are described using the law of mass action

$$v_1 = p_1 u K_1 \qquad v_2 = p_2 K_2, \tag{6.14a}$$
$$v_3 = p_3 K_2 KK_1 \qquad v_4 = p_4 K_2 KK_2, \tag{6.14b}$$
$$v_5 = p_5 KK_3 \qquad v_6 = p_6 KK_2, \tag{6.14c}$$
$$v_7 = p_7 KK_3 KKK_1 \qquad v_8 = p_8 KK_3 KKK_2, \tag{6.14d}$$
$$v_9 = p_9 KKK_3 \qquad v_{10} = p_{10} KKK_2. \tag{6.14e}$$

In the following, the model is used to illustrate/discuss a few aspects of the proposed methodology. 6.3 In all figures, simulations using the parameters values shown in Table 6.1 generated artificial data subsequently used by the observer. Further, in all figures, the following design specifications for solving the observer LMIs (6.10) were chosen: $\epsilon = 1$, $\sigma^R_{\min} = 1$, $\delta = 21$. The observer nonlinearity was bound with $-\Psi_{\min} = \Psi_{\max} = 10$.

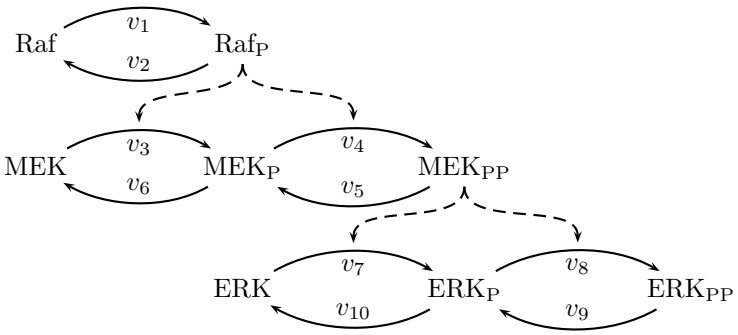

Figure 6.2: Example of a MAPK system: Raf-MEK-ERK

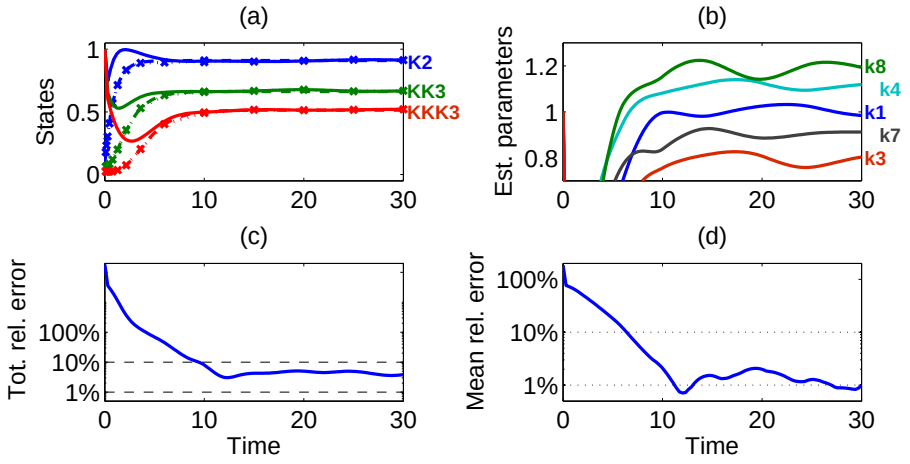

Figure 6.3: Estimation of the MAPK model with input, i.e. $u(t) = 0.01 \forall t < 0$, $u(t) = 1 \forall t \geq 0$. **(a)** Trajectories for measurements (x-marks), fitted outputs (dashed lines) and observed trajectories (solid lines). **(b)** Parameter estimates. **(c)** Total state estimation error relative to true values. **(d)** Mean parameter estimate error relative to true values.

6.5.1 Observability issues, known parameters and rate measurements

Application of Theorem 6.3 requires that the pair (A, C) is observable. With A given in (6.11), this means that the output has to be chosen accordingly. It follows from the structure of A that $c(t)$ has to be included in the output. In addition some reaction rates have to be included in the output if the stoichiometric matrix N possesses linearly dependent columns. For example, due to the dependencies of N in (6.13) either the phosphorylation or the dephosphorylation rate in each phosphorylation cycle has to be included in the output. In the following it is assumed that the output comprises all concentrations as well as the dephosphorylation fluxes, i.e.

$$y^T = \begin{bmatrix} c^T & v_2 & v_5 & v_6 & v_9 & v_{10}. \end{bmatrix}$$

Clearly, measuring all the required quantities is unrealistic in a real-world experimental scenario, in particular when it comes to measuring reaction rates. Measuring reaction rates can be circumvented by assuming that the corresponding parameters are known. Here, we assume that the dephosphorylation parameters are known, and calculate the flux directly from the concentration measurements, i.e.

$$y^T = \begin{bmatrix} c_{\text{measured}}^T & v_{\text{dephos}}(c_{\text{measured}}, p_{\text{known}})^T \end{bmatrix}. \tag{6.15}$$

Figure 6.4 illustrates that the stability of the observer is not lost, even if the assumed parameters are not known exactly (see also Table 6.2). In an identification where the known parameters are accurately known, the estimate of the remaining parameters is also accurate. However, when the known parameters are incorrectly known, a systematic error is introduced, i.e. the parameter estimates are off by an constant term (compare panels (a) and (b) in Fig. 6.4).

It is possible to further reduce the amount of time course measurements by exploiting conserved moieties, i.e linearly dependent rows in N. For example, the total concentration of kinase in each (double-) phosphorylation cycle is constant. Assuming the total concentration is known (or measured beforehand), one concentration measurement in each conserved moiety can be reduced. For example

$$\begin{aligned}
y_1(t) &= K_1(t) = K_{\text{total}} - K_2(t) = K_{\text{total}} - y_2(t), \\
y_4(t) &= KK_2(t) = KK_{\text{total}} - KK_1(t) - KK_3(t) = KK_{\text{total}} - y_3(t) - y_5(t), \\
y_7(t) &= KKK_2(t) = KKK_{\text{total}} - KKK_1(t) - KKK_3(t) = KKK_{\text{total}} - y_6(t) - y_8(t).
\end{aligned}$$

6.5.2 Data sampling and noise

In practice, experimental data is sampled (time discrete) and noisy. Because the observer requires a continuous output, data interpolation and smoothing is necessary. There is a multitude of non-parametric and parametric interpolation, smoothing and curve fitting techniques available (Motulsky and Christopoulos, 2004). Detailing these techniques would go beyond the scope of this manuscript, note however that smoothing splines provide a popular, easy to use standard. Throughout this manuscript, we fitted smoothing to the artificially generated

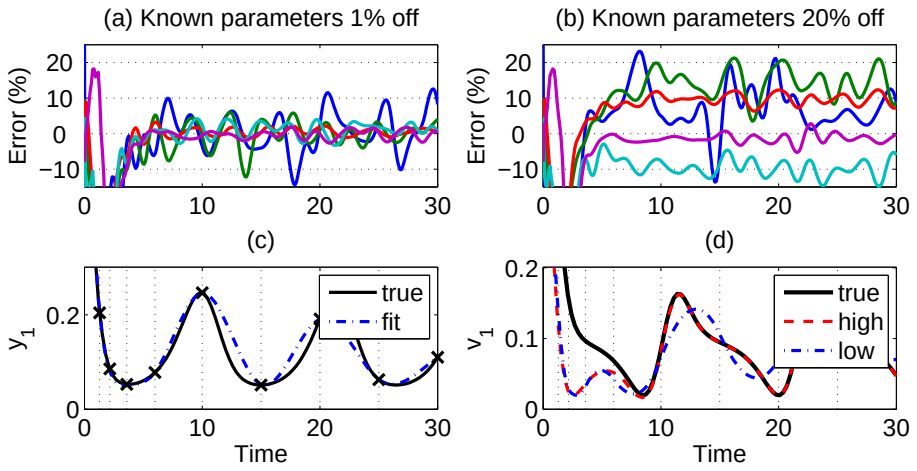

Figure 6.4: Effects of estimating only a subset of the parameters and sampling. **(a-b)** Identification with wrong values for known parameters as provided in Table 6.2; only the unknown parameters are estimated. Figures show the relative error of the estimated parameters for **(a)** known parameters 1% off the true values, **(b)** known parameters 20% off the true values. **(c-d)** Effect of insufficient sampling. **(c)** Output trajectories $y_1 = K_1$ as measured (solid) and fitted with low sampling (dash dotted). **(d)** State trajectory v_1 of the true system (solid) and the observer, i.e. the estimate, for high sampling (dashed) and low sampling (dash dotted).

Table 6.2: True, assumed and estimated parameters for the nominal model and sine input. The known parameters are 1% or 20% off the true values, i.e. the mean error of the assumed parameters is 1% or 20%. The row "estimated" presents mean values for $t > 10$ of the oscillating parameter estimate shown in Fig. 6.4.

		p_1	p_2	p_3	p_4	p_5	p_6	p_7	p_8	p_9	p_{10}
	true	1.00	0.10	0.80	1.10	0.40	0.20	0.90	1.20	0.50	0.30
1% off	assumed	-	0.11	-	-	0.49	0.27	-	-	0.48	0.23
	estimated	1.02	0.10	0.79	1.11	0.40	0.20	0.92	1.18	0.50	0.30
	% error	-2.22	-0.87	1.07	-1.78	-1.22	-0.06	-2.61	1.24	-0.00	-1.68
20% off	assumed	-	0.10	-	-	0.40	0.19	-	-	0.49	0.30
	estimated	1.17	0.11	1.11	1.35	0.50	0.27	0.72	1.17	0.48	0.24
	% error	-17.8	-14.9	-39.4	-23.1	-25.0	-39.1	19.1	2.37	2.89	19.87

data using the Matlab curve fitting toolbox. In all simulations, the stability of the observer was not compromised by the smoothing spline interpolations used, indicating that the proposed observer design is robust to measurement noise and data preprocessing.

An important aspect of smoothing and curve fitting is the associated error. Even in the noise free case when the fit perfectly retrieves the data at the sampled instances, interpolation still introduces errors and influences the quality of the subsequent state and parameter estimate. Figure 6.4(c-d) illustrates that insufficiently low sampling results in inaccurate state estimates (and thus inaccurate parameter estimates). Therefore, one has to be careful to choose sampling rate and curve fitting technique that can accurately capture the dynamics of the measured variables.

6.5.3 Unknown inputs

The observer is capable of identifying the internal parameters, even if the system is linked to other systems that have not been modelled. Mathematically, we treat the influence of non modelled dynamics as stimulation by unknown inputs. For example, the MAPK system is linked to a extracellular changes of hormone concentrations by a complex network of receptor, adaptor and scaffolding proteins.

Consider stimulation of the MAPK system with

$$v_1 = p_1 K_1 u(t), \qquad u(t) = 0.5 + A_0 \sin(2\pi t/w_0), \tag{6.16}$$

where $A_0 = 0.4$ and $w_0 = 23/2$. Further assume that the input is not measured. We therefore neglect it for setting up the observer, i.e. $u_{\text{observer}} = 1$. (instead of $v_1 = p_1 K_1 u$ we use $v_1 = p_1 K_1$ for the observer). Figure 6.5a shows that the observer still converges and that all states except v_1 are estimated correctly. The correct parameter values are obtained, with exception of the parameter p_1. This is not surprising, the observer simply included the unmodelled, unknown input into the p_1 estimate, i.e. $p_{1,\text{estimate}} = p_1 u(t)$.

6.5.4 Modelling errors

The fact that the observer is capable of estimating time varying parameters (see previous section and Fig. 6.5a) means it can be used to identify modelling errors, such as missing/unknown feedback loops. Ideally, when the model is correct, the parameter estimate is constant but time-varying in the case of an incorrect model (see Fig. 6.5b). This hypothesis was tested in several instances, by altering the system that generated the artificial data. Several modelling errors such as faulty reaction orders and unmodelled feedback loops were considered, and could all be identified. For simplicity of illustration, one one modelling error is presented here. In particular, consider a unmodelled feedback interaction of ERK to v_1, i.e the the data generating (true) system is

$$v_1 = 5 p_1 K K K_1 K_1 u,$$

whereas the observer design remains based on the simple nominal system

$$v_1 = p_1 K_1 u.$$

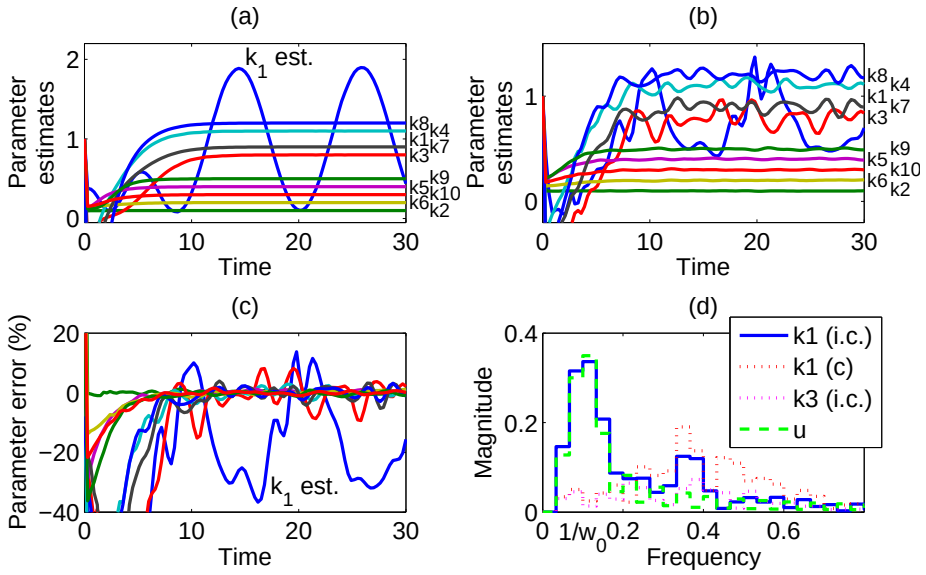

Figure 6.5: Identification of modelling errors of MAPK model with sine input. **(a)** Unknown input observer resulting in time dependent parameter $k_{1,\text{est.}} \hat{=} k_1 u(t)$. (no noise for illustration purposes) **(b-c)** Identification of modelling error in v_1. Data was generated using model alteration A1, with a feedback from ERK to v_1, i.e. $v_{1,\text{true}} = 5k_1KKK_1K_1u$, whereas the estimation was performed using the (faulty) nominal model for the observer, i.e. $v_{1,\text{obs}} = k_1K_1u$. (1% measurement noise.) **(b)** Relative parameter error for faulty model. **(c)** Discrete Fourier transform of (some representative) parameter estimates and input.

All extended states are estimated correctly by the observer. However, for the altered system, the parameter p_1 is not estimated correctly due to the modelling error in the corresponding reaction v_1. Instead of the true value, the observer estimated $p_1 KKK_1$. In order to see the modelling error the system must not be in steady state, because a faulty parameter estimate in steady state can not be distinguished from correct, constant estimates. We can only see the error if the system is moving, since then the faulty modelled parameter is time-varying (Fig. 6.5b).

Under noise free condition, a faulty modelled reaction is easy to spot. In a real world scenario, it might be more difficult depending on the level of noise, because noise causes (all) parameter estimates to vary. Nevertheless, the modelling error can be identified easily because the corresponding parameter estimate is highly correlated to the input. This can be seen by computing the discrete Fourier transform (DFT). In contrast to the DFT of all other parameters, the DFT of the p_1 estimate shows a frequency pattern very similar to that of the input (Fig. 6.5c).

In practice, it might be difficult to stimulate a stationary system with oscillations due to limitations of experimental techniques. Step and pulse stimulations might be much easier to achieve and they suffice to identify modelling errors. Instead of an oscillatory parameter estimate, one gets a raising or declining estimate for the parameter corresponding to the faulty reaction. Figure 6.6 shows an example in which the system was stimulated with the input $u(t) = 1/2(1 + 0.8 \tanh(15 - t))$ and reaction v_3 was modelled erroneous. The real system that generated the data had a feedback of ERK to v_3

$$v_3 = 7 p_3 KKK_1 p_2 KK_1,$$

whereas the observer design was again based on the simple nominal system

$$v_3 = p_3 K_2 KK_1.$$

The parameter estimate p_1 oscillates at around $t = 15$ because of the input change but returns to its previous value. In contrast p_3 raises toward a new steady state, indicating a modelling error.

6.6 Summary and conclusions

This chapter presented the design of a dissipative observer and its use for parameter estimation in the context of the model extension presented in Chapter 4. From a theoretical perspective, sufficient conditions for the observer design were given in the form of a linear matrix inequality that can be solved efficiently using programming packages such as YALMIP and SeDuMi (Löfberg, 2004; Sturm, 1999). From an application perspective, practical aspects such as limited number of measurement-outputs, measurement noise, sampling and modelling errors have been discussed. Using the MAPK system as a template, the examples illustrated that usual drawbacks of observer based approaches, such as the requirement of continuous measurements and sensitivity to noise, can be overcome by data preprocessing in the form of curve fitting. Curve fitting also allows to dissect the system into subsystems that can be estimated separately in a modular fashion. Therewith the methodology is well scalable to large systems.

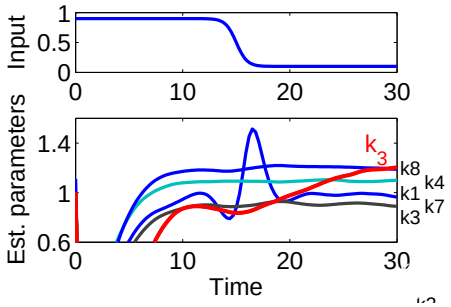

Figure 6.6: Identification with step like input. Stimulation with input $u(t) = 1/2(1+0.8\tanh(15-t))$ and the resulting parameter estimate, whereby reaction v_3 was modelled erroneous The data was generated with $v_3 = 7p_3KKK_1p_2KK_1$ (feedback of ERK to v_3), whereas the observer used the nominal model, i.e. $v_3 = p_3K_2KK_1$. Parameter estimate p_1 oscillates at around $t = 15$ because of the input change but returns to its previous value. In contrast p_3 raises toward a new steady state, indicating a modelling error.

An important advantage of the presented methodology is that it guarantees a unique parameter estimate by mathematical proof and that it can be used to estimate time varying parameters. The capability of the methodology to handle unknown inputs and estimate time varying parameters reveals modelling errors and pinpoints unmodelled effects. This is of particular relevance in gene regulation and signal transduction networks, which are generally associated with a great deal of uncertainty.

Chapter 7

Summary and perspective

Molecular systems biology aims in a detailed, dynamic understanding of cell function. To that end, mathematical models have to be constructed and calibrated using experimental data. Models of evolved biochemical reaction systems differ in a multitude of points from humanly engineered systems, rendering classical system identification methodologies unsuitable. However, biological systems have particular properties that can be exploited to develop novel methodologies. Here, I exploited the particular nonlinearity of biochemical systems in form of rational functions.

Chapter 3 presented a methodology to invalidate entire parameter regions by proving inconsistency of model and data. The method can be used to reduce the space of feasible parameters or to invalidate competing models. The methodology requires measurements at a few time points, such that derivatives can be calculated. Further, the states of the model have to be observable. Identifiability of the parameters is not required. Both, insufficient data and structural unidentifiability result in parameter dependencies, which are returned by the method as result. The main advantages of the methodology is that it does not require to solve or simulate the differential equations, and that entire parameter regions can be analysed. The main drawbacks of the methodology is that it can only invalidate, i.e. disprove parameters. This drawback is an artifact of the relaxation, for which we allowed solutions of the sdp of arbitrary rank. In the static case, Kuepfer et al. (2007) used rank one solutions as parameter estimates. In how far a low rank solution is a valid solution of the parameter estimation problem and how we can get low rank solutions are open question that can be considered in future research.

Chapters 4, 5 and 6 presented a methodology to estimate actual parameter values. The methodology relies on a state space extension that transforms the system into parameter free coordinates. The actual estimation is performed by special nonlinear observers that are particularly tailored to the parameter free system. Two observer design have been presented. In theory, the normal form observer can be applied even when only a few states are measured. However, it requires Lie algebraic computations and the inversion of the nonlinear observability map, which limits the size of systems for which the observer is applicable in praxis. The inversion of an observability map containing Lie derivatives of orders higher than two or three is probably not feasible. Further, normal form observers are not readily extendable to systems with inputs and are sensitive to

measurement noise. Avoiding these drawbacks motivated the design of a dissipative observer. The linear matrix inequalities developed in Section 6 provide a straight forward design that can be solved numerically in a matter of seconds (using YALMIP and SeDuMi). As demonstrated in numerous examples, the dissipative observer is robust against measurement noise and sampling. The main advantage of the observer based approach is that it estimates unknown influences and pinpoints modelling errors, giving valuable insight for further model development.

In contrast to the approach for parameter invalidation in Chapter 3 it is not possible to incorporate known parameter dependencies into the observer based approach due to the nature of the state space extension. The extension introduces a state variable for each reaction and Hill term. Even if two reaction share the same parameter, the corresponding state variables are different. This artificially increased the dimension of the identification problem. Future research should address this issue, as it is particularly important in the context of domain oriented modelling (Conzelmann et al., 2008).

Observability

The concept of observability is the common factor of the developed methodologies. In the context of parameter invalidation (Chapter 3), observability allowed us to solve for the unmeasured states and formulate conditions on the parameters in terms of the measured outputs and their derivatives. If the system is not observable, then the elimination of all unmeasured states is not possible, and the equations do not restrict the parameter space. Therewith, observability is a necessary condition for identifiability (see Theorem 3.3). To identify the parameters, we have to evaluate the parameter condition at different time points of the measured trajectory, which gives different manifolds of consistent parameters in the parameter space. If the resulting manifolds intersect in a single point only, the system is identifiable and the intersection point is the parameter estimate. This requires that we find at least $n + 1$ linearly independent functions in the observability space, where n is the number of states in the system. Assuming that only one parameter condition is used, the output and its derivatives need to be measured at at least n_p different time points t_i, where n_p is the number of states in the system. Of course the measurement vectors $[y(t_i), \dot{y}(t_i), \ldots]$ need to be independent of each other, which requires that the system is sufficiently exited.

In the context of parameter estimation using the extended system (Chapter 4), observability of the parameter free systems implies identifiability. In fact, observability of the parameter free system means that the reconstruction of all parameters is possible at any point in time. Given the output and its derivatives at one point on the trajectory, the parameter can be directly calculated (by inverting the observability map). In contrast to the requirements discussed in the previous section, observability of the parameter free system is a rather strong condition. In fact, it means we need to find at least $n + n_p$ linearly independent functions in the observability space.

Curve fitting

Experimental data is sampled and noisy. This is especially true in molecular biology, where modelers are faced with low sampling rates (often only a couple of time points are measured), and high levels of noise, rendering the task of model identification very challenging. In particular, calculating derivatives from experimental data, as required in Chapter 3, greatly amplifies measurement noise. Further, observer based approaches, as developed in Chapters 5 and 6 assume continuous measurements and thus require some sort of interpolation. Curve fitting can not only reduce measurement noise, but is also a means of obtaining derivatives and interpolation. Further, curve fitting allows for a modularized approach, in which some fitted curves act as inputs decoupling the subsystems as described in Chapter 6. Several standard techniques for curve fitting exist, such as fitting periodic functions or polynomials using least squares regression, most of which are implemented in the Matlab curve fitting toolbox used in this thesis. Fitting standard regressors, such as splines, gives good results for high sampling rates. The lower the sampling rate, the more carefully the smoothing parameter has to be tuned. The smoothing parameter describes how trustworthy the data points are. A smoothing parameter of 1 means the fitted spline goes through each data point. Lower smoothing parameters allow for a mismatch of data and fit, acknowledging that the data is corrupted by noise. It can therefore be used to capture the shape of the trajectory but not the noise. I found that tuning the smoothing parameter by visual inspection greatly enhances the results, a fact that is probably related to the low sampling rates and high levels of noise. Under certain conditions, fitting user defined function is beneficial because prior knowledge can be incorporated. For example, we know that the phosphorylation cycles in Chapter 3 exhibit exponential or sigmoidal trajectories, which can be captured using special, non-standard exponential functions.

Semidefinite programming

Semidefinite programming has become very popular within the control community in recent years. This is probably due to the fact that many problems of robust and optimal control can be readily formulated in terms of linear matrix inequalities, which are a special case of semidefinite programmes. This thesis utilised semidefinite programming to solve the parameter conditions in Chapter 3 and to solve the linear matrix inequalities for the observer in Chapter 6. The assumptions under which the observer design problem in Chapter 6 can be relaxed to a linear matrix inequality are rather strict. Using some ideas from Chapter 3, such as the sum of squares decomposition, it might be possible to find alternative, less stringent formulations.

Part II

Modelling the Morris water maze

Chapter 8

Background and literature review

The Morris water maze is an experimental procedure in which animals learn to escape swimming in a pool using environmental cues. Despite its success in neuroscience and psychology for studying spatial learning and memory, the exact mnemonic and navigational demands of the task are not well understood. To shed light on how rats solve the task, part two of this thesis develops a mathematical model of rat swimming dynamics on a behavioural level. Before doing this, the following sections provide the necessary background.

8.1 Morris water maze

In 1981, Morris described a simple, yet effective device to analyse spatial navigation, learning and memory (Morris, 1981; Morris et al., 1982; Morris, 1984). The Morris water maze consist of a large circular pool filled with opaque water such to hide an escape platform under the water surface. Using navigational cues, animals learn the location of the platform over several training trials and escape from the pool. Since its first application, the Morris water maze task has become one of the most frequently used tool in behavioural neuroscience utilised in more than 2000 research reports (D'Hooge and Deyn, 2001).

Undoubtedly, one of the reasons for its success is the simplicity and ease of use, offering this task many advantages over other spatial task. The use of water allows to control odour cues, and serves as an excellent motivation factor for animals to learn the platform location.

Despite the relative simplicity of the task, it remains unclear how the animals use the navigational cues for spatial learning and navigation.

8.2 Neuronal networks

On the neuronal level, the probably most common theory is the cognitive map theory (O'Keefe, 1990). The cognitive map is a neuronal network in the Hippocampus encoding a detailed spatial map of the environment in which each point in the environment evokes firing of at least one neuron. Experimentally,

the cognitive map theory is supported by reports of so called place cells. Place cells are neurons in the Hippocampus that express firing patterns depending on the position of the animal in space. Critic on the cognitive map theory argues that Hippocampal neurons do not map physical space explicitly, but rather encode spatial-temporal relationships and sequences (Eichenbaum et al., 1999).

Theoretical studies using the cognitive map theory have demonstrated that artificial neuronal networks can be used to learn spatial locations and navigate to them (Blum and Abbott, 1996; Brown and Sharp, 1995; Burgess et al., 1994). The resulting models are conceptually based on cognitive map theories, initially described by O'Keefe (1990), and hypothesise patterns of connection between different kinds of neurons such as place cells, head direction cells and grid cells (Moser et al., 2008; Burgess and O'Keefe, 1996). These studies have either focused on neuronal structures or on application of artificial networks for navigation of robots (Burgess, 2008; Tamosiunaite et al., 2008; Strösslin et al., 2005; Brown and Sharp, 1995).

8.3 Behavioural strategies

Despite the advances on the neurological level, spatial navigation and learning is not well understood on the *behavioural* level (Sutherland and Hamilton, 2004). In contrast to neurological studies, which focus on how neurons or networks of neurons process information, behavioural studies focus on higher level functions. such as different learning protocols. The result is a rather simple model that explains the observed behaviour (i.e. swimming path in the water maze) using environmental conditions os stimuli (i.e. available cues) and the strategy employed by the subject (e.g. random swimming, searching, ...).

This thesis takes such an behavioural approach in order to explain the animals swimming behaviour in the MWM.

The literature proposes multiple spatial strategies for orientation and navigation in animals and humans (Aggleton et al., 2000; Pearce et al., 1998). So called egocentric strategies define the relation of an object or goal relative to the subject. Egocentric mechanism include predefined sequences of motor movements, or approaching navigational cues directly, whereby little information about the relations between the cues themselves is used (Brown, 1992; de Bruin et al., 2001). In contrast, so called allocentric strategies define the relation of an object or goal relative to subject-independent locations. Allocentric mechanisms include the use of particular spatial relations between several cues, such as distances and directions between them. Triangulation of three or more distal cues allows the animal to triangulate its position and learn the goal location accurately (Hamilton et al., 2004; McGauran et al., 2004; Benhamou, 2003; Poucet and Benhamou, 1997). It has been suggested that animals have an entire hierarchy of strategies at their disposal with the preferred one used depending on the context and demands of the task. An animal might even use several different strategies in a single trial and change the employed pattern of strategies with training (Kealy et al., 2008a; McGauran et al., 2008; Choi et al., 2006; Gerlai et al., 2002; Packard and McGaugh, 1996). Harvey et al. (2008) argues that even under well controlled conditions navigation in the MWM is constantly changing, employing dynamic expression patterns of different cue-dependent ego- and allocentric strategies.

8.4 Analysis of water maze experiments

Nearly all experimental studies concerning the MWM rely on statistical analysis of the animals performance, such as the time passed until the animal finds the platform (escape latency), or the time the animal spends in different areas of the pool. In conjunction with neurological, surgical and pharmacological methods, simple performance analysis helped to reveal a great deal about learning and memory, especially on the neurological level (Maei et al., 2009; D'Hooge and Deyn, 2001; McNamara and Skelton, 1993). From a behavioural perspective however, those rather crude statistics clearly possess limitations. Statistics can coarsely describe, but not explain the rats swimming behaviour. Detailed, sophisticated mathematical models are necessary.

8.5 Dynamic modelling

Computational models can capture and parameterise essential features of the rats behaviour such as search strategies and learning protocols. Such models can be used to control experimental conditions in computer experiments to an extend that can not by achieved in web lab experiments. Other branches of the life sciences successfully utilised dynamic modelling to explain phenomena such as neuronal spiking, circadian rhythms, oscillations in population dynamics and animal movements of simple organisms (Jeanson et al., 2003). In concordance to the latter, we use dynamic modelling to explain and analyse rat movements in a water maze pool. By fitting the models to different conditions, e.g. trained versus untrained rat, one can exactly identify which parameters change. Clearly this approaches offers a richer, more detailed analysis compared to simple performance statistics.

Chapter 9

Stochastic process modelling of rat movements

This chapter develops a dynamic model conceptually based on a random walk that mimics rat swimming behaviour. The aim is to obtain a simple, time discrete model that can be identified easily from recorded swimming paths.

9.1 Introduction

Random walk models have been used in the literature to describe movements of simple organisms such as cockroaches and squid (Jeanson, et al., 2003; Schmitt & Laurent, 2001). In a simple random walk, either the displacements in each coordinate direction, or the step size and direction follow random variables. Clearly, such a simple model does barely justice to real rat movements, considering that rat have a tail and a head, and thus a somewhat coherent heading into a particular direction. The following sections develop a model of rat movement based on a directed random walk (Figure 9.1). In contrast to the common random walk, the direction is not a simple random variable, but depends on a random process in which the change of direction is driven by a random variable This model is developed in Section 9.3. In addition to the free swimming in the interior, rats also tend swim along the pool border. This behaviour is termed thigmotaxis and modelled in Section 9.4. The random variables in the model are identified from experimentally recoded swimming paths. The next section briefly comments on how the data was collected.

9.2 Experimental data

The data was obtained by Harvey et al. (2009). Male Wistar rats (aged 3 months 250-350g, Biomedical Facility, University College Dublin) were divided into two groups (1 cue and 3 cues). All animals (n=16) were given 4 trials per day for 5 days to acquire the water maze task. The Morris water maze consisted of a circular pool (1.7m diameter). Rats could escape from swimming by locating a hidden platform (9cm diameter) located in all experiments in the middle of the northeast quadrant of the pool. The platform was submerged 2cm, rendering

it invisible to the rats. The pool was surrounded by a black curtain located approximately 50cm from the pool wall. Different numbers of cues suspended on the inside of the curtains were available for the different groups. The 3 cues group had two light bulbs (in the northwest and northeast corner), and a rectangular sheet of white paper (55cm x 81cm, east side). The 1 cue group had a single light bulb located in the northeast corner. Collected data consists of recordings of rat swimming paths (x-y coordinates) in successive trials with neglectable positional error and a temporal resolution of 0.2s over at most 60s (after which the trial classifies as unsuccessful), resulting in 50 to 300 data points per trial.

9.3 Modelling free swimming inside the pool

The dynamic model is conceptually based on a directed random walk (Fig. 9.1) and a feedback loop of the heading change having a modular structure (Fig. 9.2). The random walk is modelled as a discrete-time system:

$$x_t = x_{t-\Delta t} + \Delta r_t \sin(\alpha_t), \tag{9.1a}$$
$$y_t = y_{t-\Delta t} + \Delta r_t \cos(\alpha_t), \tag{9.1b}$$
$$\alpha_t = \alpha_{t-\Delta t} + \Delta\alpha_t, \tag{9.1c}$$

where x_t, y_t and α_t denote position and heading of the rat at time t. Δt is the sampling time of the experimental data. The step size Δr_t and the heading change $\Delta\alpha_t$ are random processes to be identified from the data. Based on our data analysis, we assume that the step size is an independent random variable (the crosscorrelation between step size and heading change shows a high p-value of > 0.2 and values $20\times$ smaller than the autocorrelation of the heading change), whereas the heading change is a standard autoregression model extended by an input term u:

$$\Delta\alpha_t = \sum A_i \Delta\alpha_{t-i\Delta t} + u, \tag{9.2}$$

where A_i are coefficients describing the relative contributions of the past values on the current value. Two considerations motivated (9.2). First, rats do not change their heading completely randomly, as they tend to swim coherent curves. For example, when the rat turns left at one time instant, it tends to keep turning left for a certain amount of time, thus swimming a left curve. This effect can be modelled mathematically by making the change of heading dependent on previous heading changes, i.e. nonzero coefficients A_i. Second, rats are able to control their change of heading, which is mathematically modelled by the input term u realising a feedback mechanism:

$$u_t = K\hat{e}_t + \nu_t. \tag{9.3}$$

Here, $\hat{e}_t$ is the rat's estimate of its heading error, K is a proportional feedback gain and ν_t a normal distributed random number (Gaussian noise). The higher the gain, the faster the desired heading is achieved. We assume that the error estimate is realised as a low pass filter

$$\hat{e}_t = (1-F)\hat{e}_{t-1} + F(\alpha_{\text{desired}} - \alpha_t), \tag{9.4}$$

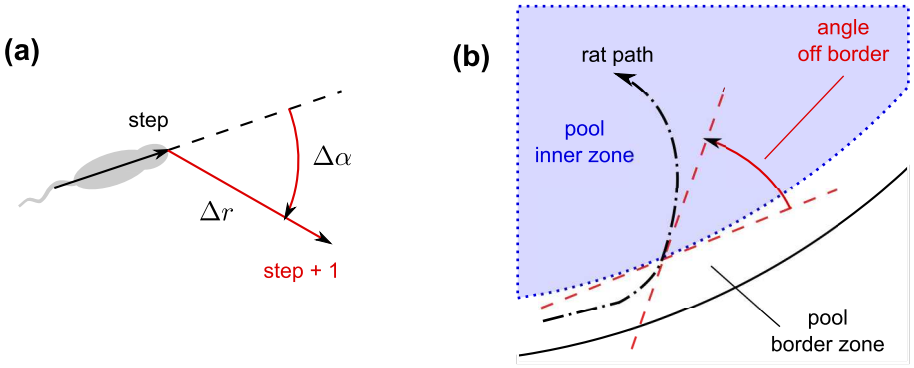

Figure 9.1: Sketch of the model. **(a)** Illustration of the random walk with Δr denoting the step size and $\Delta\alpha$ the heading change. **(b)** Illustration of the angle at which the rat leaves the pool border.

where $0 \leq F \leq 1$ is a weighting factor. Loosely speaking, the higher the weighting factor, the more the rat trusts its visual input; the smaller the weighting factor, the more the rat trusts its memory. Using an error estimate rather than the actual error directly achieves a much better model fit to the data (Sec. 10) and is further interpreted in Section 11.

9.4 Modelling thigmotaxis at the pool border

The above considerations mainly concern the rats swimming behaviour in the interior of the pool. Along the pool border, rats exhibit a distinct swimming behaviour termed thigmotaxis (Fig. 9.1b). Searching for a way out of the water, the rat swims along the pool border for a certain amount of time. The complete model captures both behaviours, free swimming in the pool and thigmotaxis, and is summarised in Table 9.1. Basically the simulated rat starts swimming in the pool as described in the previous section. When it hits the border, it chooses to swim along the border, whereby the probability to leave the border after each step is constant (see results section).

9.5 Perspective

The behaviour of rats in the water maze changes depending on the experimental conditions and the training regime used. The modelling framework developed in this chapter can be used to identify which parameters change in the model. Using the model, different navigational strategies can be tested in isolation and combination revealing the contribution and usefulness of these strategies and giving valuable insight into the MWM task. The next chapter illustrates how this can be done in particular.

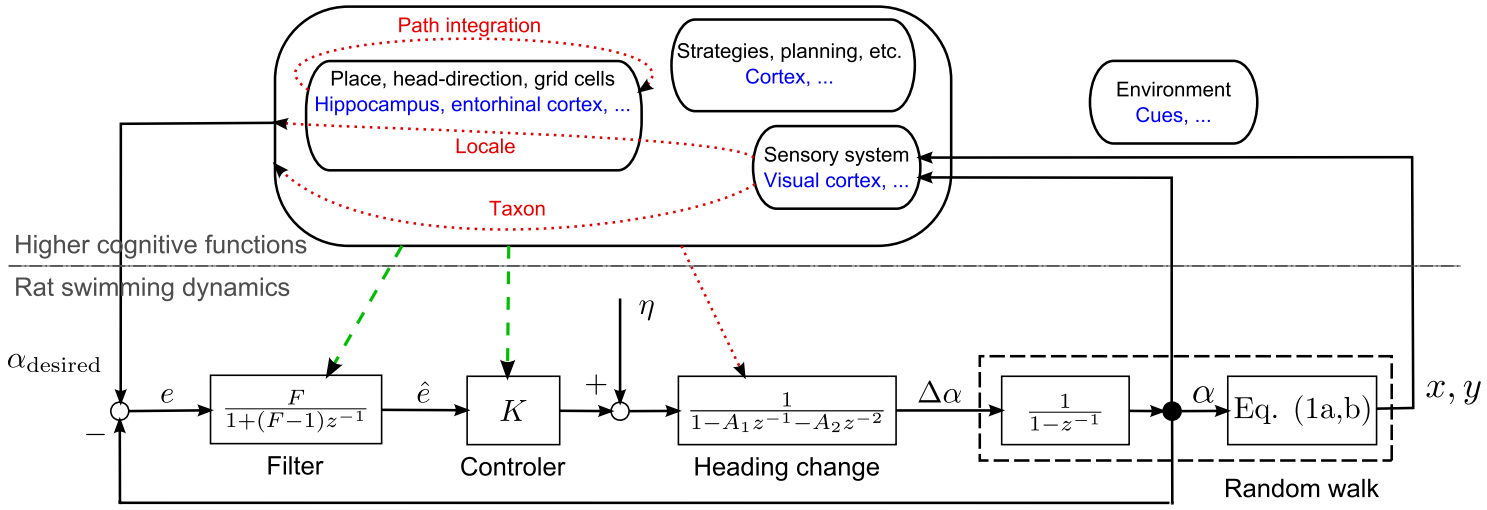

Figure 9.2: Overview of the heading change model (dynamics) and its relations to the neurophysiology (cognitive functions). On the path dynamics level, x, y is the rat's location, α is the rat's actual heading, α_{desired} the rats desired heading, e the heading error, $\hat{e}$ the rats estimate of the heading error, u the input to the heading change model and η a random variable with a normal distribution. The variable z arises from the z-Transform of the system, and can be understood as a time shift operator, i.e. $z^{-i}x(t) = x(t - i\Delta t)$. The neurological level comprised different brain regions and neuronal pathways and determines α_{desired} as well as the model parameters F, K and A_i.

Table 9.1: Overview of the model and the distributions identified from the data.

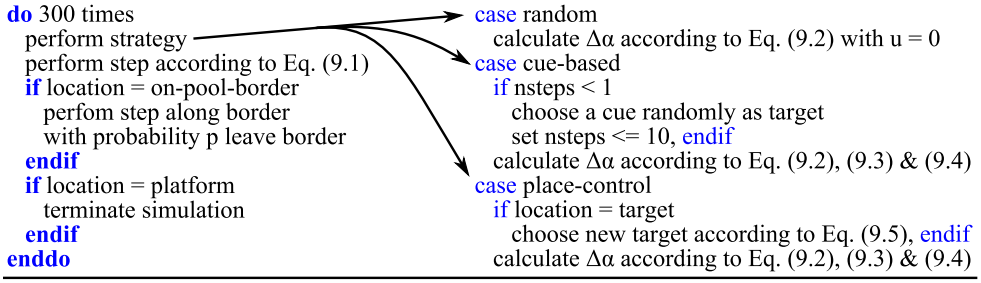

Process	Distribution	Probability density function	Parameters
Step size	Rayleigh	$\frac{x}{b^2}\exp(\frac{-x^2}{2b^2})$	$b = 8$
Heading change	Normal	$\frac{1}{\sigma\sqrt{2\pi}}exp(\frac{-(x-\mu)^2}{2\sigma^2})$	$\mu = 0, \sigma = 10$
Probability to leave border	Constant	p	$p = 1/8$
Angle off border	Log-normal	$\frac{1}{\sigma\sqrt{2\pi}}exp(\frac{-(\ln x-\mu)^2}{2\sigma^2})$	$\mu = 3.5, \sigma = 0.78$

Chapter 10

Identification and analysis of the model

This section identifies the mathematical model from experimental data and analyses different navigational strategies. Estimating all parameters from the recorded swimming paths is possible because the described model is simple and largely linear. In fact, the only nonlinearity is the calculating the displacements in (x, y) coordinates from the heading in (9.1).

10.1 Thigmotaxis

The distribution of the path length along the border was identified by analysing the recorded swimming paths using the Matlab statistics toolbox. A histogram shows good accordance with an exponential distribution, suggesting a constant probability to leave the border at each time step (0.2s) (Fig. 10.1). As there is no escape from the water at the border, the rats learn to avoid the border over time (Fig. 10.2). Avoiding thigmotaxis occurs on a much longer timescale in a matter of days. For the model we can therefore safely assume the following. In a single trial, the probability of leaving the border in each time step remains approximately constant, yielding an exponential distribution of the path length. Learning to avoid thigmotaxis can be modelled by changing the probability to leave the border from one trial to the next, or even from one day to the next.

10.2 Learning not reflected in the distribution, but in the autocorrelation of the heading change

The probability density functions of the random variables were identified by analysing the recorded swimming paths using the Matlab statistics toolbox (Fig. 10.1). The distributions of step size and heading change do not change significantly with training (Fig. 10.3a-b). This is not surprising, because those variables do not contain positional information. However, the autocorrelation of the heading change, which describes how current heading changes correlate

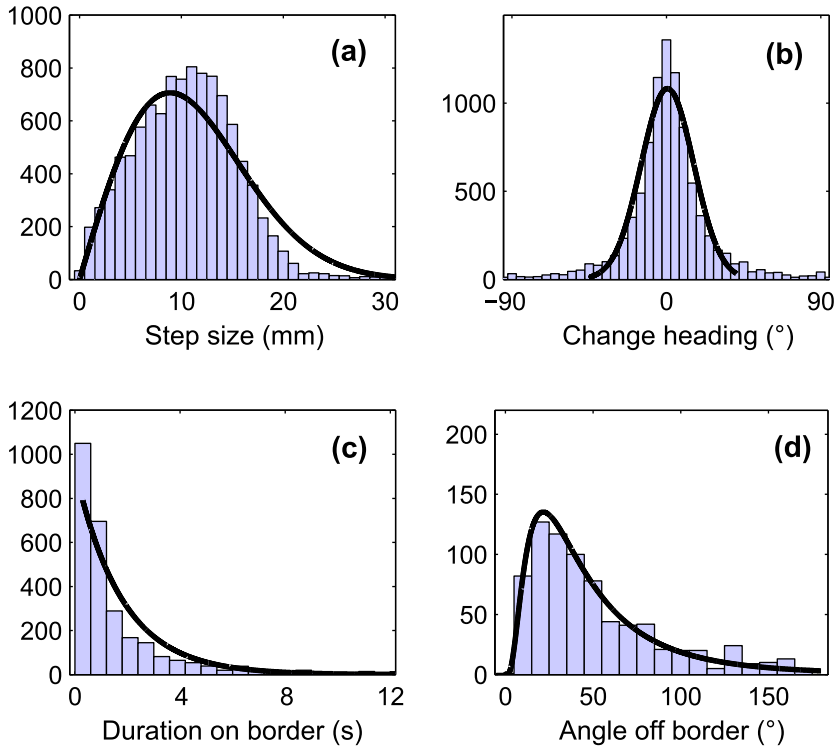

Figure 10.1: Visualisation of the random variables distributions: histograms show the data, solid lines the fitted probability density functions as used in the model. **(a)** Rayleigh distribution of the step size **(b)** normal distribution of the heading change **(c)** exponential distribution of the path length on the pool border **(d)** log-normal distribution of the angle at which rats leave the border

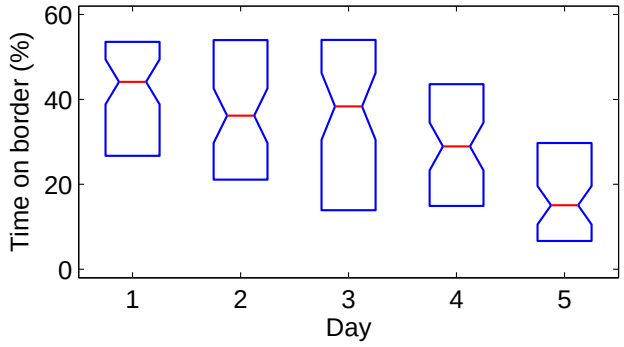

Figure 10.2: Percentage of time the rats spent at the pool border. Middle lines indicate medians, boxes upper and lower quartile, indicating a significant statistical difference between day 1 and day 5.

to past heading changes for one time step back (lag one, i.e. 0.2s), two time steps back (lag two, i.e. 0.4s) and so forth: $\sum_i \Delta\alpha_i \Delta\alpha_{i-lag}$, increases over days, reflecting the rats learning progress (Fig. 10.3c).

10.3 Open loop model mimics swimming behaviour of day one

We identified the parameters A_i of the heading change model in open loop using the data of day one, when we assume the rat's swimming behaviour is not directed towards a particular goal ($\alpha_{\text{desired}} = \alpha$) and the input u is Gaussian noise ($u_t = \nu_t$). This renders (9.2) a simple autoregressive model that can be identified using the Yule-Walker equations. We found that a second order model (i.e. $A_i = 0$ for $i > 2$) explains the observed autocorrelation sufficiently well (Fig. 10.3d, see also next section). Only slightly different coefficients were obtained for the 3-cues and 1-cue group. The simulated swimming paths and the resulting simulated escape latencies are in good accordance with those of the wet lab experiments (Fig. 10.4).

10.4 Selecting the model order based on behaviour

Selecting the model order (i.e. $A_i = 0$ for $i >$ model order) is an important step in systems identification, which involves a certain trade off. On the one hand, a higher model order, i.e. a greater number of free parameters, improves the model's fit to the observed autocorrelation. On the other hand, an oversized model describes random errors or noise particular to the respective data set instead of the underlying relationship. Such overfitted models generally have poor predictive performance, exaggerating minor fluctuations in the data. Therefore, great care has to be taken into choosing the model order.

There is a rich literature on how to choose the model order optimally, mainly taking an information theoretical perspective. Famous examples are the Akaike's information criterion or the Bayesian (also called Schwarz) information criterion (Ljung, 1999; Koehler and Murphree, 1988). Often, different criteria return different model orders, especially if the stochastic is not mere (measurement) noise but the major driving force of the system, as in our case. We can obtain a meaningful model (in the predictive sense) by identifying different models of different order on subsets of the data and comparing preserved features/behaviour. From a systems theoretical point of view, the behaviour of a systems is best described by its poles and zeros, as we can directly see stability, oscillatory behaviour etc. Figure 10.5 shows the poles (there are no zeros in an autoregressive model) of the identified models for different model orders (1-5). Two poles are particularly well preserved, a real pole at ≈ 0.4 and a real pole at ≈ -0.3. These poles of the second order model are very similar in the 1-cue and 3-cues case, do not change significantly over days of training and also occur reliably in higher order models (order > 3). Further, these two poles are the most prominent in higher order models (order > 3), i.e. their respective gains in a partial fraction decomposition are considerably higher compared to the remaining poles. In conclusion, a second order model seems to capture the main features of the underlaying behaviour reliably.

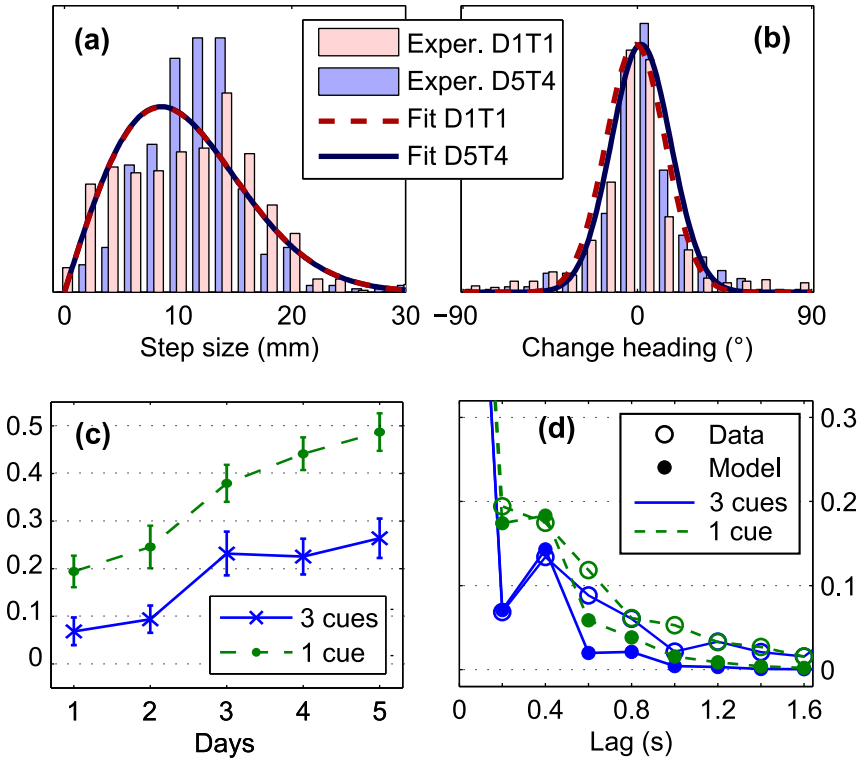

Figure 10.3: Identification of the open loop model. **(a,b)** Comparison of the distributions for untrained (day 1, trial 1) vs. trained rats (day 5, trial 4). Fitted distributions show no significant difference. **(c)** Lag 1 (0.2s) autocorrelation of the heading change over days. Markers indicate the mean over 8 rats and 4 trials, errorbars indicate the standard error of the mean (SEM). **(d)** Fit of the open loop model autoregressive model (2nd order), i.e. identification of the parameters A_i. Solid: 3 cues case. Dashed: 1 cue case.

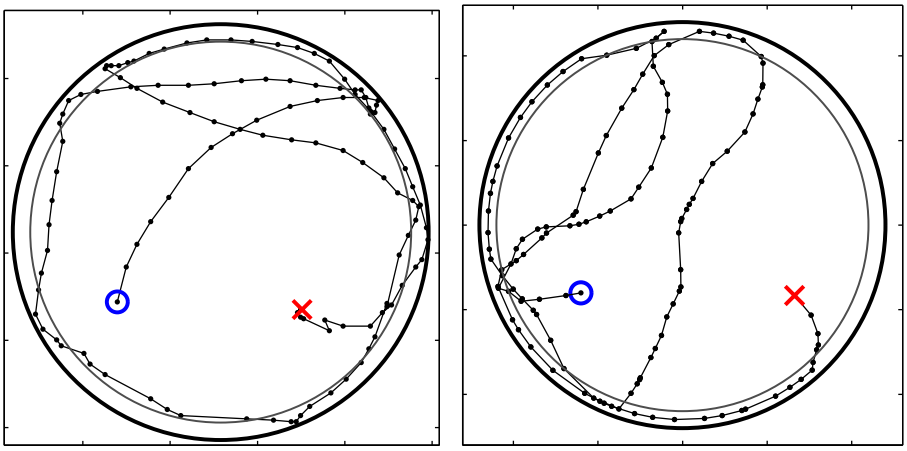

Figure 10.4: Exemplary swimming path of a real rat on day one (left) and a simulated rat using the open loop model (right). The circle indicates the starting point, the x-mark the end point. In the shown trial, both rats succeeded in finding the platform indicated by the x-mark.

10.5 Closed loop model reveals different feedback mechanisms

We identified the parameters K and F of controller and filter in closed loop using the data of day five, when the rats direct their heading using the described feedback mechanism. Here, the Yule-Walker equations are not applicable due to the feedback. Instead, we used simulations to minimise the least squares error of the autocorrelation of the heading change (Fig. 10.6).

We found an inherent difference in the navigational control strategy depending on whether one or three cues were available. Despite the fact that learning occurs equally fast in both cases, 3-cues rats employ a stronger feedback ($K = 0.42$), compared to the 1-cue rats ($K = 0.32$). In addition, the 3-cues group seem to rely only on the currently observed error, i.e. $F = 1$, whereas the 1-cue group rely to 24% on their memorised estimate, i.e. $F = 0.76$. We repeated this analysis using different, more complex control models (data not shown). All gave similar results, showing higher, immediate control for 3-cue rats, and lower, delayed control for 1-cue rats.

10.6 Model analysis assesses efficiency of navigational strategies

10.6.1 Avoiding the pool border

A first simulation experiment implemented a purely egocentric strategy in which rats learn to avoid the border (platform located somewhere in the interior of the pool). Border avoidance is modelled by a change of the probability to leave the border. Simulations revealed that solely avoiding the border slightly decreases

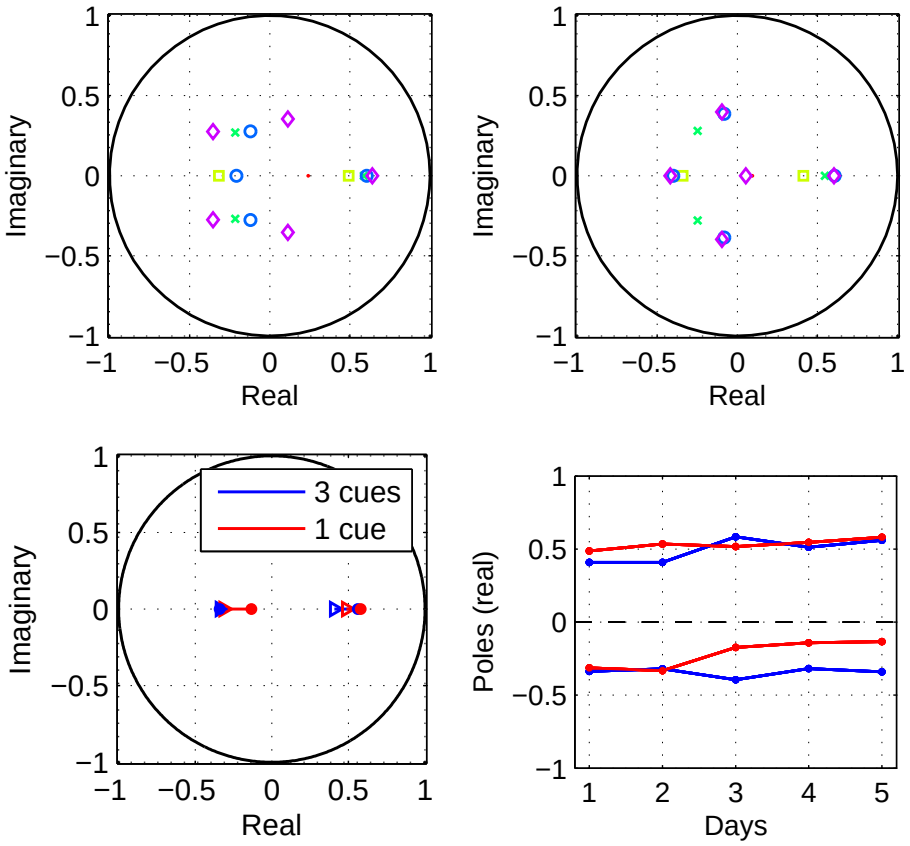

Figure 10.5: Poles of identified autoregression models of the heading change in open loop. **(a,b)** Poles in the complex plane for identified models of different orders. Dot: 1st order, square: 2nd order, x-mark: 3rd order, circle: 4th order, diamond: 4th order. **(a)** 1-cue case **(b)** 3-cue case **(c)** Root locus of poles for increasing days showing how the poles move in the complex plane with training. **(d)** Changes of the (real part) poles over days.

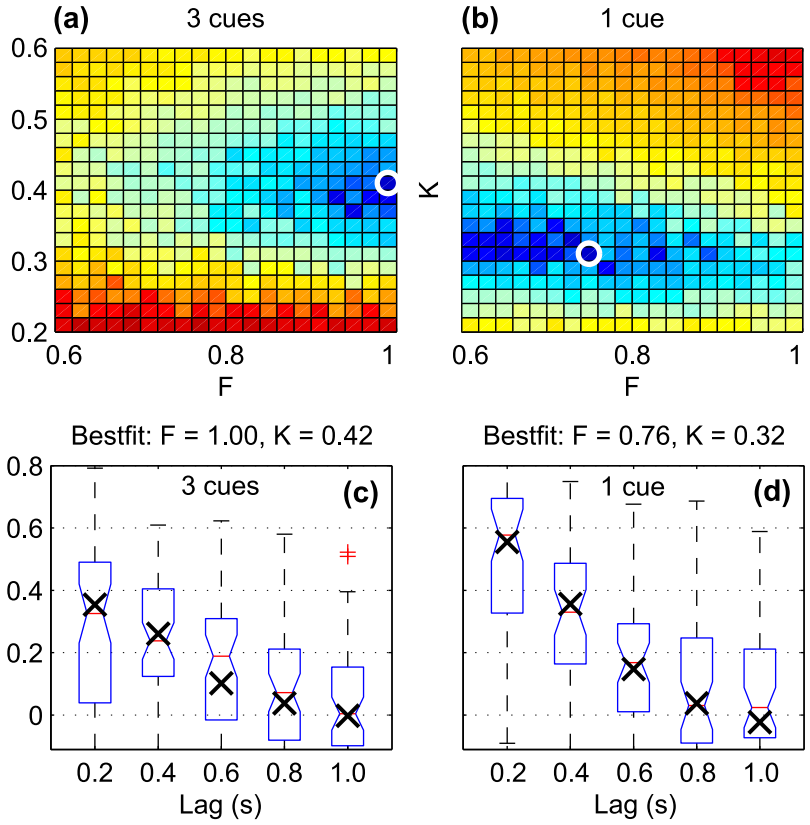

Figure 10.6: Fit of the closed loop model, i.e. identification of the feedback parameters K and F. **(a,b)** Colour contour plot visualising the values of the cost-function (sum of squares error of the autocorrelation function) for different control parameters. Darker, blue areas correspond to a better fit, the white circle indicates the best fit. **(c,d)** Comparison of the autocorrelation function of the heading change of data and model. Box plots show the data, horizontal lines indicate the median, notches the 95% confidence interval, boxes the lower and upper quadrille, whiskers the extreme values and "+" outliers. The x-marks "×" indicate the mean autocorrelation function of the model as obtained from > 500 simulation runs.

the escape latencies, but that this effect is rather minor (Fig. 10.7a).

10.6.2 Cue-based egocentric strategy

A second simulation experiment implemented a cue-based egocentric strategy in which the rats approach different cues for a certain (random) amount of time. Unsurprisingly, the analysis of the resulting escape latencies shows that this cue-based egocentric strategy is more efficient in the 3-cues case than in the 1-cue case (Fig. 10.7b). Although the escape latencies were significantly reduced compared to random swimming (50% and 32% for 3-cues and 1-cue group, respectively), they did not reach the performance of fully trained rats. For example, Figure 3b demonstrates that simulated animals in the 3-cues group reach escape latencies of 19 seconds whereas animals in the laboratory typically reach 10 seconds or less following 5 days of training (Kealy et al., 2008a). At this point it is important to note that simulating the one cue experiment with the strong control parameters (as identified from the 3-cues data) increases the escape latencies significantly compared to the nominal control parameters (as identified from the 1-cue data) for cue usages of more than 60%. This decrease of performance worsens the more the rat uses the cue (Fig. 10.7b), red-dash-dotted line). A weaker control is therefore beneficial in a 1-cue scenario, explaining the difference of feedback strength identified in the previous section ($K_{\text{3-cues}} > K_{\text{1-cue}}$).

10.6.3 Allocentric place navigation

A third simulation experiment, implemented an allocentric place navigation strategy, assuming the rats know the platform location with varying degrees of uncertainty (similar to a cognitive map, Burgess 2008). These uncertainties were represented by two dimensional Gaussian distributions with varying degrees of standard deviation. The simulated rats' assumed platform location is the true platform location plus a random deviation drawn from the uncertainty distribution:

$$x_{\text{PF, rat}} = x_{\text{PF, true}} + \rho \sin(\theta), \tag{10.1}$$

$$y_{\text{PF, rat}} = y_{\text{PF, true}} + \rho \cos(\theta), \tag{10.2}$$

where ρ is a normally distributed random number with zero mean and θ a uniformly distributed random number in the interval $[0, 180)$. Once the simulated rat successfully navigated to its assumed platform location while realising there was no platform, it dropped that assumption and chose a new platform location, again by drawing from the uncertainty distribution. An analysis of the resulting escape latencies demonstrates that animals possessing little knowledge of the platform location (large uncertainty) can solve the task very effectively. Indeed, an uncertainty of about half the pool radius is sufficient to explain the escape latencies after 5 days of training (10 seconds, Fig. 10.7c). The situation of a perfectly learned platform location, i.e. with no uncertainty, results in very low escape latencies (4 seconds). Such low escape latencies have been observed for over-trained rats (12 days of training, Kealy et al. 2008a).

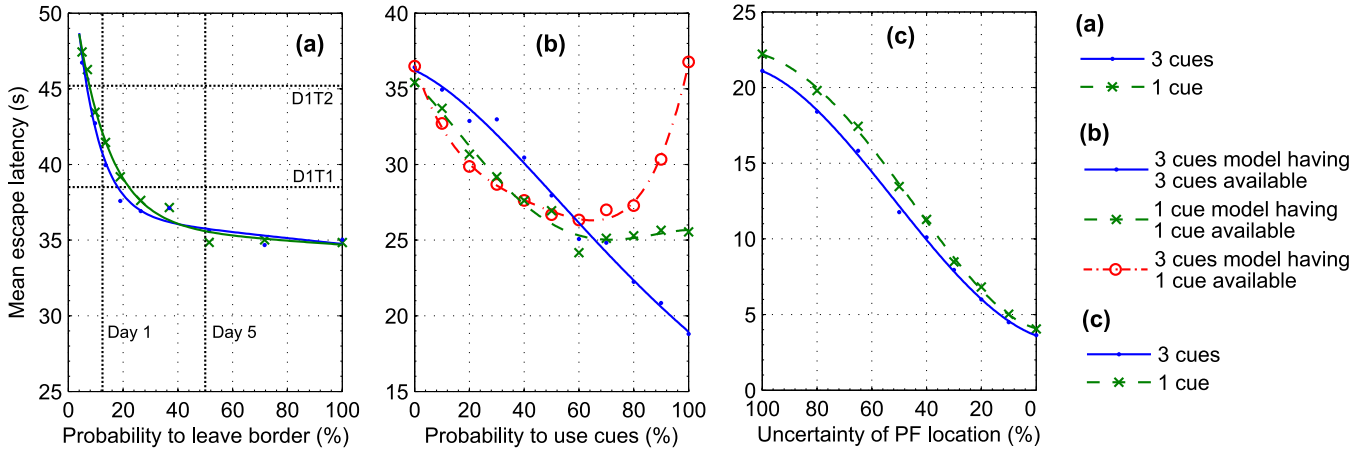

Figure 10.7: Analysis in terms of mean escape latency (y-axis for all plots). Markers present mean values of at least 500 simulations with SEM's < 1s (dots for 3-cues, x-marks for 1-cue model). Lines present a smooth fit to the simulated data (solid for 3-cues, dashed for 1-cue model). **(a)** Strategy for leaving the border: At each time step the simulated rat leaves the border with a certain probability. The two open loop models ($\alpha_{\text{desired}} = \alpha$) were simulated for a range of probabilities to leave the border (x-axis). Thick vertical dotted lines indicates the probability to leave the border as estimated from the experimental data of day 1 and 5. Horizontal dash-dotted lines indicate the mean escape latencies of the experimental data in trials 1 & 2 of day 1. **(b)** Egocentric cue-based strategy: The simulated rat swims in episodes of random length in which the rat either approaches a cue ($\alpha_{\text{desired}} = \alpha_{cue}$) or swims randomly ($\alpha_{\text{desired}} = \alpha$). In the 3-cue case, the target cue was chosen randomly with equal probability. The two models were simulated in their corresponding environment for a range of probabilities to choose a cue (x-axis). We also simulated the 3-cues model (K high, $F = 1$) in the 1-cue environment (circles, dash-dotted line). **(c)** Allocentric place navigation strategy: In each episode, the simulated rat swims to a randomly chosen target location ($\alpha_{\text{desired}} = \alpha_{\text{PF, rat}}$). Once reached, another episode begins and the rat chooses a new target. Target location is the platform location plus a random error with a Gaussian distribution of zero mean. The two models were simulated for a range of standard deviations of the error, which can be understood as the uncertainty with which the rat knows the platform location (x-axis).

10.7 Model predictions

10.7.1 Physical parameters

Water maze experiments depend on several factors: physical ones such as pool size and platform or cue location as well as behavioural ones. All are reflected as model parameters, which can easily be altered in simulations for generating model-based predictions. This is illustrated at the example of two types of experiments.

First, changing the pool size has a major effect for untrained rats (random walk strategy), but not for trained rats (place-control strategy), see Fig. 10.8a. This is not surprising, because the difficulty of finding the platform depends on the ratio of pool size to platform size. The greater this ratio, the more difficult it is to find the platform using a random search strategy.

Second, having the platform on the opposite side of the clues is more difficult with a cue-based strategy, but identical for a place navigation (Fig. 10.8b). Using a cue based strategy, the rat learn to swim away from the cues, heading in the opposite direction. In contrast to approaching the cues, turning away from the cues results a wide spread of swimming paths and the platform is missed more often. The place navigation strategy is by definition not affected by the cue position. Place navigation assumes that the rat knows its own and the platform position and therefore swims directly to the target. It is important to note that the question of how the rat infers the positions, for example by constructing a mental map, is neglected.

10.7.2 Probe test performance

Probe test are used by experimentalists to assess the learning success after training. In a probe test, the platform is removed from the pool and the rat is given a 60s retention trial. The rats (learning) performance is then assessed usually using one of the following measures

- Percent quadrant time (Q). Amount of time mice searched a virtual quadrant (i.e., 25% of total pool surface area), centred on the location of the platform during training (Morris, 1984; Morris et al., 1982; Morris, 1981).
- Percent zone. Amount of time mice searched virtual target zones (20 [Z20], 15 [Z15] and 10 [Z10] cm in radius, centred on the location of the platform during training) during the 60-s test (de Hoz et al., 2004; Moser et al., 1993; Moser and Moser, 1998). These zones represent 1/9th (11.1%), 1/16th (6.25%) and 1/36th (2.8%) of the total pool surface area, respectively.
- Crossings (X). Number of times mice cross the exact location of the platform (5 cm in radius) during the 60-s test (Morris, 1984; Morris et al., 1982; Morris, 1981).
- Proximity (P) measure (Gallagher's measure). Average distance in centimetres of mice from centre of the platform location across the 60-s test (Gallagher et al., 1993).

Using the model, simulated retention trials allow for comparison of different strategies and performance measures. For example, the Gallagher measure is

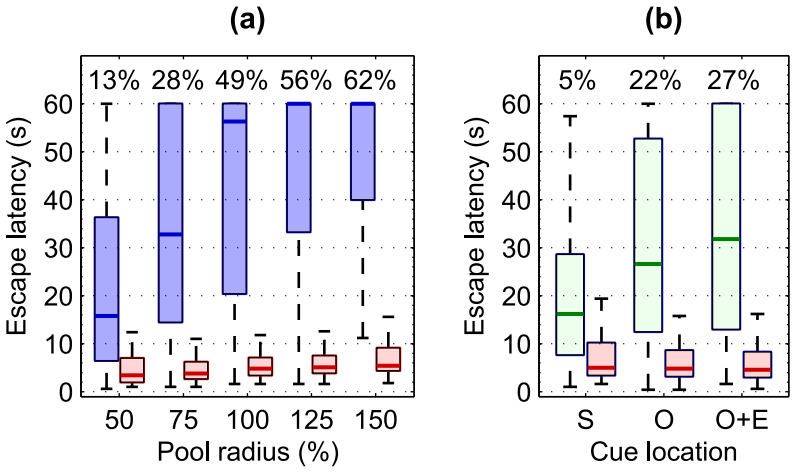

Figure 10.8: Prediction of expected escape latencies (y-axis), middle lines indicate medians, boxes upper and lower quartile, percentage on top of each box is the percentage of unsuccessful trials. **(a)** Different pool sizes (x-axis). Blue, left-hand-side: Random walk model (untrained rats of day one, i.e. probability to leave border = 1/8). Red, right-hand-side: Place control model (trained rats of day five, i.e. probability to leave border = 1/2).**(b)** Different cue locations. Green, left-hand-side: Egocentric cue-based strategy (3 cues, probability to use cues = 100%); S: cues in same quadrant as platform, simulated rats approach cues ($\alpha_{\text{desired}} = \alpha_{\text{cues}}$); O: cues in opposite quadrant as platform, simulated rats swim away from cues perfectly ($\alpha_{\text{desired}} = \alpha_{\text{cues}} + 180°$); O+E: cues in opposite quadrant as platform, simulated rats swim away from cues but with an directional error ($\alpha_{\text{desired}} = \alpha_{\text{cues}} + 180° + \epsilon$, where ϵ is normal distributed with zero mean and standard deviation 10°). Red, right-hand-side: Place-control strategy (uncertainty = 30%); S, O: rat swims to its assumed platform location directly ($\alpha_{\text{desired}} = \alpha_{\text{PF, rat}}$), O+E: rat swims to its assumed platform location with an directional error ($\alpha_{\text{desired}} = \alpha_{\text{PF, rat}} + \epsilon$).

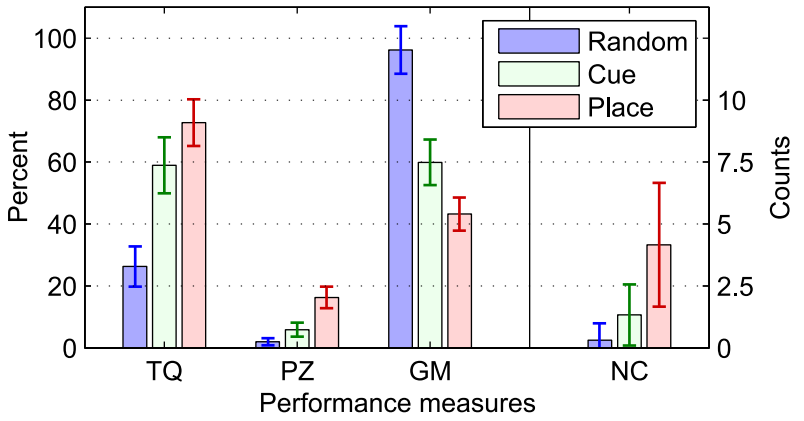

Figure 10.9: Predictions of different performance measures for the random walk model (blue, left-hand-side bars), the egocentric cue-based strategy with 3 cues (green, middle boxes) and the place-control strategy (red, right-hand-side bars). In the simulations, trained rats are allowed to swim for 60s without an escape platform. Errorbars indicate standard variations. TQ: Time in quadrant, i.e. percentage of time the rat swims within the correct pool quadrant. PZ: Percentage zone, i.e percentage of time the rat swims within a circular zone around the correct location. (Zone covers 1/9 of the total pool area.) GM: Gallagher measure or average distance (in percent, normalised to pool radius), i.e the mean distance to the correct location over the trial. NC: Number of crossings, i.e. the number of times the rat swims over the correct location.

best suited to distinguish different behavioural strategies (no overlap of errorbars, Fig. 10.9), closely followed by the percentage zone measure, which performs slightly worse for distinguishing the random from the cue-based strategy. The time in quadrant measure has difficulties distinguishing the cue-based from the place-control strategy. Finally, the number of crossings measure fails to distinguish reliably either the random or the place-control strategy from the cue-based strategy, due to large variations between samples. Summarising, such model prediction are helpful in screening through possible experimental setups to uncover the most promising ones that should be performed in a real experiment.

10.8 Conclusion

This chapter illustrated how the modelling framework developed in Chapter 9 can be used to analyse Morris water maze experiments, test different behavioural strategies and make model predictions. In particular, identifying the model revealed inherent differences for two groups of rats, one group trained with three extra-maze cues available, the other group trained with one extra-maze cues available. The next chapter discusses the differences of the 3-cue and 1-cue model from a control theoretical and neurophysiological perspective.

Chapter 11

Discussion of the model and relation to neurophysiology

11.1 The role of feedback control

Developing a control system that robustly tracks a desired variable is a problem commonly faced by engineers. The standard solution is integral feedback control, in which the time integral of difference between actual value and desired value, is fed back into the system. A heating system controlled by a thermostat is one well-known example. Because temperature, which is proportional to the integral of heat (the output of the heater), is compared to the desired temperature and fed back into this closed-loop system, the difference between the room temperature and the desired temperature approaches zero despite external environmental disturbances or variations in the heater. Here, we have the same situation. The heading, which is the integral of the heading change, is fed back (Fig. 9.2). Hereby, the role of the integrator is taken by the random walk model. It is therefore not necessary to use integral action within in the controller in order to achieve a zero tracking error in steady state.

The identified feedback parameters ($K_{\text{1-cue}} < K_{\text{3-cues}}$, see Chapter 10) suggest that the more navigational cues are available, the more the animal seems confident, i.e. applies a stronger, more stringent control strategy. Our simulations showed the advantage of weaker, more moderate control in the one cue case as it allows for exploring a greater area.

11.2 The role of the filter

In engineering, a low pass filter is a simple but effective way to reduce (measurement) noise. Here we have a somewhat noisy situation in the one cue case where the rats positional inference is impaired. It makes therefore sense that rats use a filter if only few or uncertain navigational cues are available ($F_{\text{1-cue}} < F_{\text{3-cues}}$, see Chapter 10). A biological interpretation of this result is that animals navigating with more available cues rely on their immediate visual information, whereas animals with a limited number of available cues rely more on past information.

11.3 Fitting the model into underlying neural circuits

The neurophysiology of spatial memory and learning involves different brain regions depending on environment, experimental conditions and strategy employed by the rat (Fig. 9.2). For example, the taxon (egocentric) pathway directly projects the visual cortex onto motor neurons in the striatum (Sheynikhovich et al., 2009). In contrast, the locale (allocentric) pathway additionally involves hippocampal and parahippocampal regions and the brain's spatial representation system. In these (para) hippocampal regions, the rats location and head direction is represented by neurons called place cells and head direction cells, respectively (O'Keefe and Dostrovsky, 1971). In the parahippocampus, grid cells of the entorhinal cortex are thought of incorporating the rats self movements (motor actions) in a process called path integration (Burgess, 2008; O'Keefe and Burgess, 2005; Hafting et al., 2005).

There is an extensive literature modelling the neuronal processes, which ultimately cause the animal's movements, see for instance Sheynikhovich et al. (2009) or Burgess (2008). In contrast, the here proposed behavioural model focuses on the dynamics of the resulting movements. Models on both levels, the neuronal and the behavioural one, are necessary for a complete picture in which the loop can be closed via the environment (Fig. 9.2). We suggest that the parameters of the dynamic model change depending on which neuronal pathway is activated. For example, the higher control gain K in the 3-cue case might be linked to the synaptic projections from place cells to motor neurons in the nucleus accumbens in the ventral striatum (locale system). Further, the increased filter constant F in the 1-cue case could be linked to increased activation of the projections from view cells to motor neurons in the caudate putamen in the dorsal striatum (taxon system, Sheynikhovich et al. 2009). However, the parameters K and F are probably not independent from each other and both are likely to be influenced by several, possibly overlapping neuronal processes.

11.4 Conclusion

The here presented modelling results concerning the 3-cues and 1-cue group are in concordance with earlier reports. Harvey et al. (2009) revealed no significant difference between the groups in terms of the gross measures used (e.g escape latencies) demonstrating that both groups learned the task effectively, but also found different behavioural patterns. Here, this thesis provides a mathematical model explaining the group differences and revealing that both groups control their movements differently. The parameters of the heading change model were identified in open loop and seem not to differ considerably. In contrast, the feedback parameters as identified in closed loop are clearly distinct. This demonstrates that the model can reveal inherent procedural differences not visible in gross measures.

The model parameters are influenced by several factors that could be controlled in experiments (e.g. brain lesions, training schemes). This makes the model a useful tool for analysis of experiments for which swimming paths are recorded. The fitted model parameters can be understood as higher level measures reflecting behavioural and neurophysiological differences. Further research

should address the issue of mapping the neurophysiology to the model parameters.

Part III

Concluding remarks

Coming back to the introduction, building models from observed data is at the heart of science, and particularly challenging in the biological sciences. This thesis demonstrates that approaching this challenge from a systems theoretical perspective can improve current identification methodologies (Part I) and shed new light on old biological problems (Part II). I believe it is fair to say that biological systems are messy, often containing a great deal of uncertainty and stochasticity. The cell is a crowded place where many hundreds and thousands of components interact simultaneously. Because of this complexity, we need to surround biology with unambiguous mathematical formalisms that can guide our intuition. I think biology can no longer shy away from the complexity that ultimately lies at its core. Likewise, mathematics (systems theory) can no longer neglect the messiness of biological systems and work with simple approximations, for example in terms of linearisations and discretisations. Not if we are, at any point, to solve the question Schrödinger (1943) put so nicely: What is life? Asking this question triggered the field of molecular biology and propelled biology forward for over 50 years. I also think it fair to say that we now know what life *is* in the sense that we know what it is composed of, namely DNA, RNA, proteins and so forth. In the spirit of systems biology, we should therefore go one step further. It is probably time to reformulate Schrödiner's question in order to tackle what he really had in mind and ask: How does life work?

Therewith I conclude my final remarks, hoping that my thesis inspired the reader.

Bibliography

Aggleton, J. P., Vann, S. D., Oswald, C. J., and Good, M. (2000). Identifying cortical inputs to the rat hippocampus that subserve allocentric spatial processes: a simple problem with a complex answer. *Hippocampus*, 10(4):466–474.

Agrawal, A. (1999). New institute to study systems biology. *Nat Biotechnol*, 17(8):743–744.

Aldridge, B. B., Burke, J. M., Lauffenburger, D. A., and Sorger, P. K. (2006a). Physicochemical modelling of cell signalling pathways. *Nat Cell Biol*, 8(11):1195–1203.

Aldridge, B. B., Haller, G., Sorger, P. K., and Lauffenburger, D. A. (2006b). Direct Lyapunov exponent analysis enables parametric study of transient signaling governing cell behavior. *IEE Proceedings—Systems Biology*, 153(6):457–466.

Anderson, J. and Papachristodoulou, A. (2009). On validation and invalidation of biological models. *BMC Bioinformatics*, 10:132.

Audoly, S., Bellu, G., D'Angiò, L., Saccomani, M. P., and Cobelli, C. (2001). Global identifiability of nonlinear models of biological systems. *IEEE T Biomed Eng*, 48(1):55–65.

Ayala, F. J. (1968). Biology as an autonomous science. *Am Sci*, 56(3):207–221.

Baldi, E., Lorenzini, C. A., and Corrado, B. (2003). Task solving by procedural strategies in the Morris water maze. *Physiol Behav*, 78(4-5):785–793.

Barry, C. and Burgess, N. (2007). Learning in a geometric model of place cell firing. *Hippocampus*, 17(9):786–800.

Benhamou, S. (2003). Bicoordinate navigation based on non-orthogonal gradient fields. *J Theor Biol*, 225(2):235–239.

Beyer, H.-G. and Schwefel, H.-P. (2002). Evolution strategies a comprehensive introduction. *Natural Computing*, 1:3–52. 10.1023/A:1015059928466.

Blum, K. I. and Abbott, L. F. (1996). A model of spatial map formation in the hippocampus of the rat. *Neural Comput*, 8(1):85–93.

Borchers, S., Rumschinski, P., Bosio, S., Weismantel, R., and Findeisen., R. (2009). Model invalidation and system identification of biochemical reaction networks. In *Proc of the 15th IFAC Symposium on Systems Identification, Saint Malo, France*.

Boyd, S. and Vandenberghe, L. (2004). *Convex optimization*. Cambridge University Press.

Brown, M. A. and Sharp, P. E. (1995). Simulation of spatial learning in the Morris water maze by a neural network model of the hippocampal formation and nucleus accumbens. *Hippocampus*, 5(3):171–188.

Brown, M. F. (1992). Does a cognitive map guide choices in the radial-arm maze? *J Exp Psychol Anim Behav Process*, 18(1):56–66.

Bullinger, E., Fey, D., Farina, M., and Findeisen, R. (2008). Identifikation biochemischer Reaktionsnetzwerke: Ein beobachterbasierter Ansatz. *AT-Automatisierungstechnik*, 56(5):269–279.

Burgess, N. (2008). Spatial cognition and the brain. *Ann N Y Acad Sci*, 1124:77–97.

Burgess, N. and O'Keefe, J. (1996). Neuronal computations underlying the firing of place cells and their role in navigation. *Hippocampus*, 6(6):749–762.

Burgess, N., Recce, M., and O'Keefe, J. (1994). A model of hippocampal function. *Neural Netw.*, 7(6-7):1065–1081.

Cain, D. P. and Saucier, D. (1996). The neuroscience of spatial navigation: Focus on behavior yields advances. *Rev Neurosci*, 7(3):215–231.

Cannon, W. (1932). *The Wisdom of the Body*. W. W. Norton, New York.

Chalfie, M., Tu, Y., Euskirchen, G., Ward, W. W., and Prasher, D. C. (1994). Green fluorescent protein as a marker for gene expression. *Science*, 263(5148):802–805.

Choi, S. H., Woodlee, M. T., Hong, J. J., and Schallert, T. (2006). A simple modification of the water maze test to enhance daily detection of spatial memory in rats and mice. *J Neurosci Methods*, 156(1-2):182–193.

Conzelmann, H., Fey, D., and Gilles, E. D. (2008). Exact model reduction of combinatorial reaction networks. *BMC Systems Biology*, 2:78.

Cornish-Bowden, A. (2004). *Fundamentals of Enzyme Kinetics*. Portland Press, third edition.

Costenoble, R., Müller, D., Barl, T., van Gulik, W. M., van Winden, W. A., Reuss, M., and Heijnen, J. J. (2007). ^{13}C-labeled metabolic flux analysis of a fed-batch culture of elutriated *Saccharomyces cerevisiae*. *FEMS Yeast Res*, 7(4):511–526.

Cressant, A., Muller, R. U., and Poucet, B. (1997). Failure of centrally placed objects to control the firing fields of hippocampal place cells. *J Neurosci*, 17(7):2531–2542.

Csete, M. E. and Doyle, J. C. (2002). Reverse engineering of biological complexity. *Science*, 295(5560):1664–1669.

de Bruin, J. P., Moita, M. P., de Brabander, H. M., and Joosten, R. N. (2001). Place and response learning of rats in a Morris water maze: differential effects of fimbria fornix and medial prefrontal cortex lesions. *Neurobiol Learn Mem*, 75(2):164–178.

de Graauw, M. (2009). *Phospho-Proteomics Methods and Protocols*, volume 527 of *Methods in Molecular Biology*. Springer Verlag.

de Hoz, L., Martin, S. J., and Morris, R. G. M. (2004). Forgetting, reminding, and remembering: the retrieval of lost spatial memory. *PLoS Biol*, 2(8):E225.

D'Hooge, R. and Deyn, P. P. D. (2001). Applications of the Morris water maze in the study of learning and memory. *Brain Res Rev*, 36(1):60–90.

Dochain, D. (2003). State and parameter estimation in chemical and biochemical processes: a tutorial. *J Process Control*, 13(8):801–818.

Dojer, N., Gambin, A., Mizera, A., Wilczynski, B., and Tiuryn, J. (2006). Applying dynamic bayesian networks to perturbed gene expression data. *BMC Bioinformatics*, 7:249.

Draghici, S., Khatri, P., Eklund, A. C., and Szallasi, Z. (2006). Reliability and reproducibility issues in dna microarray measurements. *Trends Genet*, 22(2):101–109.

EcoCyc (2010). (http://ecocyc.org/), last visited december 2010.

Eichenbaum, H., Dudchenko, P., Wood, E., Shapiro, M., and Tanila, H. (1999). The hippocampus, memory, and place cells: is it spatial memory or a memory space? *Neuron*, 23(2):209–226.

Eissing, T., Waldherr, S., Allgwer, F., Scheurich, P., and Bullinger, E. (2007). Steady state and (bi-) stability evaluation of simple protease signalling networks. *Biosystems*, 90(3):591–601.

Farina, M., Bullinger, E., Findeisen, R., and Bittanti, S. (2007). An observer based strategy for parameter identification in systems biology. In *Proc of the 2nd Conf Foundations of Systems Biology in Engineering, Stuttgart, Germany*, pages 521–526. FOSBE.

Farina, M., Findeisen, R., Bullinger, E., Bittanti, S., Allgöwer, F., and Wellstead, P. (2006). Results towards identifiability properties of biochemical reaction networks. In *Proc of the 45th IEEE Conf on Decision and Control, San Diego, USA*, pages 2104–2109. IEEE.

Fell, D. (1997). *Understanding the Control of Metabolism*. Portland Press, London.

Feng, X.-J., Hooshangi, S., Chen, D., Li, G., Weiss, R., and Rabitz, H. (2004). Optimizing genetic circuits by global sensitivity analysis. *Biophys J*, 87(4):2195–2202.

Feng, X.-J. and Rabitz, H. (2004). Optimal identification of biochemical reaction networks. *Biophys J*, 86(3):1270–1281.

Fey, D. and Bullinger, E. (2009). A dissipative approach to the identification of kinetic reaction networks. In *Proc of the 15th IFAC Symposium on Systems Identification, Saint Malo, France*, pages 1259–1264.

Fey, D. and Bullinger, E. (2010). Limiting the parameter search space for dynamic models with rational kinetics using semi-definite programming. In *Proc of the 15th Symposium on Computer Applications in Biotechnology, Leuven, Belgium*, pages 150–155.

Fey, D. and Bullinger, E. (2011). Identification of kinetic parameters and modelling errors for biomolecular reaction systems using dissipative observers. *(submitted)*.

Fey, D., Commins, S., and Bullinger, E. (2010). Feedback control strategies for spatial navigation revealed by dynamic modelling of learning in the Morris water maze. *J Comput Neurosci*. (in press).

Fey, D., Findeisen, R., and Bullinger, E. (2008). Parameter estimation in kinetic reaction models using nonlinear observers facilitated by model extensions. In *Proc of the 17th IFAC World Congress, Seoul, Korea*, pages 313–318.

Fey, D., Findeisen, R., and Bullinger, E. (2009). Identification of biochemical reaction networks using a parameter-free coordinate system. In Iglesias and Ingalls (2009), pages 297–316.

Gadkar, K. G., Gunawan, R., and Doyle III, F. J. (2005). Iterative approach to model identification of biological networks. *BMC Bioinformatics*, 6:155.

Gallagher, M., Burwell, R., and Burchinal, M. (1993). Severity of spatial learning impairment in aging: development of a learning index for performance in the Morris water maze. *Behav Neurosci*, 107(4):618–626.

Garnier, H., Mensler, M., and Richard, A. (2003). Continuous-time model identification from sampled data implementation issues and performance evaluation. *Int J Control*, 76(13):1337–1357.

Garnier, H. and Wang, L., editors (2008). *Identification of Continuous-time Models from Sampled Data*. Springer Verlag, London.

Gauthier, J. P., Hammouri, H., and Othman, S. (1992). A simple observer for nonlinear systems applications to bioreactors. *IEEE T Automat Contr*, 37(6):875–880.

Geffen, D., Findeisen, R., Allgöwer, F., and Guay, M. (2007). The question of parameter identifiability for biochemical reaction networks considering the NF-κB signal transduction pathway. In *Proc of the 2nd Conf Foundations of Systems Biology in Engineering, Stuttgart, Germany*, pages 509–514.

Gerlai, R. T., McNamara, A., Williams, S., and Phillips, H. S. (2002). Hippocampal dysfunction and behavioral deficit in the water maze in mice: an unresolved issue? *Brain Res Bull*, 57(1):3–9.

Gilles, E. (2002a). Control—key to better understanding biological systems. *AT-Automatisierungstechnik*, 50:7–17.

Gilles, E. (2002b). Regelung — Schlüssel zum Verständnis biologischer Systeme. *AT-Automatisierungstechnik*, 50:7–17.

Goldbeter, A. and Koshland, D. E. (1981). An amplified sensitivity arising from covalent modification in biological systems. *Proc Natl Acad Sci U S A*, 78(11):6840–6844.

Gstaiger, M. and Aebersold, R. (2009). Applying mass spectrometry-based proteomics to genetics, genomics and network biology. *Nat Rev Genet*, 10(9):617–627.

Hafting, T., Fyhn, M., Molden, S., Moser, M.-B., and Moser, E. I. (2005). Microstructure of a spatial map in the entorhinal cortex. *Nature*, 436(7052):801–806.

Hamilton, D. A., Rosenfelt, C. S., and Whishaw, I. Q. (2004). Sequential control of navigation by locale and taxon cues in the Morris water task. *Behav Brain Res*, 154(2):385–397.

Harrison, F. E., Reiserer, R. S., Tomarken, A. J., and McDonald, M. P. (2006). Spatial and nonspatial escape strategies in the Barnes maze. *Learn Mem*, 13(6):809–819.

Harvey, D. R., Brant, L., and Commins, S. (2009). Differences in cue-dependent spatial navigation may be revealed by in-depth swimming analysis. *Behav Processes*, 82(2):190–197.

Harvey, D. R., McGauran, A.-M. T., Murphy, J., Burns, L., McMonagle, E., and Commins, S. (2008). Emergence of an egocentric cue guiding and allocentric inferring strategy that mirrors hippocampal brain-derived neurotrophic factor (bdnf) expression in the Morris water maze. *Neurobiol Learn Mem*, 89(4):462–479.

Heinrich, R. and Schuster, S. (1996). *The Regulation of Cellular Systems*. Chapman and Hall, New York.

Hodgkin, A. L. and Huxley, A. F. (1952). A quantitative description of membrane current and its application to conduction and excitation in nerve. *J Physiol*, 117(4):500–544.

Huang, C. Y. and Ferrell, J. E. (1996). Ultrasensitivity in the mitogen-activated protein kinase cascade. *Proc Natl Acad Sci U S A*, 93(19):10078–10083.

Ideker, T. (2004). Systems biology 101 – what you need to know. *Nat Biotechnol*, 22(4):473–475.

Ideker, T., Galitski, T., and Hood, L. (2001). A new approach to decoding life: Systems biology. *Annu Rev Genomics Hum Genet*, 2:343–372.

Iglesias, P. A. and Ingalls, B. P., editors (2009). *Control Theory and Systems Biology*. MIT Press, Cambridge/MA.

Inouye, S. and Tsuji, F. I. (1994). Evidence for redox forms of the *Aequorea* green fluorescent protein. *FEBS Lett*, 351(2):211–214.

Ireton, R., Montgomery, K., Bumgarner, R., Samudrala, R., and McDermott, J., editors (2009). *Computational Systems Biology*, volume 541 of *Methods in Molecular Biology*. Springer Verlag.

Irish, J. M., Kotecha, N., and Nolan, G. P. (2006). Mapping normal and cancer cell signalling networks: towards single-cell proteomics. *Nat Rev Cancer*, 6(2):146–155.

Jeanson, R., Blanco, S., Fournier, R., Deneubourg, J. L., Fourcassi, V., and Theraulaz, G. (2003). A model of animal movements in a bounded space. *J Theor Biol*, 225(4):443–451.

Karnaukhov, A. V. and Karnaukhova, E. V. (2003). Application of a new method of nonlinear dynamical system identification to biochemical problems. *Biochemistry (Moscow)*, 68(3):253–259. Translated from Biokhimiya, Vol. 68, No. 3, 2003, pp. 309–317.

Kealy, J., Diviney, M., Kehoe, E., McGonagle, V., O'Shea, A., Harvey, D., and Commins, S. (2008a). The effects of overtraining in the Morris water maze on allocentric and egocentric learning strategies in rats. *Behav Brain Res*, 192(2):259–263.

Kealy, J., Diviney, M., Kehoe, E., McGonagle, V., O'Shea, A., Harvey, D., and Commins, S. (2008b). The effects of overtraining in the Morris water maze on allocentric and egocentric learning strategies in rats. *Behav Brain Res*, 192(2):259–263.

Keener, J. and Sneyd, J. (2001). *Mathematical Physiology*, volume 8 of *Interdisciplinary Applied Mathematics*. Springer-Verlag, New York, second edition.

KEGG (2010). (http://www.genome.ad.jp/), last visited december 2010.

Kholodenko, B. N. (2000). Negative feedback and ultrasensitivity can bring about oscillations in the mitogen-activated protein kinase cascades. *Eur J Biochem*, 267(6):1583–1588.

Kholodenko, B. N. (2006). Cell-signalling dynamics in time and space. *Nat Rev Mol Cell Biol*, 7(3):165–176.

Kholodenko, B. N., Demin, O. V., Moehren, G., and Hoek, J. B. (1999). Quantification of short term signaling by the epidermal growth factor receptor. *J Biol Chem*, 274(42):30169–30181.

Kholodenko, B. N., Hancock, J. F., and Kolch, W. (2010). Signalling ballet in space and time. *Nat Rev Mol Cell Biol*, 11(6):414–426.

Kholodenko, B. N., Kiyatkin, A., Bruggeman, F. J., Sontag, E., Westerhoff, H. V., and Hoek, J. B. (2002). Untangling the wires: a strategy to trace functional interactions in signaling and gene networks. *Proc Natl Acad Sci U S A*, 99(20):12841–12846.

Kitano, H. (2000). Perspectives on systems biology. *New Generation Computing*, 18(3):199–216.

Kitano, H., editor (2001a). *Foundations of Systems Biology*. MIT Press, Cambridge/MA.

Kitano, H. (2001b). Preface. In Kitano (2001a), pages xiii–xv.

Kitano, H. (2001c). Systems biology: Towards system-level understanding of biological systems. In Kitano (2001a), pages 1–29.

Kitano, H. (2002). Systems biology: a brief overview. *Science*, 295(5560):1662–1664.

Klipp, E., Herwig, R., Kowald, A., Wierling, C., and Lehrach, H. (2005). *Systems Biology in Practice: Concepts, Implementation and Application*. Wiley-VCH, Weinheim.

Koehler, A. B. and Murphree, E. S. (1988). A comparison of the akaike and schwarz criteria for selecting model order. *Applied Statistics*, 37(2):187–195.

Kremling, A. and Saez-Rodriguez, J. (2007). Systems biology—an engineering perspective. *J Biotechnology*, 129(2):329–351.

Kuepfer, L., Sauer, U., and Parrilo, P. A. (2007). Efficient classification of complete parameter regions based on semidefinite programming. *BMC Bioinformatics*, 8:12.

Le Novère, N., Bornstein, B., Broicher, A., Courtot, M., Donizelli, M., Dharuri, H., Li, L., Sauro, H., Schilstra, M., Shapiro, B., Snoep, J., and Hucka, M. (2006). BioModels Database: A free, centralized database of curated, published, quantitative kinetic models of biochemical and cellular systems. see also `http://www.ebi.ac.uk/biomodels/` , last visited 11 Dec 2010.

Lee, W.-P. and Tzou, W.-S. (2009). Computational methods for discovering gene networks from expression data. *Brief Bioinform*, 10(4):408–423.

Leggio, M. G., Neri, P., Graziano, A., Mandolesi, L., Molinari, M., and Petrosini, L. (1999). Cerebellar contribution to spatial event processing: characterization of procedural learning. *Exp Brain Res*, 127(1):1–11.

Leloup, J.-C. and Goldbeter, A. (2008). Modeling the circadian clock: from molecular mechanism to physiological disorders. *Bioessays*, 30(6):590–600.

Leloup, J. C., Gonze, D., and Goldbeter, A. (1999). Limit cycle models for circadian rhythms based on transcriptional regulation in Drosophila and Neurospora. *J Biol Rhythms*, 14(6):433–448.

Li, C., Donizelli, M., Rodriguez, N., Dharuri, H., Endler, L., Chelliah, V., Li, L., He, E., Henry, A., Stefan, M. I., Snoep, J. L., Hucka, M., Le Novère, N., and Laibe, C. (2010). BioModels Database: An enhanced, curated and annotated resource for published quantitative kinetic models. *BMC Syst Biol*, 4:92. see also `http://www.ebi.ac.uk/biomodels/` , last visited 11 Dec 2010.

Li, H., Xuan, J., Wang, Y., and Zhan, M. (2008). Inferring regulatory networks. *Front Biosci*, 13:263–275.

Ljung, L. (1999). *System Identification — Theory for the User*. Prentice Hall, Upper Saddle River, NJ, second edition.

Ljung, L. (2003). Challenges of non-linear identification. Bode Lecture, 42$^{\text{th}}$ IEEE Conf on Decision and Control, Maui, Hawaii, USA.

Ljung, L. (2010). Perspectives on system identification. *Annual Reviews in Control*, 34(1):1–2.

Ljung, L. and Glad, T. (1994). On global identifiability for arbitrary model parametrizations. *Automatica*, 30(2):265–276.

Löfberg, J. (2004). Yalmip : A toolbox for modeling and optimization in MATLAB. In *Proceedings of the CACSD Conference*, Taipei, Taiwan.

Maei, H. R., Zaslavsky, K., Teixeira, C. M., and Frankland, P. W. (2009). What is the most sensitive measure of water maze probe test performance? *Front Integr Neurosci*, 3:4.

McGauran, A.-M. T., Harvey, D., Cunningham, L., Craig, S., and Commins, S. (2004). Retention of cue-based associations in the water maze is time-dependent and sensitive to disruption by rotating the starting position. *Behav Brain Res*, 151(1-2):255–266.

McGauran, A.-M. T., Moore, J. B., Madsen, D., Barry, D., O'Dea, S., Mahon, B. P., and Commins, S. (2008). A possible role for protein synthesis, extracellular signal-regulated kinase, and brain-derived neurotrophic factor in long-term spatial memory retention in the water maze. *Behav Neurosci*, 122(4):805–815.

McGauran, A.-M. T., O'Mara, S. M., and Commins, S. (2005). Vestibular influence on water maze retention: transient whole body rotations improve the accuracy of the cue-based retention strategy. *Behav Brain Res*, 158(1):183–187.

McNamara, R. K. and Skelton, R. W. (1993). The neuropharmacological and neurochemical basis of place learning in the Morris water maze. *Brain Res Rev*, 18(1):33–49.

Mesarović, M. D. (1968). Systems theory and biology – view of a theoretician. In Mesarović, M. D., editor, *Systems Theory and Biology*, pages 59–87. Springer Verlag.

Moghaddam, M. and Bures, J. (1996). Contribution of egocentric spatial memory to place navigation of rats in the Morris water maze. *Behav Brain Res*, 78(2):121–129.

Moles, C. G., Mendes, P., and Banga, J. R. (2003). Parameter estimation in biochemical pathways: a comparison of global optimization methods. *Genome Res*, 13(11):2467–2474.

Moreno, J. A. (2008). Observer design for bioprocesses using a dissipative approach. In *Proc of the 17th IFAC World Congress, Seoul, Korea*, 15559–15564.

Morris, R. (1984). Developments of a water-maze procedure for studying spatial learning in the rat. *J Neurosci Methods*, 11(1):47–60.

Morris, R. G., Garrud, P., Rawlins, J. N., and O'Keefe, J. (1982). Place navigation impaired in rats with hippocampal lesions. *Nature*, 297(5868):681–683.

Morris, R. G. M. (1981). Spatial localization does not require the presence of local cues. *Learning and Motivation*, 12(2):239–260.

Moser, E., Moser, M. B., and Andersen, P. (1993). Spatial learning impairment parallels the magnitude of dorsal hippocampal lesions, but is hardly present following ventral lesions. *J Neurosci*, 13(9):3916–3925.

Moser, E. I., Kropff, E., and Moser, M.-B. (2008). Place cells, grid cells, and the brain's spatial representation system. *Annu Rev Neurosci*, 31:69–89.

Moser, M. B. and Moser, E. I. (1998). Distributed encoding and retrieval of spatial memory in the hippocampus. *J Neurosci*, 18(18):7535–7542.

Motulsky, H. and Christopoulos, A. (2004). *Fitting Models to Biological Data Using Linear and Nonlinear Regression: A Practical Guide to Curve Fitting*. Oxford University Press, USA.

Muller, R. U. and Kubie, J. L. (1987). The effects of changes in the environment on the spatial firing of hippocampal complex-spike cells. *J Neurosci*, 7(7):1951–1968.

Murray, J. D. (2007). *Mathematical Biology: I. An Introduction*. Springer.

Nature office (2001). Lab automation: Automation by lab robots PC control and integration. *Nature*, 411:869–870.

Needham, C. J., Bradford, J. R., Bulpitt, A. J., and Westhead, D. R. (2007). A primer on learning in bayesian networks for computational biology. *PLoS Comput Biol*, 3(8):e129.

Noble, D. (1960). Cardiac action and pacemaker potentials based on the Hodgkin-Huxley equations. *Nature*, 188:495–497.

Nurse, P. (2000). A long twentieth century of the cell cycle and beyond. *Cell*, 100(1):71–78.

O'Keefe, J. (1990). A computational theory of the hippocampal cognitive map. *Prog Brain Res*, 83:301–312.

O'Keefe, J. and Burgess, N. (2005). Dual phase and rate coding in hippocampal place cells: theoretical significance and relationship to entorhinal grid cells. *Hippocampus*, 15(7):853–866.

O'Keefe, J. and Dostrovsky, J. (1971). The hippocampus as a spatial map. Preliminary evidence from unit activity in the freely-moving rat. *Brain Res*, 34(1):171–175.

Osorio, M. and Moreno, J. A. (2006). Dissipative design of observers for multivalued nonlinear systems. In *Proc of the 45th IEEE Conf on Decision and Control, San Diego, USA*, pages 5400–5405.

Packard, M. G. and McGaugh, J. L. (1996). Inactivation of hippocampus or caudate nucleus with lidocaine differentially affects expression of place and response learning. *Neurobiol Learn Mem*, 65(1):65–72.

Parillo, P. A. (2003). Semidefinite programming relaxations for semialgebraic problems. *Math Prog*, 96(2, Ser B):293–320.

Pearce, J. M., Roberts, A. D., and Good, M. (1998). Hippocampal lesions disrupt navigation based on cognitive maps but not heading vectors. *Nature*, 396(6706):75–77.

Peifer, M. and Timmer, J. (2007). Parameter estimation in ordinary differential equations for biochemical processes using the method of multiple shooting. *IET Syst Biol*, 1(2):78–88.

Polisetty, P. K., Voit, E. O., and Gatzke, E. P. (2006). Identification of metabolic system parameters using global optimization methods. *Theor Biol Med Model*, 3:4.

Poucet, B. and Benhamou, S. (1997). The neuropsychology of spatial cognition in the rat. *Crit Rev Neurobiol*, 11(2-3):101–120.

Poucet, B., Lenck-Santini, P. P., Hok, V., Save, E., Banquet, J. P., Gaussier, P., and Muller, R. U. (2004). Spatial navigation and hippocampal place cell firing: the problem of goal encoding. *Rev Neurosci*, 15(2):89–107.

Poucet, B., Lenck-Santini, P.-P., Paz-Villagrn, V., and Save, E. (2003). Place cells, neocortex and spatial navigation: a short review. *J Physiol Paris*, 97(4-6):537–546.

Prasher, D. C., Eckenrode, V. K., Ward, W. W., Prendergast, F. G., and Cormier, M. J. (1992). Primary structure of the *Aequorea* victoria green-fluorescent protein. *Gene*, 111(2):229–233.

Roche, R. A. P., Mangaoang, M. A., Commins, S., and O'Mara, S. M. (2005). Hippocampal contributions to neurocognitive mapping in humans: a new model. *Hippocampus*, 15(5):622–641.

Rosen, R. (1967). *Optimality Principles in Biology*. Butterworth, London.

Rumschinski, P., Borchers, S., Bosio, S., Weismantel, R., and Findeisen, R. (2010). Set-base dynamical parameter estimation and model invalidation for biochemical reaction networks. *BMC Syst Biol*, 4:69.

Santos, S. D. M., Verveer, P. J., and Bastiaens, P. I. H. (2007). Growth factor-induced mapk network topology shapes erk response determining pc-12 cell fate. *Nat Cell Biol*, 9(3):324–330.

Schaffner, J. and Zeitz, M. (1999). Variants of nonlinear normal form observer design. In Nijmeijer, H. and Fossen, T., editors, *New Directions in nonlinear observer design*, volume 244 of *Lecture Notes in Control and Information Sciences*, pages 161–180. Springer Berlin / Heidelberg. 10.1007/BFb0109926.

Schaum, A., Moreno, J. A., and Vargas, A. (2005). Global observability and detectability analysis for a class of nonlinear models of biological processes with bad inputs. In *Proc of the 2nd Int Conf Electrical and Electronics Engineering, Mexico City, Mexico*, pages 343–346.

Schilling, M., Maiwald, T., Bohl, S., Kollmann, M., Kreutz, C., Timmer, J., and Klingmüller, U. (2005). Computational processing and error reduction strategies for standardized quantitative data in biological networks. *FEBS J*, 272(24):6400–6411.

Schrödinger, E. (1943). What is life. Dublin Institute for Advanced Studies, February 1943.

Schrödinger, E. (1944). *What is Life? The physical aspect of the living cell*. Cambridge University Press, Cambridge.

Sheynikhovich, D., Chavarriaga, R., Strsslin, T., Arleo, A., and Gerstner, W. (2009). Is there a geometric module for spatial orientation? insights from a rodent navigation model. *Psychol Rev*, 116(3):540–566.

Shu, Y. and Hong-Hui, L. (2004). Transcription, translation, degradation, and circadian clock. *Biochem Biophys Res Commun*, 321(1):1–6.

Singer, A. B., Taylor, J. W., Barton, P. I., and Green, W. H. (2006). Global dynamic optimization for parameter estimation in chemical kinetics. *J Phys Chem A*, 110(3):971–976.

Sontag, E. (2005). Molecular systems biology and control. *European J Control*, 11(4–5):396–435.

Sontag, E., Kiyatkin, A., and Kholodenko, B. N. (2004). Inferring dynamic architecture of cellular networks using time series of gene expression, protein and metabolite data. *Bioinformatics*, 20(12):1877–1886.

Sorger, P. K. (2005). A reductionist's systems biology: Opinion. *Curr Opin Cell Biol*, 17(1):9–11.

STKE (2010). Signal transduction knowledge environment (http://stke.sciencemag.org/cm/), last visited december 2010.

Strösslin, T., Sheynikhovich, D., Chavarriaga, R., and Gerstner, W. (2005). Robust self-localisation and navigation based on hippocampal place cells. *Neural Netw*, 18(9):1125–1140.

Sturm, J. F. (1999). Using sedumi 1.02, a MATLAB toolbox for optimization over symmetric cones. *Optimization Methods and Software*, 11–12:625–653.

Sutherland, R. J. and Hamilton, D. A. (2004). Rodent spatial navigation: at the crossroads of cognition and movement. *Neurosci Biobehav Rev*, 28(7):687–697.

Szallasi, Z. (2006). Biological data acquisition for system level modeling – an exercise in the art of compromise. In *System Modeling in Cellular Biology*, pages 201–220. MIT Press, Cambridge/MA.

Szallasi, Z., Stelling, J., and Periwal, V., editors (2006). *Systems Modelling in Cellular Biology*. MIT Press, Cambridge, MA.

Tamosiunaite, M., Ainge, J., Kulvicius, T., Porr, B., Dudchenko, P., and Wrgtter, F. (2008). Path-finding in real and simulated rats: assessing the influence of path characteristics on navigation learning. *J Comput Neurosci*, 25(3):562–582.

Thattai, M. and van Oudenaarden, A. (2002). Attenuation of noise in ultrasensitive signaling cascades. *Biophys J*, 82(6):2943–2950.

Tucker, W., Kutalik, Z., and Moulton, V. (2007). Estimating parameters for generalized mass action models using constraint propagation. *Math Biosci*, 208(2):607–620.

Vargas, A. and Moreno, J. A. (2000). Approximate high-gain observers for uniformly observable nonlinear systems. In *Proc of the 39th IEEE Conf on Decision and Control, Sydney, Australia*, pages 784–789. IEEE.

Vargas, A. and Moreno, J. A. (2005). Approximate high-gain observers for non-Lipschitz observability forms. *Int J Control*, 78(4):247–253.

Vargas, A., Moreno, J. A., and Zeitz, M. (2003). Event-based observer design for observable nonlinear systems with bad input points. In *Proceedings of the European Conference of Control, Cambridge, UK*.

Vayttaden, S. J., Ajay, S. M., and Bhalla, U. S. (2004). A spectrum of models of signaling pathways. *Chembiochem*, 5(10):1365–1374.

von Bertalanffy, L. (1968). *General System Theory: Foundations, Development, Applications*. George Braziller, New York.

Waldherr, S., Findeisen, R., and Allgöwer, F. (2008). Global sensitivity analysis of biochemical reaction networks via semidefinite programming. pages 9701–9706.

Watson, J. D. (1968). *The Double Helix: A Personal Account of the Discovery of the Structure of DNA*. Atheneum.

Watson, J. D. and Crick, F. H. (1953). Molecular structure of nucleic acids; a structure for Deoxyribose Nucleic Acid. *Nature*, 171(4356):737–738.

Wellstead, P., Bullinger, E., Kalamatianos, D., Mason, O., and Verwoerd, M. (2008). The rôle of control and system theory in systems biology. *Annual Reviews in Control*, 32(1):33 – 47.

Wiener, N. (1948). *Cybernetics—Control and Communication in the Animal and the Machine*. John Wiley & Sons, New York/NY.

Willems, J. C. (1972a). Dissipative dynamical systems — Part I: General theory. *Archive for Rational Mechanics and Analysis*, 45(5):321–351.

Willems, J. C. (1972b). Dissipative dynamical systems — Part II: Linear systems with quadratic supply rates. *Archive for Rational Mechanics and Analysis*, 45(5):352–393.

Wolkenhauer, O. (2001). Systems biology: The reincarnation of systems theory applied in biology? *Brief Bioinform*, 2(3):258–270.

Wolkenhauer, O. and Mesarović, M. D. (2005). Feedback dynamics and cell function: Why systems biology is called Systems Biology. *Molecular BioSystems*, 1(1):14–16.

Wolkenhauer, O., Sreenath, S. N., Wellstead, P., Ullah, M., and Cho, K. H. (2005). A systems- and signal-oriented approach to intracellular dynamics. *Biochem Soc Trans*, 33(3):507–515.

Xia, X. and Moog, C. H. (2003). Identifiability of nonlinear systems with application to HIV/AIDS models. *IEEE Trans Autom Control*, 48(2):330–336.

Xia, X. and Zeitz, M. (1997). On nonlinear continuous observers. *Int J Control*, 66:943–954.

Zak, D. E., Gonye, G. E., Schwaber, J. S., and Doyle III, F. J. (2003). Importance of input perturbations and stochastic gene expression in the reverse engineering of genetic regulatory networks: Insights from an identifiability analysis of an in silico network. *Genome Res*, 13(11):2396–2405.